5-2019

Novel wet laid nonwoven carbon fiber mats and their composites

Hicham Kheir Ghossein
University of Tennessee, hghossei@utk.edu

To the Graduate Council:

I am submitting herewith a dissertation written by Hicham Kheir Ghossein entitled "Novel wet laid nonwoven carbon fiber mats and their composites." I have examined the final electronic copy of this dissertation for form and content and recommend that it be accepted in partial fulfillment of the requirements for the degree of Doctor of Philosophy, with a major in Mechanical Engineering.

Uday Vaidya, Major Professor

We have read this dissertation and recommend its acceptance:

Chad Duty, Amit Naskar, Ahmed Hassen, Vincent Paquit

Accepted for the Council:

Dixie L. Thompson

Vice Provost and Dean of the Graduate School

(Original signatures are on file with official student records.)

Novel wet laid nonwoven carbon fiber mats and their composites

A Dissertation Presented for the
Doctor of Philosophy
Degree
The University of Tennessee, Knoxville

Hicham Kheir Ghossein
May 2019

DEDICATION

This work is dedicated to my parents, Kheir and Nawal. Their faith in my potential allowed me to become the man that I am today. To my late Grandfather Chafic for imbedding in me the love for science and knowledge, and to my late aunt Raheel, her faith in me was my guide throughout the darkest of days.

ACKNOWLEDGEMENTS

This work has been possible thanks to the consistent support of my siblings especially my brother Ziad, and the continuous guidance of my advisor Dr. Uday vaidya. I would like to offer a special thanks to my committee members, Dr. Chad Duty, Dr. Amit Naskar, Dr. Ahmed Arabi Hassen and Dr. Vincent Paquit, for their input, support and mentoring in order to make this work possible. I would also like to acknowledge my collaborators Dr. Seokpum Kim and Dr. Jessie Ault from Oak Ridge National Lab and Dr. Stephen Langer from the National Institute of Science and Technology for their invaluable assistance with the computational work of this project. A special thanks to Neenahfibers, MiniFibers, eSpin Technologies, Zoltek Inc., Ashland Chemicals, and Nalco Water an Ecolab Company for their assistance with raw material and scientific support. This work was financially supported by the Department of Energy (DOE) - Institute of Advanced Composite Manufacturing Innovation, the University of Tennessee's Mechanical Aerospace and Biomedical Engineering Department, and the now defunct DOE-Graduate Automotive Technology Education program.

ABSTRACT

In the wake of lightweight and specific strength, composite materials are increasingly used for few decades. In order to meet the industry production rates, a novel mixing method has been developed in this work that provides more control on fiber length and homogeneity in wet-laid (WL) carbon fiber (CF) mats. The WL process has been adopted from papermaking industries to produce non-woven CF fiber mats.This work investigates the production of CF mats in three main phases; (a) First, the mixing regime of the WL method is explored to optimize the process of fiber dispersion. Experimental and theoretical computational fluid dynamics (CFD) studies have been conducted to understand the different factors of the process, in order to obtain the most optimal time of production. Mats produced are imaged through the Back Light Scattering (BLS) technique and computationally analyzed using a Matlab generated code to determine the fiber density distribution through pixel counts and compare the improved results of the mixing method developed in this work to the traditional propeller mixing. Processing time was reduced by 60% to produce a mat on laboratory scale with optimal characteristics; (b) Second composites were made from mats produced by each of the two mixing methods presented in the first part of the work. An object oriented finite element analysis (OFF) investigated the isotropic nature of the composites. The mechanical properties of these composites were evaluated in tensile, flex and inter laminar shear (ILSS). Tensile data showed improvement in standard deviation between samples collected from plates made with mats produced through the innovated mixing method when comparing them to composites made with the mats produced through the traditional

method; and (c) Third, the in-plane permeability of the mats was analyzed in respect to changes in the fiber length and mats grammage per square meter (gsm) and a link between local permeability in response to changes in complex geometries is investigated.

The novel mixing method for fiber distribution in WL discussed in this work presents an innovation in composites production, leading to improved production rate of nonwoven CF mats, ease of production and reproducibility of composites.

TABLE OF CONTENTS

LIST OF TABLES

LIST OF FIGURES

INTRODUCTION

The use of composite materials is growing in the aerospace, automotive, military and industrial sectors [1–3]. Composites possess high strength-to-weight and stiffness-to-weight ratio, low fatigue susceptibility and capability to offer lightweight advantages over metallic products [4–5]. The Corporate Average Fuel Economy (CAFÉ) mandates fuel efficiency of vehicles of 50 mpg by 2025 [6], and with vehicle emissions requirements getting more restrictive in Europe, automakers in general see vehicle light-weighting as one major way to remain in compliance.

Carbon fiber (CF), as is well known, offers many advantages over steel or aluminum such as light weight, high strength, and durability [7]. The full benefit of its use in composites as reinforcement is defined by factors such as aspect ratio (length to diameter), orientation, bonding with the matrix and processing conditions [8 – 10]. CF reinforced polymer (CFRP) composites are produced in various ways such as Sheet Molding Compound (SMC) for thermoset resin and Injection Molding (IM) and Extrusion Compression Molding (ECM) for thermoplastic polymers. But it is well known that IM and ECM suffer from fiber length attrition, and SMC material have limited shelf-life and can present a challenge in design with fiber flow. A new method has emerged recently that gives more control on these aspects, and that is non-woven design of fiber mats that offers higher control on fiber length retention and more isotropic composites like the Wet-laid (WL) method [11]. The WL nonwoven material have been developed in a way to combine excellent property characteristics at low economical cost [12]. WL process has distinct advantages like high productivity, homogeneous preform material,

control of fiber orientation, ability to use recycled fibers and fiber blends, functionalization by addition of fillers, possibility of in-line impregnation [13]. WL has traditionally been used in paper making and textile industries [14]. This process involves uniform dispersion of fibers in water and to produce a mat via filtration by transporting it onto a fine mesh screen.

WET-LAID NONWOVENS

Definition

The North America's Association of Nonwoven Fabric Industry (INDA) describes nonwoven fabrics as sheet or web structures bonded together by entangling fibers or filaments, by various mechanical, thermal and/or chemical processes [15]. While the European Disposables and Nonwoven Association (EDANA), definition for Wet Laid (WL) nonwovens: "Wet laid webs are nonwovens provided they contain a minimum of 50% of man-made fibers or other fibers of non-vegetable origin with a length to diameter ratio equals or superior to 300, or a minimum of 30% of man-made fibers with a length to diameter ratio equals or superior to 600, and a maximum apparent density of 0.40 g/cm³" [16]. In lab scale WL web formation, fibers are deposited onto a forming surface using filtration process.

State of the art

Smithers Apex [17] analyzed the global nonwovens market, and stated that it represents a $37.4 billion industry. WL products comprise a $534 million global industry, with annual projected growth of 5.1% projected for WL nonwovens through 2019. The

motivation toward WL nonwovens is its fabric-like attributes and paper-like production. Ahrens [18] proved that the WL system allows a great flexibility in the blending of different kinds of fibers, this is still reflected today with the work of several researchers as will be discussed in this section. Yeole et al. [19] worked on a recycled Glass Fiber/PA6 Composite. Ramasubramanian et al. [20] did computational fluid dynamics study (CFD) for the dispersion of the synthetic fibers in WL forming. Li et al [21] looked into the effect of beating revolution on dispersion of flame attenuated glass wool suspension. Wood et al. [22] worked on natural fibers scaffold reinforcements using soy fiber. Wang et al. [23] produced kenaf fiber/High Density Polyethylene composites using kenaf fiber mats produced through the WL system. Only handful of examples of CF being used in WL systems can be found, while more work is done with glass and natural fibers . Caba et al. [4] explored the fiber to fiber interactions in carbon mat thermoplastic consisting of 12.7 mm long chopped carbon fibers in a polypropylene matrix but they did not discuss the dispersion method. Lu [24] characterized mechanical performance of Carbon/Polyethylene Terephtalate composites prepared through a WL machine, but did not discuss the dispersion method. The current state of the art systems for WL nonwoven production use a combination of propellers with baffles and surfactants addition to improve the fibers wettability. The following section discusses the challenges of the currently used WL systems when it comes to processing CF.

CHALLENGES IN CF DISPERSION

Surfactants

Reinforcing fibers like glass and carbon do not easily disperse in water and require surfactants [25]. This is due to the hydrophobic nature of these fibers. Surfactants or surface-active agents are chemicals that contains both hydrophilic and hydrophobic moieties. Hydrophobic moieties attach to the hydrophobic fiber surface and the hydrophilic moieties attracts water through hydrogen bonds allowing better wetting of the fibers.

For long fibers above 6 mm in length, surfactants alone will not provide full dispersion in water and assistance from mechanical agitation is still required.

Dispersion of fibers

Mechanical agitation serves to separate fiber bundles, as fibers used in WL have to be chopped. CF is thin with diameter smaller than 7 μm in general. At length above12.7 mm the aspect ratio of the fiber becomes high and despite the stiff nature of the fiber, the chance of fiber buckling increase and cause fiber clumps and entanglement. Chapter 1 of this dissertation will discuss this topic in depth. Shiffler [26] defined various fiber properties that can resist dispersion in aqueous system, like the adhesive forces between the fibers *i.e.* surface tension, and inter-fiber friction. CF is known for its high surface area and increased surface tension. Fathi-Khalfbadam et al. [27] discussed the critical force concept to overcome the forces that resists fiber dispersion. Establishing a foundation that explains how light fibers, similar to CF, can adopt their velocity to that of

the fluid body once rigid body motion is achieved negating in its turn the effect of the mechanical agitation.

Time and flow patterns

Extended agitation time allows in concept improve the dispersion of logs, as more of them approach the propeller and get exposed to higher hydrodynamic force. While this reduces the logs amount, as it will be discussed in chapter one, the vortex pattern leads to fibers entanglement and formation of flocs as discussed by Das et al. [28]. In particular, vortex patterns are known to favor rope formation when the vortex diameter exceed the length of the fiber in use.

Crowding factor importance

Relative to conventional paper forming, which typically involves fibers volume concentrations up to 1% while formation of a nonwoven textile requires a volume concentration level of 0.1% to avoid fiber entanglement since WL nonwoven uses long fiber at minimum length of 3 mm. This is considered to provide each of the filaments with enough space to be suspended in especially when rigid body motion is reached.

OBJECTIVES

The objectives of this work are as follows:

1) **Innovative method for enhancing carbon fibers dispersion in wet laid nonwovens:** This first chapter discusses the fundamentals of fiber dispersion and the limitations of the current method used in the WL systems that prevents optimal dispersion of CF. It expands into proposing an innovative method with computational

fluid dynamics (CFD) study based on the hypothesis of chaotic advection. A full systematic study is presented to quantify the amount of fiber distribution and to investigate the reproducibility of the WL CF nonwoven mats.

2) **Mechanical Analysis of composites made from innovated carbon fiber wet laid mats:** The second chapter expands the work into building and evaluating CF/epoxy composites from WL CF nonwoven mats prepared from both dispersion methods, the traditional and the proposed innovative one. The composites microstructure is evaluated through object oriented fundamental element analysis considering isotropic nature of the mats. OOF is a National Institutes of Standards (NIST) software for studying the relationship between the microstructure of a fibrous material and determination of its mechanical properties based on the microstructure (micrograph) using finite element analysis. The composite mechanical performance is compared in terms of tensile, flexural and inter laminar shear properties.

3) **Effects of fiber length and crowding factor on wet laid mats formation, their in-plane permeability and local permeability of complex shape parts:** The aim of the third chapter is to analyze the in-plane permeability of the mats with respect to variables such as fiber length and crowding factor of the optimized CF mats. The evaluation of the permeability constant can be used as input for resin transfer molding and design of experiment for fabrication of future composites using the WL CF mats. The analysis considered local permeability with respect to complex shapes and its relation to mechanical performance of the composite in such geometries, affected by the local distribution of fiber to resin ratio.

REFERENCES

[1] Boria S, Scattina A, Belingardi G. Experimental evaluation of a fully recyclable thermoplastic composite. Composite Structures. 2016;140:21-35.

[2] J.G Carrillo RAG, E.A. Flores-Johnson, P.I. Gonzalez-Chi. Ballistic performance of thermoplastic composite laminates made from aramid woven fabric and polypropylene matrix. Polymer testing 31. 2012:512-9.

[3] Haibin Ning SP, Uday k. Vaidya. Design and development of thermoplastic composite roof door for mass transit bus. Materials & Design 30. 2009:983-91.

[4] Shahzad A, Nasir SU. Validation of fatigue damage model for composites made of various fiber types and configurations. J Compos Mater 2018;52:1183–91. doi:10.1177/0021998317722402

[5] Chung DDL. Review: Materials for vibration damping. Journal of Materials Science 36. 2001:5733-7.

[6] https://www.nhtsa.gov/laws-regulations/corporate-average-fuel-economy

[7] Huang X. Fabrication and properties of carbon fibers. Materials (Basel) 2009;2:2369–403. doi:10.3390/ma2042369.

[8] Baid H, Abdi F, Lee M, Vaidya U. CHOPPED FIBER COMPOSITE PROGRESSIVE FAILURE 2015.

[9] Dormohammadi S, Repupilli M, Abdi F, Wan Y, Takahashi J, Huang H. Multi-Scale Computational Modeling of Short Fiber Reinforced Thermoplastics. Am Soc Compos Thirty-First Tech Conf 2016:1–8. doi:10.1111/j.1532-5415.1991.tb04043.x.

[10] Wan Y, Straumit I, Takahashi J, Lomov S V. Micro-CT analysis of internal

geometry of chopped carbon fiber tapes reinforced thermoplastics. Compos Part A Appl Sci Manuf 2016;91:211–21. doi:10.1016/j.compositesa.2016.10.013.

[11] Wölling J, Schmieg M, Manis F, Drechsler K. Nonwovens from Recycled Carbon Fibres - Comparison of Processing Technologies. Procedia CIRP 2017;66:271–6. doi:10.1016/j.procir.2017.03.281.

[12] Caba AC, Loos AC, Batra RC. Fiber-fiber interactions in carbon mat thermoplastics. Compos Part A Appl Sci Manuf 2007;38:469–83. doi:10.1016/j.compositesa.2006.02.024

[13] Weeks, G. P. and Geary, J. E., "Fiber reinforced porous sheets", US patent 5,134,016, 1992.

[14] A. J. Fundamentals of Fiber Dispersion in Water; Master Thesis. Raleigh: North Carolina State University; 2000.

[15] Wilson A. 1 - Development of the nonwovens industry. In: Russell SJ, editor. Handb. Nonwovens, Woodhead Publishing; 2007, p. 1–15. doi:https://doi.org/10.1533/9781845691998.1.

[16] White C. 3 - Wet-laid web formation. In: Russell SJ, editor. Handb. Nonwovens, Woodhead Publishing; 2007, p. 112–42. doi:https://doi.org/10.1533/9781845691998.112.

[17] Smithers Apex, *The Future of global Nonwoven Markets to 2020,* May 2015.

[18] Ahrens, R.A. Wet-laid forming of nonwoven fabrics. TAPPI Nonwovens Symp., Myrtle Beach. Notes, 1982 pp. 39-40.

[19] Yeole P, Ning H, Hassen AA, Vaidya UK. The Effect of Flocculent , Dispersants , and Binder on Wet – laid Process for Recycled Glass Fiber / PA6 Composite 2018;26:259–7

[20] Ramasubramanian MK, Shiffler D, Jayachandran A. A Computational Fluid Dynamics Modeling and Experimental Study of the Mixing Process for the Dispersion of the Synthetic Fibers in Wet-lay Forming. 61st Appita Annu Conf Exhib Gold Coast, Aust 6-9 May 2007 Proc 2007;3:381.

[21] Li CD, Chen ZF. Effect of beating revolution on dispersion of flame attenuated glass wool suspension and tensile strength of associated glass fiber wet-laid mat. Powder Technol 2015;279:221–7. doi:10.1016/j.powtec.2015.04.017.

[22] Wood AT, Everett D, Budhwani KI, Dickinson B, Thomas V. Wet-laid soy fiber reinforced hydrogel scaffold: Fabrication, mechano-morphological and cell studies. Mater Sci Eng C 2016;63:308–16. doi:10.1016/j.msec.2016.02.078.

[23] Wang Q, Jones J, Lu N, Johnson R, Ning H, Pillay S. Development and characterization of high-performance kenaf fiber–HDPE composites. J Reinf Plast Compos 2018;37:191–200. doi:10.1177/0731684417739127.

[24] Yunkai Lu. Mechanical Properties of Random Discontinuous Fiber Composites Manufactured from Wetlay Process. Virginia Polytechnic Institue and State University, 2002.

[25] Chakrabarti, P.M. (1979a). “Method of increasing the strength of wet glass fiber mats made by the wet-laid process,” US Patent 4,178,203.

[26] Shiflller D.A. Defective Fibers in Wet-Lay Nonwoven Fabrics. Tappi Journal, 70 (6). 1998:117-21.

[27] Fathi-Khalfbadam S, Latifi M, Sheikhzadeh-Najar S, Towhidkhah F. Analysis and simulation of fiber dispersion in water using a theoretical analogous model. J Dispers

Sci Technol 2011;32:352–8. doi:10.1080/01932691003659833.

[28] Das D., Butola B.S., and Renuka S. An investigation into fiber dispersion behavior in water with reference to wet-lay nonwoven technology. J Dispers Sci Technol. 2012; 33 (8): 1225-1232. DOI: 10.1080/01932691.2011.590437

CHAPTER I

INNOVATIVE METHOD FOR ENHANCING CARBON FIBERS DISPERSION IN WET LAID NONWOVENS

This chapter is revised based on a paper published by Hicham Ghossein et al.:

Ghossein Hicham, Hassen Ahmed Arabi, Paquit Vincent, Love Lonie J, Vaidya Uday K. Innovative Method for Enhancing Carbon Fibers Dispersion in Wet-Laid Nonwovens. Mater Today Commun 2018;17:100–8. doi:10.1016/j.mtcomm.2018.08.001.

My primary contiributions to this paper include (i) identifying the challenge in CF dispersion, (ii) proposing and designing the innovative mixer based on researched theories, (iii) design and conducting of experiment for validating the performance of the proposed innovative mixer, (iii) assisting and supporting computetional programs and analysis, (iv) data processing,analysis and interpretation, (v) pulling various contributions into the paper, and (vi) majority of the writing.

ABSTRACT

The production of wet laid (WL) reinforcing fiber mats is adopted from the paper making industry to produce carbon fiber (CF) mats. The resulting mats are prone to defects induced by the mixing regime. This study explores a new mixer design that achieved fully dispersed mats with 20 minutes processing time using 25.4mm long CF. The proposed mixing method is compared against the traditional method and the density distribution of fibers is characterized using Back Light Scattering (BLS) technique. The mats showed high consistency with less than 8% standard deviation from the data collected from different regions within the mats. The innovative mixer resulted in mats with fiber distribution 70% closer to the theoretical distribution than that of the traditional

mixer. This innovative method of preparing nonwoven CF mats will create new opportunities for CF nonwoven composite applications

INTRODUCTION

The interest in composite materials is growing in the aerospace, automotive, and military fields as well as industrial applications [1–3]. High strength-to-weight and stiffness-to-weight ratio, lightweight, low fatigue susceptibility and superior damping capacity give fiber reinforced composites an advantage over conventional materials [4–6]. Continuous fiber reinforced composites are generally anisotropic in terms of mechanical properties, costly to produce and difficult to produce complex shaped parts. Contrastingly, discontinuous fiber composites can be designed to provide isotropic properties [7], and are easier to process at a low cost for parts with increased complexity [8,9]. The traditional processing methods for discontinuous fibers such as extrusion compression molding (ECM) and long fiber injection compression molding (ICM) cause fiber attrition, affecting the fiber aspect ratio thereby adversely affecting composite strength properties. With fiber above critical fiber length (lc), the full reinforcing potential of the reinforcement is realized due to higher fiber aspect ratio. The high aspect ratio increases the composite stiffness and strength, and enhances creep and fatigue endurance [10,11,12–14]. As fiber length increases, elastic modulus, tensile strength, and impact resistance of fiber composites increase [15].

The wet laid (WL) technique offers a way to produce nonwoven mats with fiber length retention and ability to tailor fiber orientation, although in general the WL mats have random fiber orientation [16]. WL has traditionally been used in papermaking and

textile industries [17]. This process involves uniform dispersion of fibers in water and to produce a mat via filtration by transporting it onto a fine mesh screen.

The WL process can be divided to three main steps as shown schematically in Figure 1. [18]: 1) Dispersion of fibers in water, 2) Continuous or discontinuous web formation on a screen belt by filtration, and 3) Solidification, drying and winding up of the nonwoven web. The process has recently been adopted to produce non-woven fiber reinforced polymer matrix composites mats, as well as carbon fiber (CF) mats for use in thermoset matrices application [19]. WL process has distinct advantages like high productivity, homogeneous preform material, control of fiber orientation, ability to use recycled fibers and fiber blends, functionalization by addition of fillers, possibility of in-line impregnation, and most important low cost of production [20].

CF is widely used as reinforcement in lightweight structural composite materials, due to its exceptional properties such as high specific modulus, strength, stiffness, electrical properties and low density. However, with the high cost of CF, alternative cost effective processing methods such as nonwoven CF reinforcement provide increased product opportunities.

The dispersion of CF in WL is not well optimized, leading to a poor mixing, with few studies that have been published exploring various methods to achieve full dispersion [21]. Poor mixing can result in unequal fiber density distribution that causes variance in performance in the final product and an increase in number of defects in the wet laid mats. The proper dispersion of fibers affects the final mechanical and functional characteristics of the produced mats and composites.

This study explores a new mixing regime that creates a chaotic advection current to insure full fiber dispersion instead of the rigid body motion created by the traditional shear mixer. The traditional mixer leads to the formation of vortices with diameter larger than the fiber length that leads to fibers defects. The processed mats are characterized using back light scattering (BLS) technique to investigate fiber density distribution and insure that full fiber dispersion is obtained. The proposed novel mixing design and development of wet laid nonwoven CF mats will provide a potential opportunity to expand applications with nonwoven CF mats.

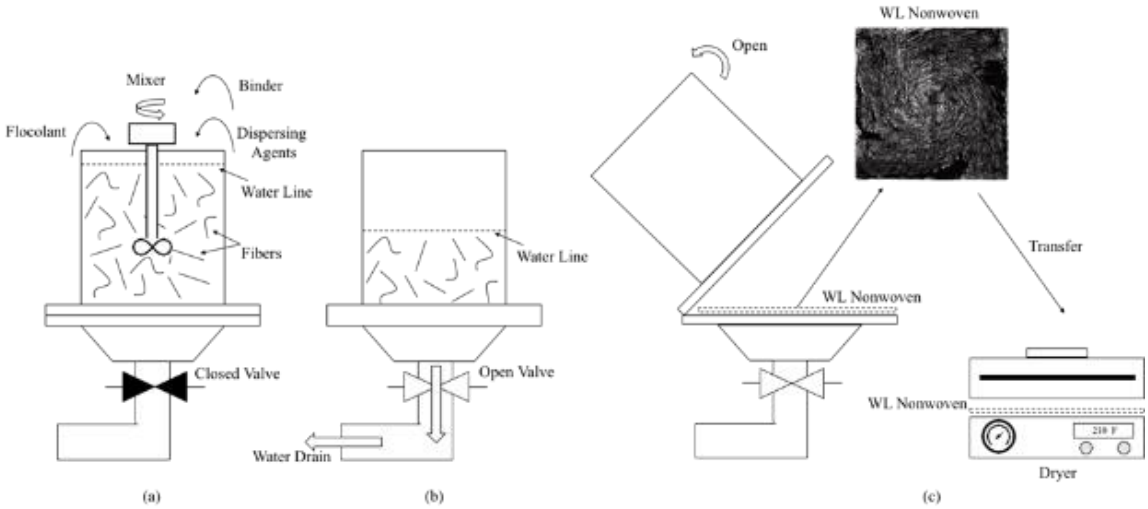

Figure 1: Schematic for the WL system; (a) Fiber dispersion in aqueous system through mechanical agitation, (b) Water drainage and fiber deposition on a screen, and

THEORETICAL BACKGROUND

Man-made fibers are less compatible with water than natural fibers as argued by Guan et al. [22]; hence, the need to add chemicals to enhance the dispersion, wettability and web formation. There are several chemicals used in the WL process. Carbon Fibers are widely used as reinforcement material in polymer composites. However, they have an inert surface and require further treatment as stated by Tiwari et al. [23]. There are several ways of improving surface wettability of fibers: - (a) surfactants are molecules that contain both hydrophilic and hydrophobic moieties, the hydrophobic moieties attach to the hydrophobic fiber and the hydrophilic moieties promote water penetration through the fiber bundle, (b) dispersing agents [24],[25] overcome the hydrophobicity of carbon by creating hydrogen bonds with water molecules, and (c) flocculent agent help the dispersion of fibers, thereby bridging fibers and forming a three dimensional web that collapses into a mat form. The fibers deposit on the screen in the form of a two-dimensional mat.

The surfactants assist in initial fiber bundle dispersion; however, mechanical agitation is still required. WL nonwoven fabrics made from synthetic fibers are prone to defects due to their dependency on mechanical agitation. There are two main types of defects that occur during the WL process of CF, such as [26]: a) log defects that can be defined as bundles of fibers that do not disperse, and b) ropes defects which are fiber assemblages that have unaligned ends that are formed by incomplete dispersion of logs or dispersed fibers that spin around each other in a vortex motion. Fiber logs are normally dispersed through the shear force exerted during the mixing process. In order to disperse

log defects, shear force must overcome the forces of friction, tension between the fibers, and the drag force applied by the water current as given by Equation 1[27]:

$F_s > F_{st}+F_d$ Eq. (1)

where F_s is the shear force in Newton exerted on the fiber bundles by agitation of the liquid, F_{st} is the combination of surface tension and friction force between the filaments obtained by $F_{st} = \gamma L$, where γ is the constant of proportionality (coefficient of liquid-surface tension), and L is the fiber length. F_d is the drag force that resists fiber dispersion given by Equation 2.

$$F_d = \frac{18\,\eta}{\rho_f d^2}\frac{C_D\,R_e}{24}\left(v_l - v_f\right) \quad \text{Eq. (2)}$$

where d and ρ_f are fiber diameter and density respectively, η is liquid dynamic viscosity, C_D is the drag coefficient, R_e is Reynolds number, v_l is liquid linear velocity, and v_f is fiber linear velocity.

The flow of a fiber filled viscous media is controlled mainly through the interactions of fibers at fiber-fiber touch points. A mathematical description of this phenomenon is provided by Dweib [28], assumed that all such interactions can be formulated as a combination of Coulomb friction between the fibers and hydrodynamic lubrication due to the thin film of liquid between the fibers as given by Equation 3.

$$\mathrm{F_s} = \eta\,\frac{\mathrm{dU}}{\mathrm{dx}} \quad \text{Eq. (3)}$$

where $\frac{dU}{dx}$ is defined as the rate of change in velocity across the flow field of the fluid. The agitation flow is characterized by Reynolds number R_e that varies between turbulent for $\mathrm{R_e} > 4000$ and laminar for $\mathrm{R_e} < 2000$, see Equation 4.

$$R_e = \omega D^2 \rho / \eta \qquad \text{Eq. (4)}$$

where ρ is defined as the fluid density, ω is the mixer rpm, and D is the vortex diameter.

The conventional method of WL production is divided into two stages. First, shear mixer is set to a velocity of 1500 RPM causing a single vortex in the same size as the mixing tank. Substituting the angular velocity in equation (4) yields a $R_e > 4000$ causing a turbulent agitation that aims to disperse the logs. At the second stage the mixer velocity is dropped to 300 RPM to obtain a $R_e < 2000$ to produce a laminar agitation, based on equation (4), in order to reduce rope formation. Shiffler [29] has indicated that turbulent flow has a powerful effect on rope formation, where the chance of their formation is greater to occur than in a laminar flow. This study concludes that the reduction of the vortex formation can be a key factor in reduction of rope formation. However, the suppression of the vortex flow did not eliminate the rope defect formation as shown in the experimental section of this paper. In single vortex system, due to constant angular velocity, the fluid reaches a steady state in rotation known as the rigid body motion [30] that causes the fibers to adjust their velocity to that of the fluid, reducing in turn the velocity gradient to a near zero value. Such reduction eliminates the effect of shear force and results in an increase in defects.

Several attempts to improve dispersion in the WL system were performed by researchers. Jayachandran [17] proposed a system with baffles in an attempt to induce chaotic advection and control vortices formation. His study is supported by a computer simulation that details the process and highlights stagnation points behind the baffles. Tafershi [31] studied the important role of baffles in vortex control and their influence on

rope formation by placing the baffles at different locations within the tank; however, in each case, the baffles were static. Sun [32] used the mixing particle semi-implicit (MPS) method to investigate the fundamental characteristics of stir mixing of viscous liquid with two rods rotating at different input speeds. He concluded that the mixing rate is affected by the stick velocity, position, number, direction of rotation, and the liquid viscosity. Still, all of these approaches were dependent on vortices generated by propellers with diameters at double the length of the fibers at least.

The formation of the vortex is the subject of some literature summarized here, and its relevance to the WL process in our work. Ahmed [33], reported that the velocity of the fiber fluctuates around the mean velocity of flow. Therefore, with higher velocity fluctuation the orientation distribution of the fibers becomes wider. This phenomenon is known as chaotic advection. Aref [34] performed a study on stirring by chaotic advection, the blinking vortex flow, and proved that it leads to better mixing. This finding was supported by several researchers that studied the enhancement of mixing by chaotic motion [35], [36],[37]. Jana [38] discussed that the velocity field that can be used as proof of obtaining chaotic advection for better mixing of a complex stokes flow is only available from numerical computations. That was proven by exploring the vortex mixing flow and expanding the investigations in driven cavity flow to multicellular cavity flows. Both studies proved the achievement of chaotic advection in order to improve the mixing in the system.

With a carbon fiber length of 25.4 mm a new system was needed that provides full dispersion through chaotic advection without causing defects in the produced mats.

This study proposes a new mixer, designed for this study with the hypothesis that it will generate chaotic advection and result in fully dispersed mats. This hypothesis is validated numerically with a computer simulation and experimentally with mat analysis through the BLS technique. For the rest of the paper the conventional shear mixing method will be referred to as Method 1, and the new mixer proposed will be referred to as Method 2.

NEW MIXER DESIGN (METHOD 2)

In the Method 2, two stirring paddles travel through a pattern resembling the "Number 8" as shown in Figure 2. The mixer was powered by a variable speed 12 V DC motor. The arm has an offset above the gears assembly in order to provide 360° clearance for the connecting arms. The connecting arms are hinged together at their ends and a mixing paddle is connected in line with the hinge axis; see Figure 2. The components of the mixer were Additively Manufactured (AM) on a Fortus 900mc using Ultem 9085. Acrylonitrile Butadiene Styrene **(**ABS) was used to fabricate the mixing paddles.

The mixing paddles motion will simulate a horseshoe map phenomenon in order to attain improved stirring and mixing by chaotic advection. The chaotic advection induced by the path crossing currents generated by the motion creates several vortices that vary in diameter but last for a short period of time due to vortex-to vortex-collision. These vortices collisions shorten the existence time of the vortices and cause them to dissipate, as discussed by Green [39]. Continuous vortex dissipation due to collisions prevents rigid body motion formation leading to a decrease in rope defect formation and increase in bundle-to-bundle collisions.

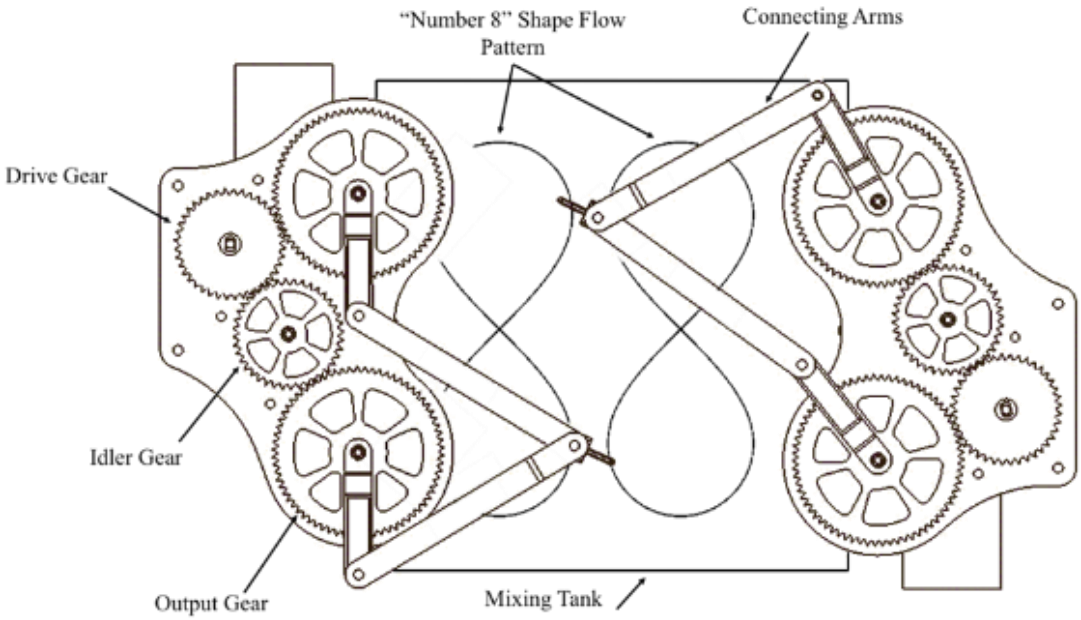

Figure 2: Schematic for innovative mixer design

MATERIALS AND METHODS

The carbon fiber used in this study was un-sized chopped Zoltek™ PX35 Type 02 CF with a length of 25.4 mm, and average diameter of 7 µm

Sample preparations and experimental setup

Two different sets of samples (CF Mats) were processed. The first set, Method 1, was processed using a conventional shear mixer; the second was prepared with the proposed innovative mixer design, Method 2, as discussed in the theoretical background section. Method 1 uses a shear mixer at two stages. First, the mixer is set to a speed of 1500 rpm, then at 300 rpm. These velocities provide a $R_e > 4000$ at 1500 RPM and $R_e < 2000$ for 300 RPM in an attempt to prevent rope defects formation. In Method 2, the design allows the mixing sticks to vary their traveling velocities providing a variable

shear leading to a chaotic advection current that causes multiple vortices collision. The chaotic advection causes a variable velocity gradient that leads to improved mixing. In order to study the effect of the mixing time on the fiber dispersion, mats were prepared using total mixing times of 10 min, 20 min and 30 min for each mixing method. In Method 1 the time is split equally between both stages of mixing. Each process is repeated three times in order to study the repeatability of the mixing method.

1.5 g of dispersant (Alkyl amine surfactant Nalco 8493™), 1.5 g of viscosity chemicals agents (anionic flocculent Nalclear 7768™), and 0.7 g of binder (polyvinyl alcohol (PVOH)) are added to the water. Chopped CF is added at fiber total volume of 1 % of the water volume to not exceed C_w. After the desired time of mixing, water is drained by gravity force and the dispersed fibers form a mat (355.6 mm x 355.6 mm (14" x 14")) on the mesh in the bottom of the tank. A vacuum machine is used to remove excess water then mats are placed in Emerson Speed Dryer (Model 145) at 210 F for 30 minutes to dry.

Wahjudi [40] stated that a high-quality WL mat is measured by its structural uniformity as it affects surface quality, strength, and aesthetic appearance of the mat. Several methods were proposed by researchers to analyze the dispersion of fibers in the WL process like X-ray techniques, microscopy and mechanical testing [41], [42],[43]. CF has an average diameter of 7 μm and low atomic number that makes the use of X-ray technique very challenging to investigate and evaluate the fabricated mats [44]. Moreover, microscopy technique is known to be laborious with an extensive sample preparation [45]; hence, the use of the BLS method in this work. The BLS technique,

shown schematically in Figure 3, was used in this work in order to characterize the mat pores distribution. LED light with a monochromatic nature that provides a high luminosity was used. Each mat is placed on a glass table with the monochromatic light source underneath allowing the light to scatter through the pores of the mat. A Nikon camera (Model 5500) was used to capture images of the mats. All pictures are analyzed using a developed Matlab software (R2017b) code.

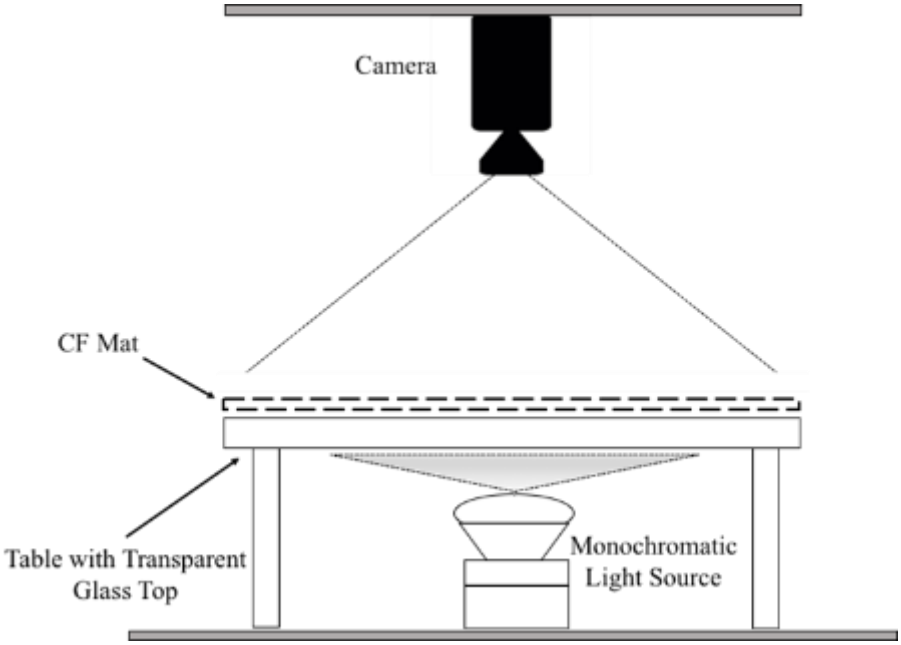

Figure 3: Schematic for BLS technique

RESULTS AND DISCUSSION

CFD for new mixer design

A Computational Fluid Dynamic (CFD) simulation was conducted using OpenFOAM software version 5.0 using PimpleDyMFoam numerical solver, which uses

the hybrid PISO-SIMPLE (PIMPLE) algorithm and dynamic meshing [46] to verify the production of chaotic advection by the proposed mixer. The simulation uses 50,240 cells in a finite volume solver, applying Direct Navier Stokes (DNS) for true simulation with continuous fluid and no slip conditions on hard surfaces. Figure 4 shows the top view for the evolution of the velocity profile across the tank, the vector orientation presents various orientations demonstrating chaotic advection pattern that is has been demonstrated to provide improved mixing as discussed in the theoretical background section. The tank is divided into four (4) equal quadrants, and the velocity components are measured at the centers of each quadrant over time, as indicated by the black markers in Figure 4b. The velocity component shows an irregular pattern associated with chaotic mixing. Furthermore, the number of vortices present in the flow increases with each cycle of the mixer, which is also indicative of chaotic motion. With every change of the paddles direction, a new vortex is generated, leading to an ever more complex velocity profile. These numerical results support the previously mentioned hypothesis that this mixer setup is efficient at generating chaotic advection.

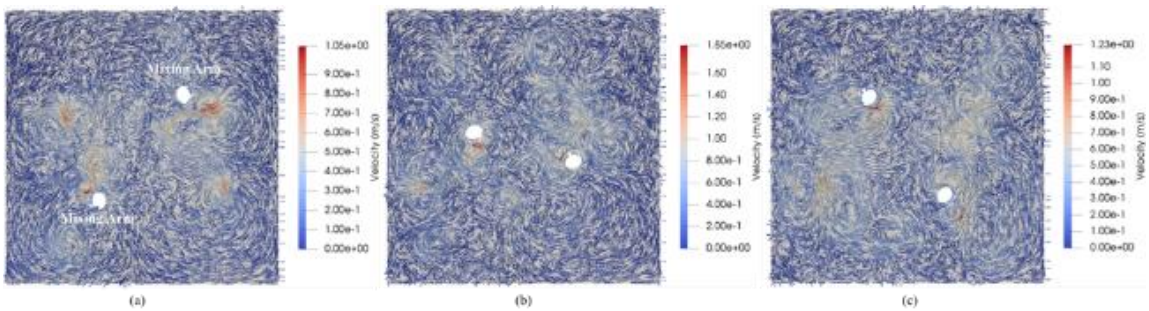

Figure 4: CFD for mixing method 2 showing velocity vector field at; (a) Time= 1.5s, (b) Time= 3s, and (c) Time= 4.5s

Experimental results

Figure 5 shows the mats produced using Method 1 and Method 2 for mixing times of 10 min, 20 min and 30 min as characterized by the BLS technique. Qualitative analysis of the images shown in Figure 5 shows the contrast difference of fibers distribution quality between the two methods, especially at 30 min mixing time. It can be noticed in Figure 5c that Method 1 at 30 min mixing time presents defects, gaps and in general poor distribution. However, Figure 5f shows that Method 2 mat at 30 min mixing time presents no defects with a good fibers distribution. As for time variable within the same method, in Method 1 it was observed that longer mixing time resulted in a reduction in the poor distribution (Observed in the corner of Figure 5a). However, rope defects were dominant at 30 min mixing time as seen in Figure 5c. The spiral pattern seen in Figure 5c falls in accordance with the theoretical background explanation of the rigid body motion and that of rope formation during such motion in large diameter vortices. Method 2 shows consistent qualitative value throughout the different mixing times, as shown in Figures 5d-f.

In order to obtain quantitative measures, images were converted to color maps based on light intensity using code written in MATLAB R2017b, the resulting color maps are shown in Figure 6. The process starts by defining the mats corners and translating them into a bounding box, so a coordinate system can be drawn for measurements collection. The images were covered by a grid system with each grid cell having the dimensions of 64 x 64 pixels and associate a value to each pixel based on light intensity threshold on a scale of 0 to 256 on the RGB scale. The resulting images are measured in

percentage of intensity threshold for every pixel with 0 representing total darkness (i.e. lack of fiber dispersion "pores") and 1 representing maximum RGB value of 256. This quantification allows the numerical measurement of the mats pores distribution (i.e. a value of 1 represents no presence of fibers and that of zero represents no presence of pores in the mat) presented in a color map format. Mean distribution of the percentage of intensity threshold for pixels in each cell was calculated, as presented in Table 1. Five regions of interest were selected, as shown in Figure 6b. Each region measured 3.5 x 3.5 inches. All measured percentage of intensity threshold pixel values were compared to the calculated theoretical value. The theoretical value was calculated by considering a perfectly isotropic mat. In such mat, fiber distribution is equal across all unit areas with equal coverage percentage of fibers. Simmonds et al. [47] showed that the probability P (n) that any given point is covered by n fibers present per unit area is given by Poisson distribution of the form, see Equation 6.

$$P(n) = \frac{e^{-k}k^{n}}{n!} \qquad \text{Eq. (6)}$$

where, k is the total coverage area of fibers per unit area of the plane. Considering that $k = nLd$, L is the fiber length and d fiber diameter. In order to calculate the theoretical value of mat's pore coverage per unit area, one must consider the value of P (0) where no fibers are present, as given by Equation 7.

$$P(0) = e^{-k} \qquad \text{Eq. (7)}$$

the constant k was evaluated at 1.97 for a nonwoven with a basis weight of 215 gsm leading to a value of P (0) = 0.14.

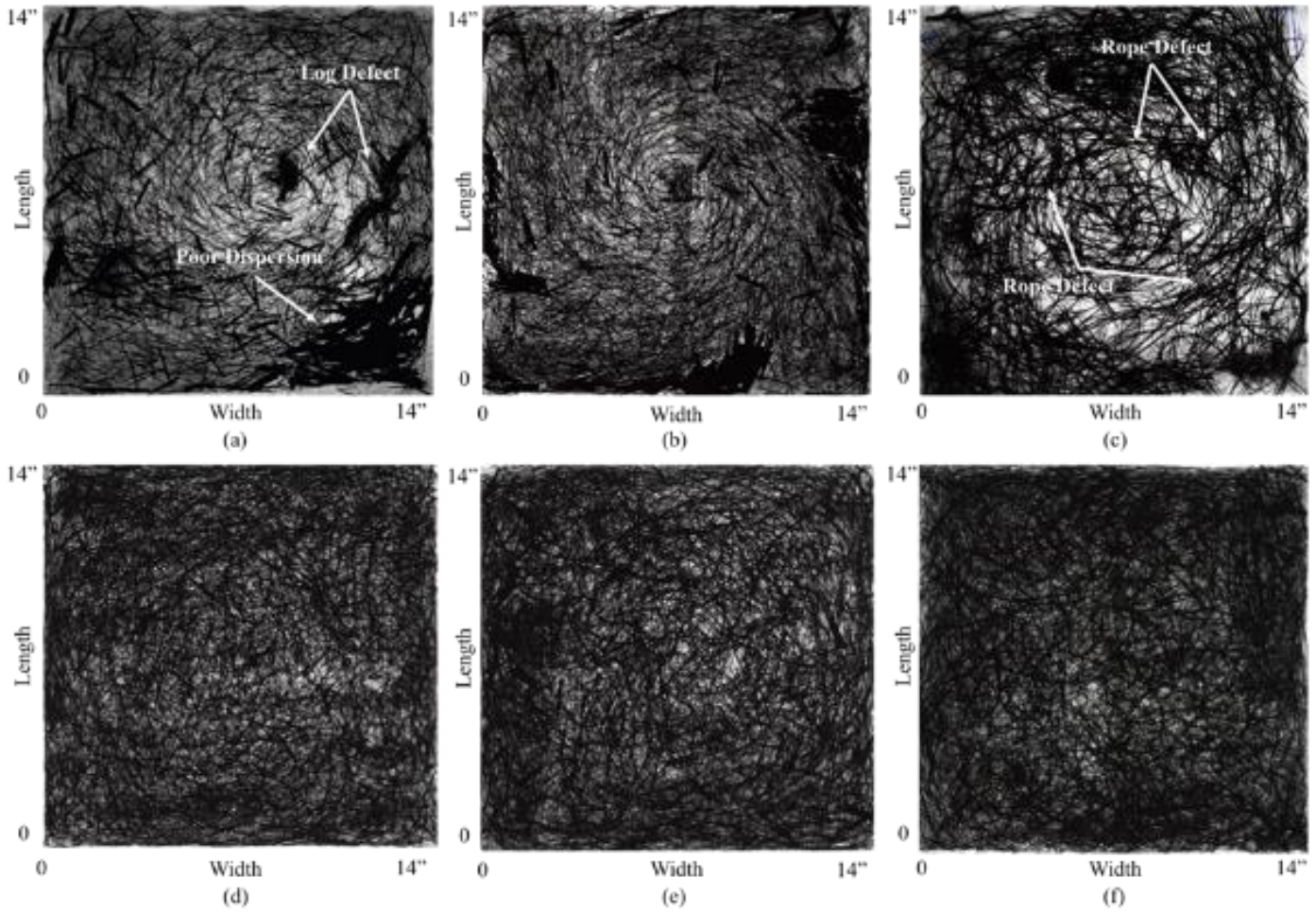

Figure 5: BLS images of mats prepared using; (a) Method 1 at 10 min, (b) Method 1 at 20 min, (c) Method 1 at 30 min, (d) Method 2 at 10 min, (e) Method 2 at 20 min, and (f) Method 2 at 30 min

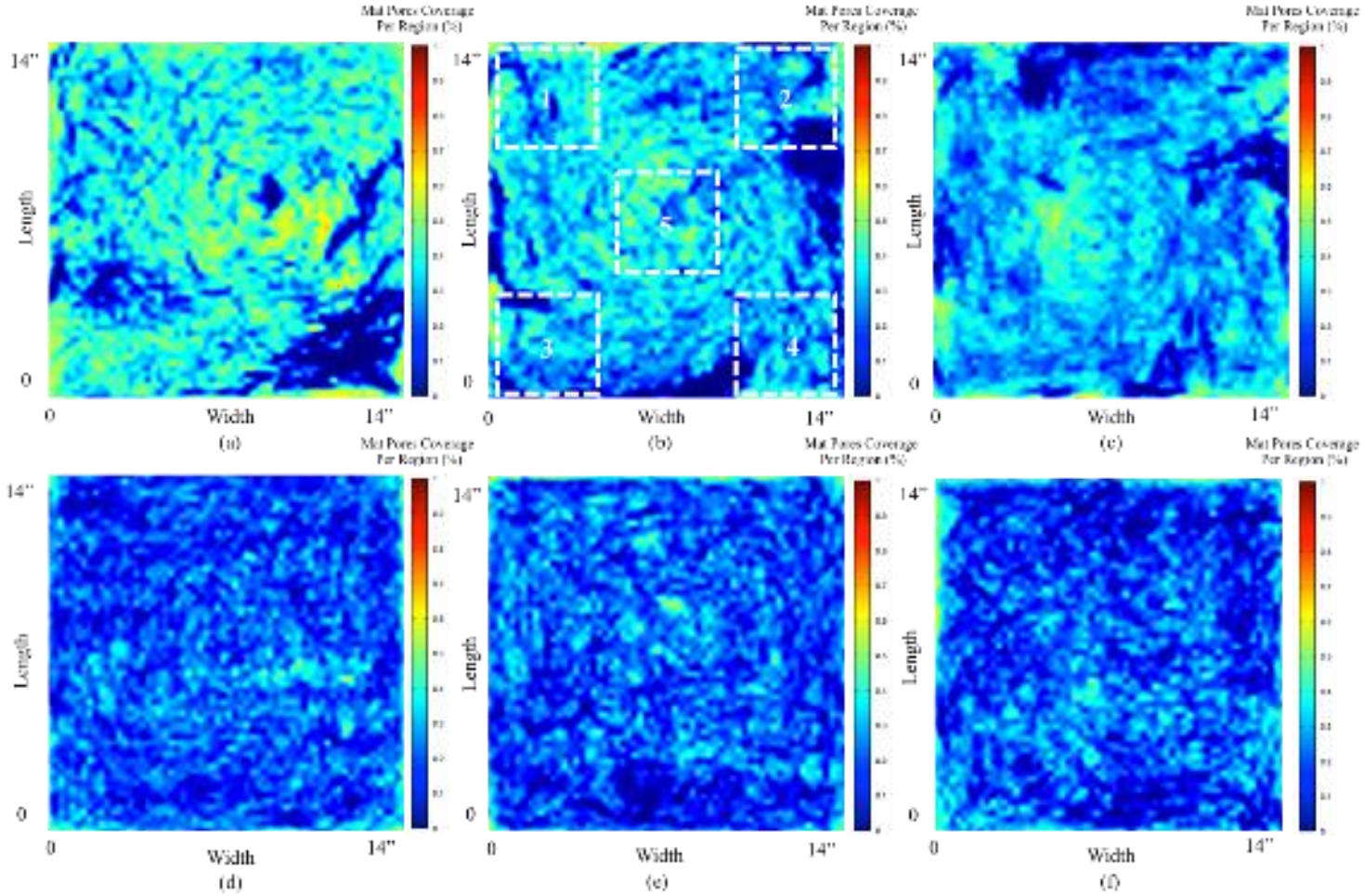

Figure 6: Color map showing mat pores coverage percentage using (a) Method 1 at 10 min, (b) Method 1 at 20 min, (c) Method 1 at 30 min, (d) Method 2 at 10 min, (e) Method 2 at 20 min, and (f) Method 2 at 30 min

Table 1: Mean distribution of mat pores coverage percentage in each region of interest

Average Porosity Distribution			Region 1		Region 2		Region 3		Region 4		Region 5	
			Mean Avg (%)	Stdv (%)	Mean Avg (%)	Stdv (%)	Mean Avg (%)	Stdv (%)	Mean Avg (%)	Stdv (%)	Mean Avg (%)	Stdv (%)
Method 1	10 min	Mat 1	34.5	10.7	39.1	8.0	35	12.3	14.3	15.9	40.6	12.5
		Mat 2	23.5	20.8	37.7	9.9	35.1	15.0	35.6	12.0	47.3	8.6
		Mat 3	39.7	10.2	37.0	14.2	41.4	13.2	37.1	14.4	42.0	13.1
	20 min	Mat 1	15.9	14.8	21.9	19.0	25.2	17.6	19.8	16.9	32.0	15.5
		Mat 2	33.7	10.0	25.6	13.5	27.9	11.5	26.7	10.9	35.9	9.9
		Mat 3	26.3	12.8	28.2	12.2	31.0	8.7	27.8	10.8	36.1	8.0
	30 min	Mat 1	32.1	15.1	27.4	14.3	23.5	14.5	28.7	14.8	32.4	14.0
		Mat 2	20.1	13.5	30.4	13.6	30.0	13.6	23.6	12.3	37	14.0
		Mat 3	25.6	13.8	33.7	14.2	25.1	14.1	18.6	14.4	33.2	15.2
Method 2	10 min	Mat 1	16.5	7.8	18.3	7.9	20.0	7.4	20.2	8.7	23.0	8.0
		Mat 2	23.1	8.5	21.9	8.7	16.9	8.9	20.8	7.4	23.9	8.1
		Mat 3	20.3	8.6	21.0	9.6	23.0	8.0	28.1	10.3	27.6	8.9
	20 min	Mat 1	22.7	7.0	21.4	7.2	20.2	7.4	20.6	6.7	22.5	6.8
		Mat 2	20.8	8.4	19.7	8.7	17.8	8.7	19.6	6.0	24.3	9.3
		Mat 3	19.6	7.6	22	6.3	22.8	7.6	23.5	5.6	22.9	7.4
	30 min	Mat 1	20.4	8.3	14.3	9.1	16.0	8.0	14.3	7.8	22.8	8.1
		Mat 2	17.7	9.2	16.6	9.2	22.2	9.7	20.7	9.9	22.8	9.2
		Mat 3	23.0	8.0	27.5	4.8	25.8	6.5	25.0	6.6	24.3	5.2

Figure 7 shows radar plots for mean distribution of the percentage of intensity threshold of pixels representing mat pores coverage percentage in each region of interest. In Figure 7a, it is noticed that mixing Method 1 at 10 min shows a low mat pores coverage percentage of 14.3 % in region 4. This is due to the fact that fibers clustered in that region due to lack of distribution. While in region 5, the mat pores coverage percentage goes up to 40.7 %. Standard deviation graph of the pixels in the region shows a value of 15.9 % for region 4 and that of 12.5 % for region 5. Standard deviation of the variation of values on the selected portion of the grid above 10% is an indication of the poor fiber distribution. Method 2 at 10 min shows higher consistency with values of 20.8 % at region 4 and that of 23.9 % at Region 5 with standard deviations of 8.7 % and 8 % respectively, providing more trust in the consistency of fiber distribution across the mat. The effect of increasing the time of mixing did not show improvement on the dispersion for Method 1, but alternatively created more rope defects. As an example, the maximum variation is observed in Region 4, as it was 14.3 %, 26.7 %, 18.6 % differences for 10 min, 20 min, and 30 min respectively. However, in Method 2 these values are observed to be 20.8 %, 20.6 %, 20.7 % differences for 10 min, 20 min, and 30 min respectively, an indication that once dispersion is achieved in Method 2 the additional time of mixing had minimal effects on the mat quality.

In order to study the reproducibility of each mixing method, three mats were produced for each mixing time. Figure 8 shows the reproducibility of the produced mats by both mixing methods for a fix mixing time of 20 min. Method 2 shows higher consistency in each region with higher confined standard deviation that did not surpass

the 10% value and less than 2% difference in the average mat pores coverage percentage in the same region between different mats. That was true across each of the 5 regions of interest. As for Method 1 the discrepancy in average values of mat pores coverage percentage between the same regions of different mats was more than 20% difference, showing a lack of reproducibility in the mats formed using this method. Figure 8f shows the averaged value for all the regions of interest, presenting the entire mat. Method 1 showed a large standard deviation values up to 15%, 19%, 18%, 17% and 15% for each of Regions 1 to 5 respectively. Despite the consistency of averaged value between all the mats, that is still remarkably high in comparison to the theoretical value. However, Method 2 shows a standard deviation below 2 % across all regions in each mat, with a higher consistency in the total mat averaging and closer result to the theoretical value. This provides an indication that Method 2 is equally dispersing the fibers across the entire regions of the mat with high repeatability. It was noticed that all the obtained values are higher than that of theoretical (i.e. an average of 14% and 6 % increase for Method 1 and Method 2 respectively). This can be attributed to the effect of fiber settling with the draining current based on their dimensional size and physical density. Such investigation is being conducted in a separate study.

CONCLUSIONS

Mat pores coverage percentage distribution in the WL mats was analyzed experimentally using the BLS technique reflecting on its turn on the quality of fiber dispersion. The data collected proved a match between experimental finding and theoretical prediction of attaining proper dispersion through chaotic advection currents,

with a significant reproducibility of results for the proposed mixer. Successfully dispersed mats with minimal defects were obtained within 20 min of mixing time of 25.4 mm long CF. The traditional method required a time of 50 min or more with no reproducibility of results. The proposed mixer results align with the theoretical work of Jayachandran [17], Ramasubramanian [26] and Fathi-Khafbadam [27]. The promotion of chaotic advection due to the crossing path of the paddles of the proposed mixer helped distribute the fibers through the volume of the tank due to an improved mixing, the variable velocity gradient and reduced drag due to opposing fluid currents helped achieve full dispersion in shorter and more significant time of processing. The innovative mixing method validated in this work will expand opportunities for nonwoven composite applications.

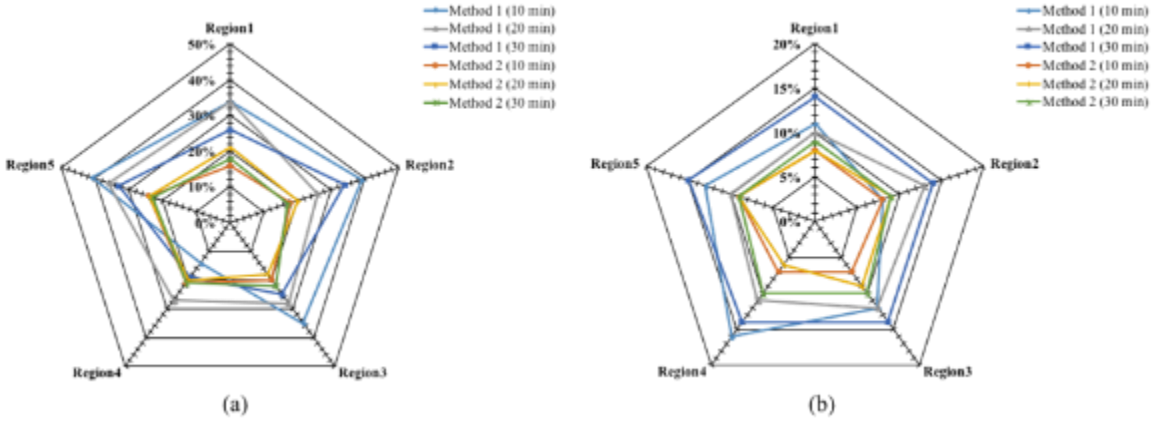

Figure 7: Effect of mixing time on the mat pores coverage percentage for Method 1 and Method 2; (a) Mat pores coverage percentage per region, and (b) Standard deviation of pixel reading per region

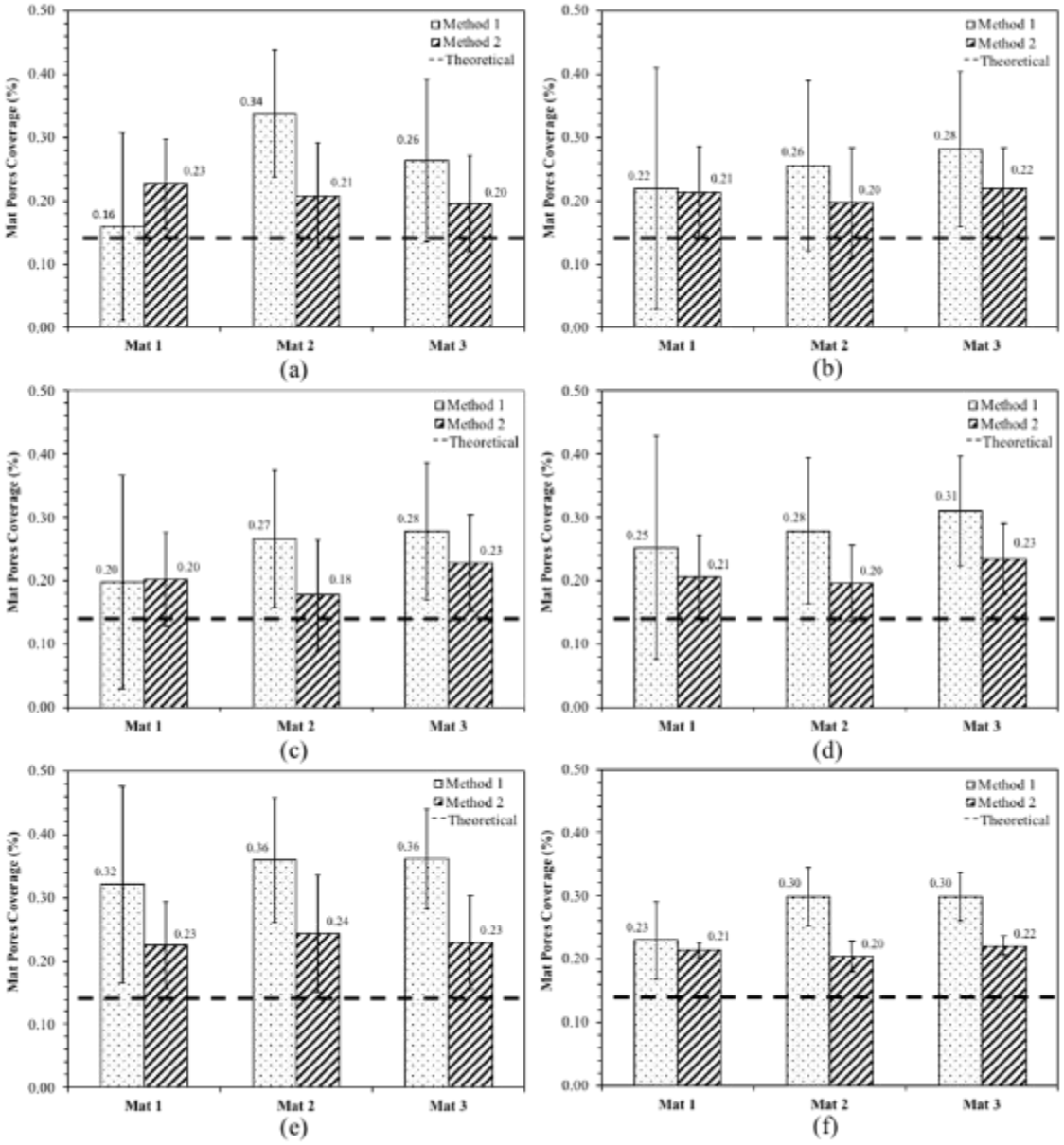

Figure 8: Mat pores coverage percentage for mats fabricated using Method 1 and Method 2 for 20 min; (a) Region 1, (b) Region 2, (c) Region 3, (d) Region 4, (e) Region 5, and (f) Average of all 5 regions representing the entire mat.

REFERENCES

[1] Boria S, Scattina A, Belingardi G. Experimental evaluation of a fully recyclable thermoplastic composite. Composite Structures. 2016;140:21-35.

[2] J.G Carrillo RAG, E.A. Flores-Johnson, P.I. Gonzalez-Chi. Ballistic performance of thermoplastic composite laminates made from aramid woven fabric and polypropylene matrix. Polymer testing 31. 2012:512-9.

[3] Haibin Ning SP, Uday k. Vaidya. Design and development of thermoplastic composite roof door for mass transit bus. Materials & Design 30. 2009:983-91.

[4] Boria S, Scattina A, Belingardi G. Impact behavior of a fully thermoplastic composite. Composite Structures. 2017;167:63-75.

[5] Chung DDL. Review: Materials for vibration damping. Journal of Materials Science 36. 2001:5733-7.

[6] Akonda MH LC, Weager BM. Recycled carbon fiber-reinforced polypropylene thermoplastic composites. Composite Part A: Applied Science and Manufacturing 43(1). 2012:79-86.

[7] Thompson JL VM, Schipper G and Krikort HGLT. Influence of fiber length and concentration on the properties of glass fiber-reinforced polypropylene: Part 3. Strength and strain failure. Composites Part A, 27A. 1996:1075-84.

[8] Thompson JL. VM. Influence of fiber length abd concentration on the properties of glass fiber-reinforced polypropylene: Part 1. Tensile and flexural modulus. Composites Part A, 27A. 1996:477-84.

[9] S.P. S. United States2000.

[10] Amaro AM, Reis PNB, Santos JB, Santos MJ, Neto MA. Effect of the electric current on the impact fatigue strength of CFRP composites. Composite Structures. 2017;182:191-8.

[11] Yang S-W CW-K. Mechanical properties of aligned long glass fiber reinforced polypropylene. I: Tensile Strength. Polymer Composites 20 (2). 1999:200-6.

[12] P.K. M. Fiber reinforced Composites: Materials, Manufacturing, and design. New York: Taylor and Francis Group; 2008.

[13] Yang S-WaC, W.-K. Mechanical Properties of Aligned Long Glass FiberReinforced Polypropylene. I: Tensile Strength. Polymer Composites. 1999;20(2):200-6.

[14] Mallick PK. Fiber reinforced composites. New York, USA: Taylor and Francis Group; 2008.

[15] Nguyen B.N. HDJ, Johnson K.I., Smith M.T. Long-Fiber Thermoplastic Injection Molded Composites: From process modeling to property prediction. SPE Automotive Composites Conference and Exposition. Troy: SPE; 2005. p. 9.

[16] Folgar F. TCLI. Orientation behaviour of fibers in concentrated suspensions. Journal of Reinforced Plastics 3. 1984:98-119.

[17] A. J. Fundamentals of Fiber Dispersion in Water; Master Thesis. Raleigh: North Carolina State University; 2000.

[18] Harbers T. EC. Highly Efficient Production and Characterization of CFRP Made from Recycled Carbon Fibers. Sampe Journal. 2014:7-13.

[19] Feraboli P. ea. Recyclability and retilization of Carbon Fiber fabric/epoxy composites. Journal of Composite Materials 0 (0). 2011:1-15.

[20] Caba AC, Loos AC, Batra RC. Fiber-fiber interactions in carbon mat thermoplastics. Compos Part A Appl Sci Manuf 2007;38:469–83. doi:10.1016/j.compositesa.2006.02.024

[21] D.A. S. Characterizing the Dispersion Kinetics of synthetic Fibers in Water. Tappi Journal, 68 (8). 1985:91-9.

[22] Guan X. QX, Yang Z. Comparison of several image analysis methods for fiber dispersion uniformity in water. Journal of Dispersion Science and Technology, 38(1). 2017:19-25.

[23] Tiwari S. BJ. Surface Treatment of Carbon Fibers - A review. Procedia Technology. 2014:505-12.

[24] R. N. United States1981.

[25] Razac S. EPU. United States1995.

[26] Ramasubramanian M.K. SDA, Jayachandran A. A Computational Fluid Dynamics Modeling and Experimental Study of the mizing process for the dispersion of the Synthetic fibers in Wet-Lay forming. Journal of Engineered Fibers and Fabrics 3(1). 2008:11-20.

[27] Fathi-Khalfbadam S. LM, Sheikhzadeh-Najar S., Towhidkhah F. Analaysis and Simulation of Fiber Dispersion in Water Using a Theoretical Analogous Model. Journal of Dispersion Science and Technology, 32(3). 2011:352-8.

[28] Dweib M.A. O-BCM. Extensional and Shearing Flow if a Glass-Mat-Reinforced Thermoplastics (GMT) Materials as a Non-Newtonian Viscous Fluid. Composites Science and Technology, 59. 1999:1399-410.

[29] Shifller D.A. Defective Fibers in Wet-Lay Nonwoven Fabrics. Tappi Journal, 70 (6). 1998:117-21.

[30] N. N. Introduction to Fluid Mechanics. Oxford: Butterworth-Heinemann; 2000.

[31] Tafreshi H.V. PB. Role of Baffles on Flow Fields Inside Wet-Lay Mixing Tanks and Their Potential Influence on Fiber Dispersion. Textile Research Journal, 73(7). 2003:575-82.

[32] Sun Z. XG, Chen X. A numerical study of stir mixing of liquids with particle method. Chemical Engineering Science 64. 2009:341-50.

[33] Ahmed S.F. ASMS. Fiber Suspensions in Turbulent flow with Two-Point Correlation. Bangladesh J Sci Res 46(2). 2011:265-70.

[34] H. A. Stirring by Chaotic advection. Journal of Fluid Mechanics, 143. 1984:1-21.

[35] Khakhar D.V. OJM. Fluid mixing (Stretching) by time periodic sequences for weak flows. Physics of Fluids. 1986:3503-5.

[36] S.W. J. The enhancment of mixing by chaotic advection. Physics of Fluids A: Fluid Dynamics, 3(5). 1998:1081-6.

[37] Meleshko V.V. AH. A blinking rotlet model for chaotic advection. Physics of Fluids, 8. 1996:3215-7.

[38] Jana S.C. MG, Ottino J.M. Experimental and Computational studies of mixing in complex Stokes Flows: The vortex mixing flow and multicellular cavity flows. Journal of Fluid Mechanics, 269. 1994:199-246.

[39] B. G. Fluid Vortices. Dordrecht: Springer Netherlands; 1995.

[40] Wahjudi U. DGG, Kibblewhite R.P. An evaluation of three formation testers using radiata pine and spruce kraft pulps. Appita Jouranl, 51. 1998:423-7.

[41] Li C.D. CZF. Effect of beating revolution on dispersion of flame attenuated glass wool suspension and tensile strength of associated glass fiber wet-laid mat. Journal of Powder technology 279. 2015:221-7.

[42] Yeole P. HAA, Ning H., Vaidya U.K. The Effect of Flocculent and Dispersants on Wet-Laid Process for Recycled Glass Fiber/PA6 Composite. Journal of Polymers & Polymer Composite, 26(3). 2018:259-69.

[43] A.E. K. The Effect of Anisotropy In-Plane Liquid Distribution in Nonwoven Fabrics. Raleigh: North Carolina State University; 2001.

[44] Yang P. ER. Porosity Content Evaluation in Carbon-Fiber/Epoxy Composites Using X-ray Computed Tomography. Polymer-Plastics Technology and Engineering, 53. 2014:217-22.

[45] U. H. Scanning probe microscopy on superconductors: Achievments and challenges. Applied Physics A, 59. 1994:41-8.

[46] Weller H.G. TG, Jasak H., Fureby C. A tensorial approach to computational continuum mechanics using obkect-oriented techniques. Computers in physics, 12(6). 1998:620-31.

[47] Simmonds G.E. BJD, Bryner M.A. Designing Nonwovens to Meet Pore Size Specifications. Journal of Engineered Fibers and Fabric, 2(1). 2007:1-15.

CHAPTER II

MECHANICAL ANALYSIS OF COMPOSITES MADE FROM INNOVATIVE CARBON FIBER WET LAID MATS

ABSTRACT

In Ghossein et al [4], the advancement and innovation in production of optimized wet laid (WL) carbon fiber (CF) mats was demonstrated to enable the formation of fully isotropic composites through dry preforms. This chapter explores the mechanical behavior of composites produced from WL CF mats in conjunction with the microstructure predicted through Object Oriented Finite Element (OOF) method. The mats used for the composites were prepared in two dispersion regimes using 25.4 mm long CF. The mixing regimes are discussed in the author's previous work [4], and are identified as Method 1 and Method 2. Method 2 is an innovative method for fiber dispersion introduced by the author. Method 1 did not yield uniform mats. Method 2 mats were uniform and fibers were optimally dispersed. Composite panels from Method 2 mats showed a tensile strength increase of 20 MPa over those from Method 1 mats. Reproducibility analysis of composites made from Method 2 mats demonstrated a 2 % standard deviation in fiber weight content, 2% in tensile modulus and 9% in tensile strength with a 12 to 17% fit to theoretical prediction from the Halpin-Tsai equations. Systematic study of the microstructure and its analysis through OOF validated the theory around the isotropy of mats produced through method 2. Reproducibility analysis of composites made from Method 1 mats demonstrated a 5 % standard deviation in fiber weight content, 5% in tensile modulus and 17% in tensile strength. This study validated the Method 2 WL CF mats to be adopted for isotropic composites production with reproducibility.

INTRODUCTION

Recent environmental issues related to global climate change and greenhouse gas emissions have prompted automotive manufacturers to focus on the development of lightweight and fuel efficient vehicles [1]. Fiber reinforced composites possess the advantage of high strength-to-weight and stiffness-to-weight ratio, lightweight, low fatigue susceptibility and superior damping capacity [2],[3]. Assessments of economic viability of carbon fiber (CF) parts production through nonwoven CF are being evaluated.

The author's in their previous work [4] explored the production of nonwoven CF wet laid (WL) mats through two methods of fiber dispersion. Method 1 used a shear mixer to break the fiber bundles, but it resulted in an unequal fiber distribution in the mats with less consistent reproducibility. Method 2 used an innovative mixer based on chaotic advection theory which provided a fully balanced fiber distribution and consistent reproducibility of the mats. Researchers [5–9] have shown that porous nonwoven fabrics like the nonwoven WL CF mats possess high specific surface area, light weight and ease of processing into complex geometries. This study investigates the mechanical properties of composite plates produced from nonwoven CF WL mats made through Method 1 and Method 2. The experimental mechanical properties of both types of composites are provided. Further, a microstructure based finite element analysis (FEA) has been conducted on the mats made by the two methods and its effect on the mechanical properties of the final composite.

The effect of microstructure on mechanical properties of a composite is well explored. Straumit et al. [10] used X-ray computed tomography to quantify the internal

structure of textile composites using an automated voxel model. Wan et al. [11] investigated the tensile and compressive properties of chopped carbon fiber tapes with respect to the changes in microstructure based on tape length and molding pressure. The authors found that increasing structural integrality improved the composite mechanical properties. Wan et al. [12] in a second study, analyzed the microstructural differences in CF composites using X-ray micro-CT. This method provided information on the morphology of the composite which was used to predict its mechanical properties. Tseng et al. [13] conducted numerical prediction of fiber orientation to predict mechanical properties for short/long glass and carbon fiber reinforced composites. The model came within 25% variance in comparison to the experimental data. Feraboli et al. [14] compared performance of different microstructures of various materials like recycled CF fabric/epoxy composites, twill laminates and sheet molding compounds (SMC), similar mechanical properties were exhibited by the twill laminates and SMC under similar microstructural conditions. Caba et al. [15] characterized the fiber-fiber interactions in carbon mat thermoplastics (CMT) produced through the wet lay (WL) technique. Their study established a foundation for understanding the relation between the fiber volume fraction and the mechanical behavior of the composites. Evans et al. [16] proposed Directed Fiber Compounding (DFC) where they produced a material similar to SMC using an automated spray deposition process of CF. They reported tensile stiffness and strength values of 36 GPa and 320 MPa for isotropic materials at 50% fiber volume. Selezneva et al. [17] investigated the mechanical properties of randomly oriented strand thermoplastic composites in effort to quantify the effect of strand size on their

mechanical properties and found that properties are dependent on the strand length. Amaro et al. [18] stated that the elastic modulus, tensile strength, and impact resistance of fiber composites increase, as fiber length increases. Thomason [19] investigated the influence of fiber length and concentration on the properties of reinforced composites, and reported that with fiber above critical fiber length (l_c), the full reinforcing potential of the reinforcement is realized due to higher fiber aspect ratio. The nonwoven WL CF mats used in this study, are produced using a 25.4 cm long CF. In order to avoid the complexity and vast data produced with X-Ray tomography to analyze the microstructure, this study refers to simpler image analysis techniques with higher precision.

Langer et al. [20] introduced an image based finite element analysis software, a novel numerical approach called: Object Oriented Finite element (OOF). OOF is a desktop software application for studying the relationship between the microstructure of a material and its overall mechanical properties using finite element models based on real or simulated micrographs. Reid et al. [21] discussed the mathematical approach and operation method for OOF and OOF2. This novel numerical approach has been used by researchers to provide fundamental insight on expectations of mechanical properties of their material [22–26]. Goel et al. [27] performed a strategic comparison between several theoretical models prediction and OOF prediction for Young's Modulus of long fiber thermoplastic (LFT), and found the closest prediction to the experimental results was achieved through the OOF software.

MATERIALS AND METHODS

This study used un-sized chopped Zoltek™ PX35 Type 02 CF with a length of 25.4 mm, average diameter of 7 µm, specific gravity of 1.81 g/cm^3, tensile strength of 4137 MPa, and tensile modulus of 242 GPa. The matrix used was a West system epoxy 105/206 mix with a specific gravity of 1.18 g/cm^3, tensile strength of 50.33 MPa and tensile modulus of 3.17 GPa.

Sample preparations and experimental setup

Two different sets of CF/epoxy plates were prepared using the Vacuum Assisted Resin Transfer Method (VARTM) technique each set contained 3 (12x12) inches plates, each plate was laid up using 5 nonwoven WL CF mats. The first set, was processed using Method 1 mats; the second was processed with Method 2 mats. The mats contain randomly distributed fiber as seen in Figure 9. All plates were prepared on a flat glass surface using the VARTM method, with a de-bulking time of 30 min, the resin was degassed for 10 min and the infusion took another 10 min until all fibers were fully wetted. After resin cure, samples were collected from each plate following the distribution seen in Figure 10. The samples distribution allowed a statistical representation from the vacuum side of the plate, the center of the plate and the resin infusion side of the plate. The three sites for sample collection allow the exploration of the effect of resin to fiber distribution on the mechanical properties of the composite. The average mechanical properties of each set was considered in the study, in order to examine the reproducibility of the composite and to understand the difference between composites made from Method 1 mats and those made using Method 2 mats.

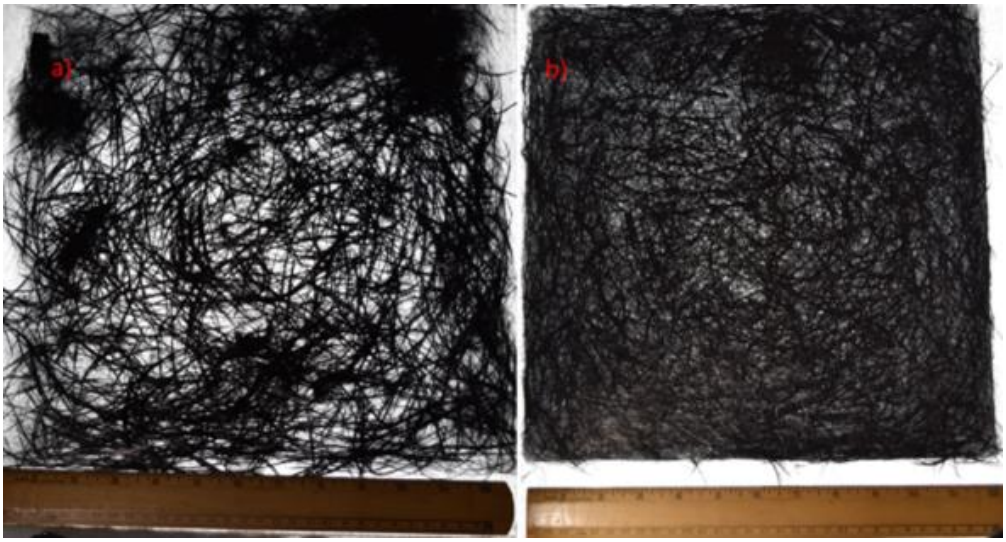

Figure 9: Images of 220 gsm mats produced by a) the traditional shear mixer showing a non-optimal fiber distribution, b) the innovated mixer presented in Chapter 1 showing optimal fiber distribution. The composites set analyzed in this study were made by stacking 5 mats of each kind to form a plate through VARTM process.

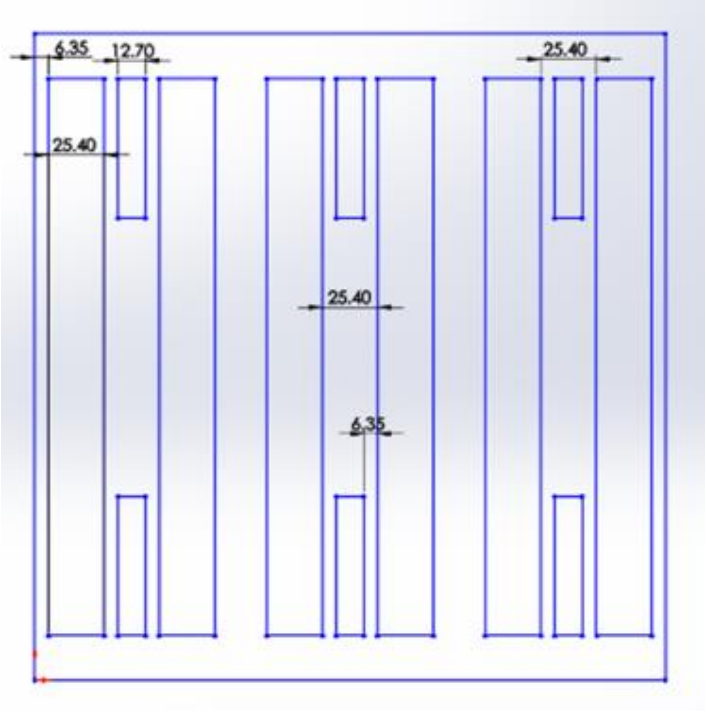

Figure 10: Location of tensile and flex samples machined from the WL nonwoven carbon fiber composite plates

All tensile samples were tested based on ASTM D5083, all flexure samples were tested based on ASTM D790 and Inter Laminar Shear Strength (ILSS) samples were tested based on ASTM 2344. Furthermore, samples of 6.45 square cm were taken from each tensile sample for a burn off test in order to confirm the fiber weight ratio to resin distribution. All samples were weighed before and after matrix burn-off for comparison. The matrix was subjected to burn-off using a Thermo Fisher Scientific 1100°C box furnace CF51800 series at 450°C for three hours. Another set of 6.45 square cm samples were selected from each tensile sample for void calculations per ASTM D2734. Scanning Electron Microscopy (SEM) analysis was conducted to observe the break surface of the tensile samples.

The effect of microstructure change from Method 1 and Method 2 mats on the composite was analyzed in order to validate the isotropy assumption of the composite. A comparison of the Young's Modulus through experimental data and prediction from the Halpin-Tsai equations [28] for oriented reinforcements is presented.

Halpin-Tsai theory and relevance

It is well known that the elastic modulus of isotropic reinforced composites are guided by the Halpin-Tsai equations for oriented reinforcements and Rule of Mixtures (ROM) [29]. Halpin[28] argued that it is possible to construct a material having isotropic mechanical properties from layers or plies of another or similar material. Mallick [30] stated that the Halpin-Tsai method is used to calculate the longitudinal and transvers properties of aligned discontinuous reinforcement composites allowing in its turn to calculate the modulus of randomly oriented reinforcement composites. This study

considers the Halpin-Tsai calculations to compute theoretical values of the composites under investigation assuming the following conditions: 1) Fiber cross section is circular; 2) Fibers are arranged in a square array; 3) Fibers are uniformly distributed throughout the matrix; 4) Perfect bonding exists between the fibers and the matrix, 5) Matrix is free of voids.

For these conditions, the tensile modulus of randomly oriented discontinuous fiber reinforced composites is calculated as:

$$E_{random} = \frac{3}{8}E_L + \frac{5}{8}E_T \quad \text{Eq (1)}$$

Where $E_L$and E_T are the longitudinal and transverse moduli respectively for a unidirectional discontinuous fiber reinforced composite and they are calculated as follow:

$$E_L = \frac{1 + 2(\frac{l_f}{d_f})\eta_L v_f}{1 - \eta_L v_f} E_m \quad \text{Eq (2)}$$

$$E_T = \frac{1 + 2\eta_T v_f}{1 - \eta_T v_f} E_m \quad \text{Eq (3)}$$

η_L and $\eta_T$are calculated as follow:

$$\eta_L = \frac{\left(\frac{E_f}{E_m}\right) - 1}{\left(\frac{E_f}{E_m}\right) + 2\left(\frac{l_f}{d_f}\right)} \quad \text{Eq (4)}$$

$$\eta_T = \frac{\left(\frac{E_f}{E_m}\right) - 1}{\left(\frac{E_f}{E_m}\right) + 2} \quad \text{Eq (5)}$$

With E_m and E_f is the matrix tensile modulus and the fiber tensile modulus respectively.

As for the theoretical strength, failure is predicted when the maximum tensile stress in the laminate equals the strength averaged over all possible fiber orientation

angles, known as the Hahn's approach [31], failure is predicted when the maximum tensile stress in the laminate equals the following strength averaged over all possible fiber orientation angles:

$$S_r = \frac{4}{\pi}\sqrt{S_L S_T} \quad \text{Eq (6)}$$

Where S_r is the strength of the random fiber laminate, S_L and S_T are respectively the longitudinal and transverse strength of a 0° laminate.

OOF analysis approach with assumption of composites isotropy and its validation

Composite microstructure has a direct influence on its mechanical properties. In order to quantify microstructural features, both morphological and material property must be characterized. Image processing is a robust technique for determination of morphological features. Computer-simulated microstructures are generated to replicate the microstructural features of actual microstructures.

The OOF2 software follows an adaptive meshing algorithm in order to conform to the boundaries of the mesh to the actual microstructure. Figure 11 displays polished surfaces of samples from Method 1 and Method 2 showing the microstructure distribution in each of the samples. A clear qualitative difference is apparent in the microstructures of the two methods. Method 1 demonstrate higher fiber agglomeration while Method 2 has clear wider fiber distribution. In both these cases a validation of the isotropic nature of the composites is required. Such validation is performed by measuring the Young's modulus in multiple directions of load application, this can be done experimentally or through computer simulation and analysis of the microstructure. Isotropy is defined by having equal Young's modulus for all load directions. In this study, the microstructure

performance, of both methods, in different load mounting directions is evaluated through computer-simulation analysis. Using OOF2 an adaptive mesh is conformed on sample sets from each method, the mesh is then subjected to a simulated deformation through ABAQUS to calculate the Young's modulus values for a tensile load in two principal directions.

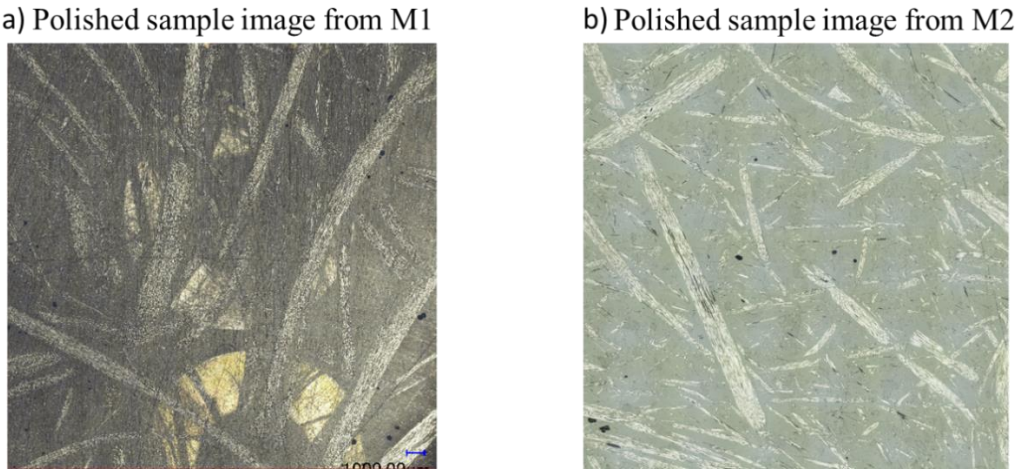

Figure 11: Polished samples showing the microstructure obtained in composite made with mats from: a) Method 1 and b) Method 2

Figure 12 and Figure 13 shows the processed images with their corresponding meshes generated by OOF2 and simulated through ABAQUS for Method 1 and Method 2 sample sets respectively. The samples area fraction varied but remains on average ~35%. The samples from Method 1 showed higher variance in area fraction which reflected on the FEA results. Samples from Method 2 had higher consistency. Such expected result is a reflection of the optimal fiber distribution of Method 2 versus the non-optimal fiber distribution of Method 1 as discussed in chapter 1.

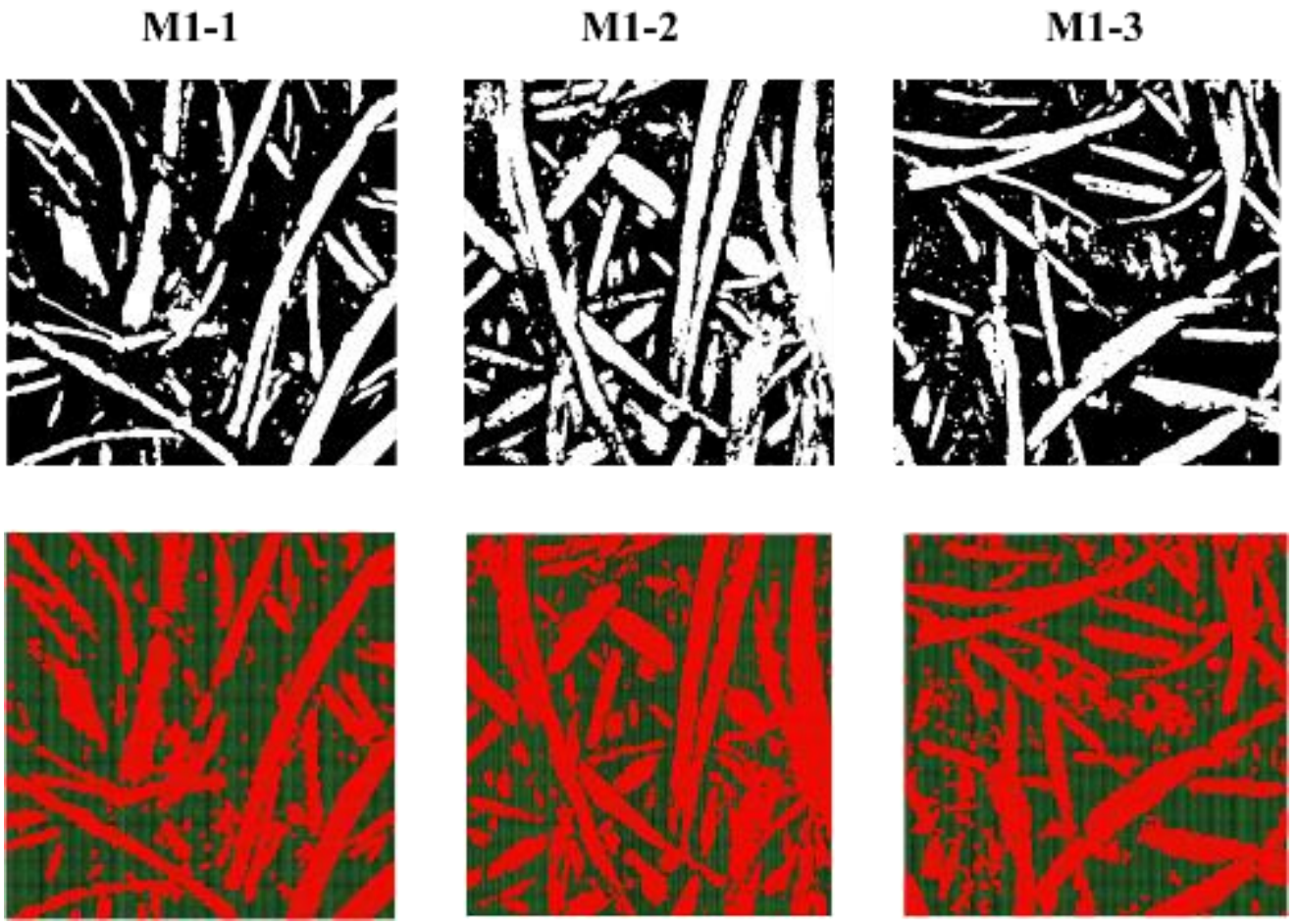

Figure 12: Method 1 modified images and their respective generated FEA meshes. M1-1 means that it is Method 1 – sample 1

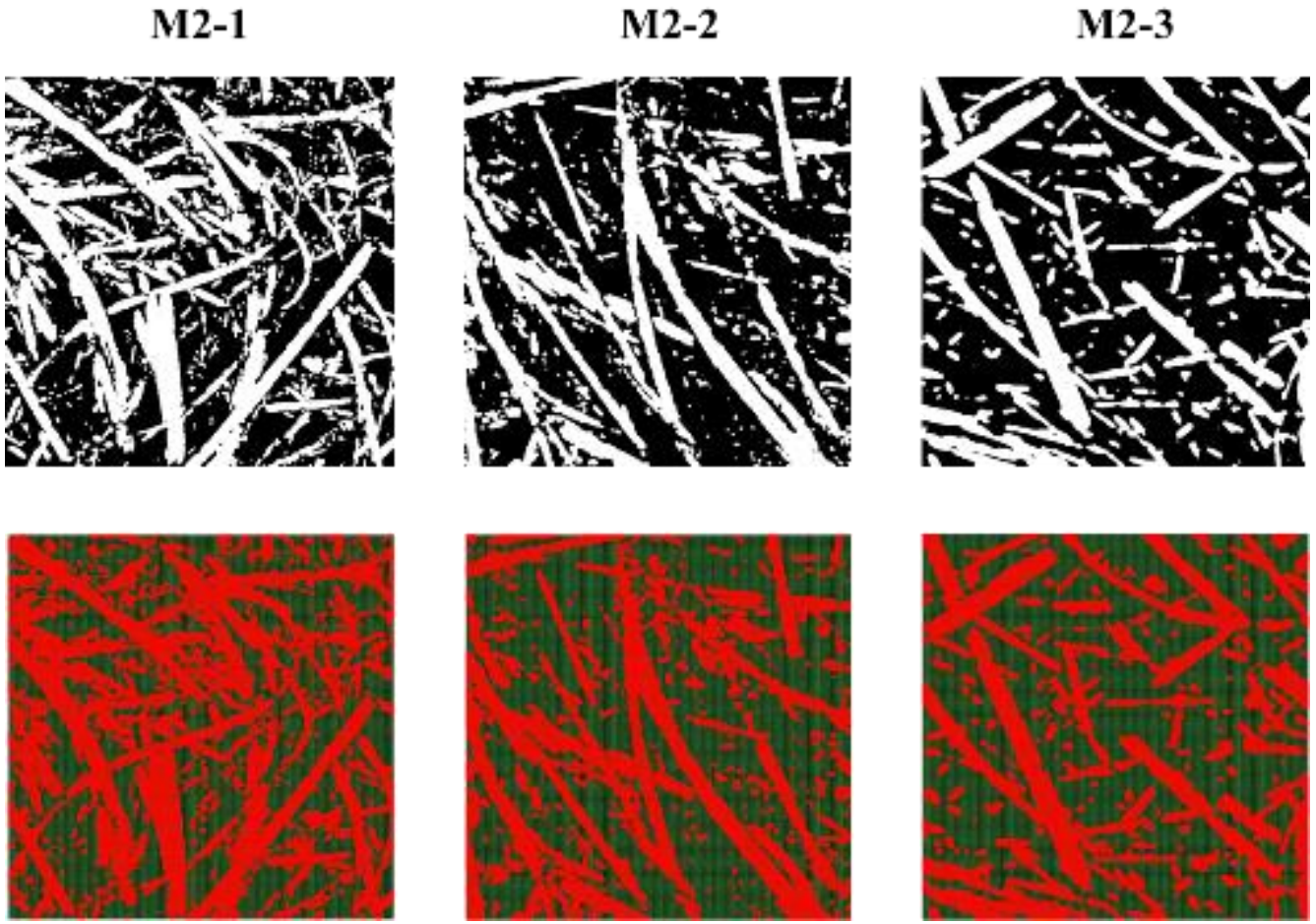

Figure 13: Method 2 modified images and their respective generated FEA meshes. M2-1 means that it is Method 2 – sample 1

The first step in this approach is to select images of a representative microstructure. The mats shown in Figure 9 were infused with epoxy resin by the same methodology of composite preparation out of several stacked layers. Three samples per method were taken from the median of the infused mats at an area of 18x18 mm each. They were mounted in epoxy resin for ease of polishing, polished to reveal the microstructure and imaged at a magnification of 100x. Note that the representative image of the microstructure is somehow subjective, thus the need for several samples for higher degree of fidelity. The samples had an area fraction average of ~ 33% which is representative of the overall volume fraction of fibers in the composite.

Before the OOF software is able to analyze the images and generates FEA meshes, some image processing filters need to be adopted. At first, the constituents within the microstructure are separated into distinct grey levels, through color thresholding and application of blurring filter and contrast adjustment as seen in Figure 14, in a similar approach to the process done by Goel et al. [27].

The next step was to assign the materials properties to respective pixel groups. The properties of the material can be found in the Materials and Methods section of this chapter. Fibers and matrix are both modeled as elastic materials since they are examined within the linear elastic regime of the stress-strain curve. The simulation was performed by applying load in two principal directions (x axis and y axis), this was done for all the samples collected for Method 1 set and Method 2 set. The rationale here is that if the mats are isotropic, they should yield comparable properties in both directions x and y as is hypothesized to result from the WL system.

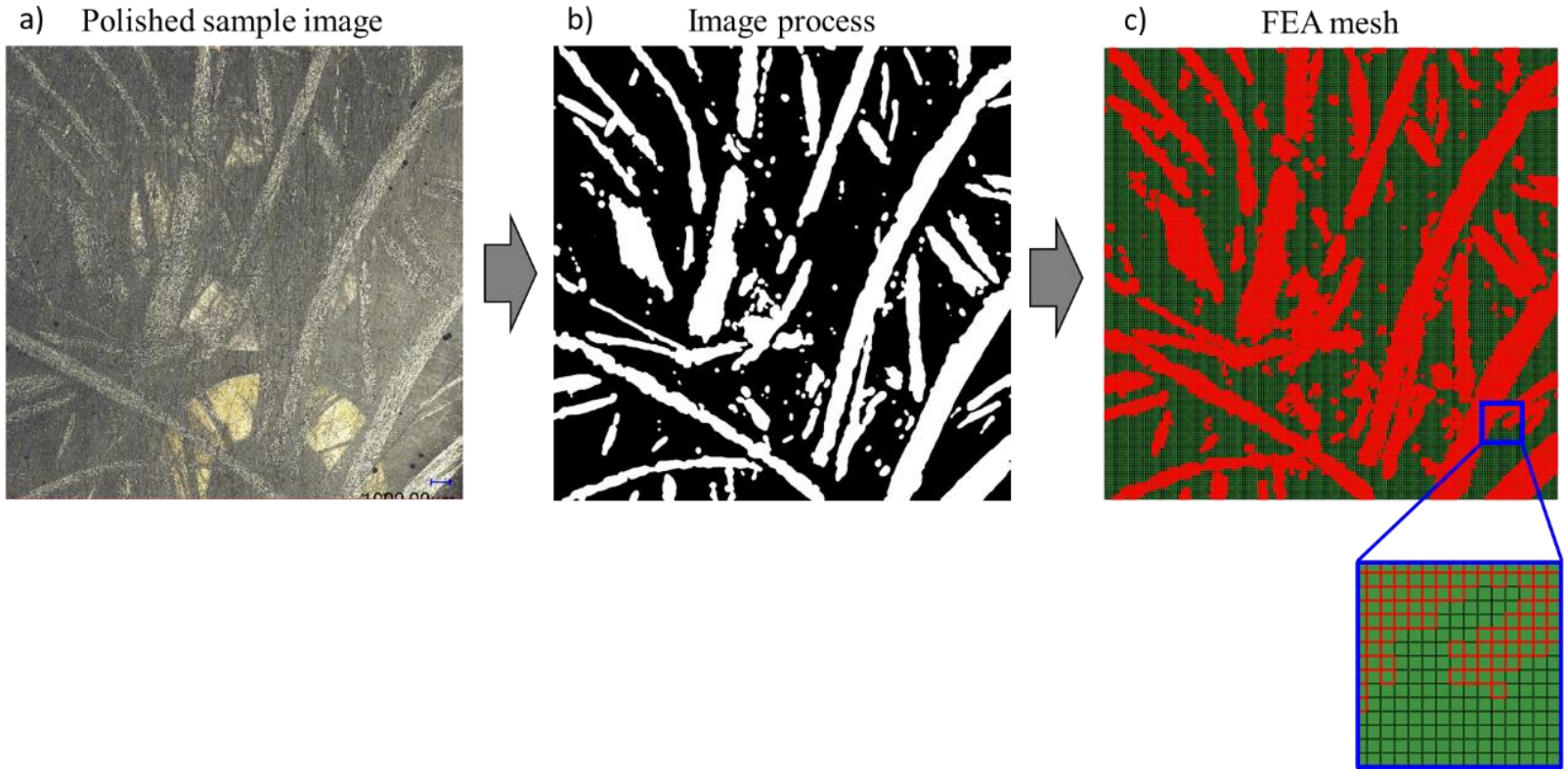

Figure 14: Image of representative microstructure and process analysis to assign a conforming mesh: a) original image collected through optical microscopy with a magnification of 100x showing the carbon fiber distribution from mixing Method 1, b) processed image after transferring to black and white and application of color threshold and blur and contrast filters the areal fiber fraction is ~36%, c) conforming mesh to the microstructure based on color separation

The following boundary conditions were used: a) at first the displacement of the left edge was fully constrained (i.e. set to zero). The displacement of the lower left node in both x and y directions was also set to zero. A force in the x direction was applied to the right of the microstructure. b) second the displacement of the lower edge was set to zero. The displacement of the lower left node in both x and y directions was also set to zero. A force in the y direction was applied to the top of the microstructure.

Results and Discussion

OOF analysis results for isotropy validation

The goal of this computational approach was to validate the isotropy of the WL mats. In chapter one, based on the density distribution, the mats were assumed to be isotropic in nature as the WL system generates random orientation for the fibers in the mats. From Table 2, the ratio of the calculated Young's modulus based on the FEA simulation shows higher isotropy in Method 2 samples over those of Method 1, validating the conclusion of Chapter 1. In isotropic samples the Young's modulus calculated in any direction should be consistent in value, this is why the ratio of the Young's modulus in different directions is considered as a measure of isotropy. Figure 16 shows an example of the FEA simulation, where the fibers in the load direction are highlighted in red due to them carrying the stress, on the other hand the fibers in normal direction to the load are indicated in colder colors based on the Von-mises scale.

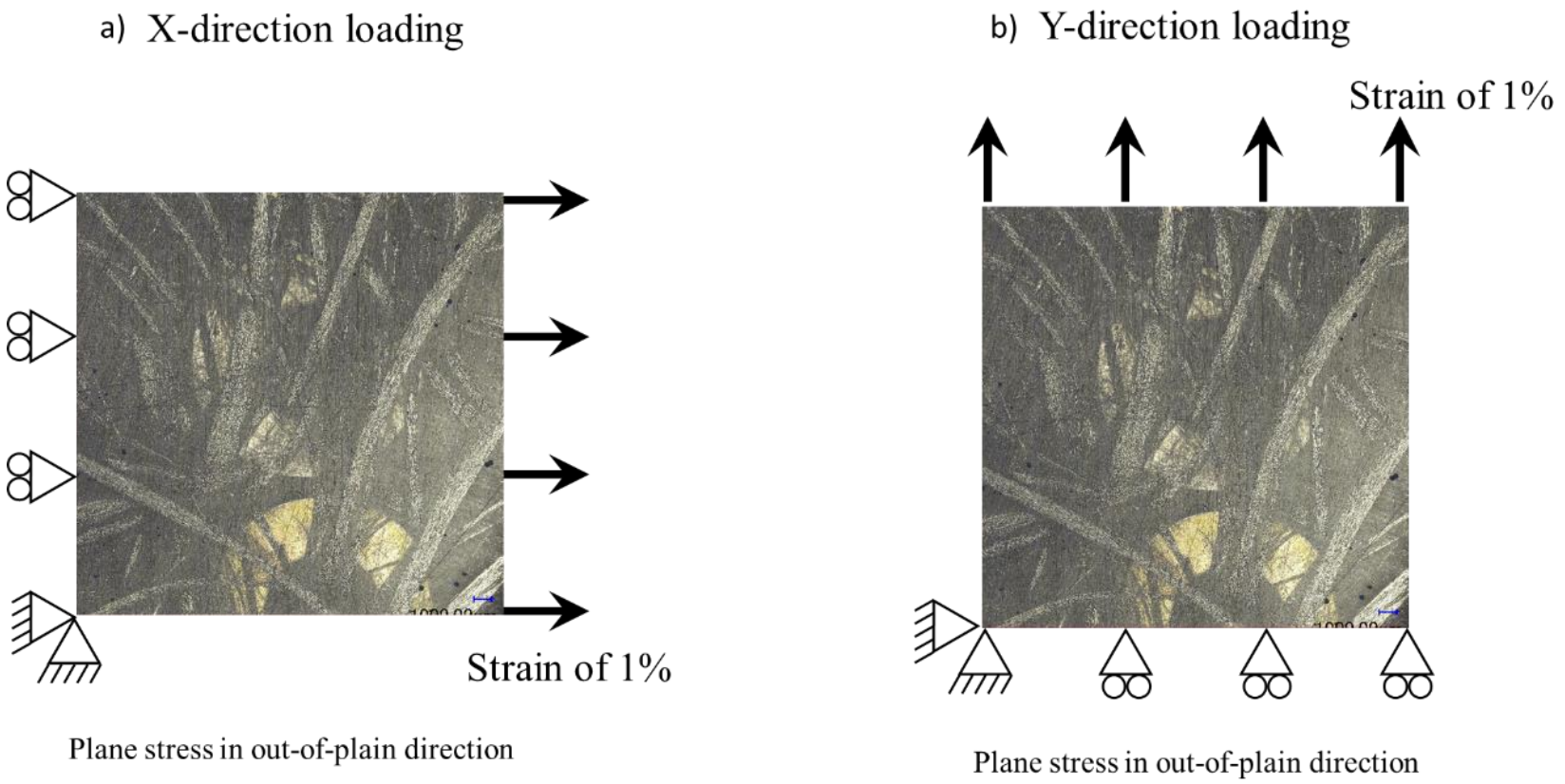

Figure 15: Boundary and loading condition for one of the original image collected through optical microscopy with a magnification of 100x. This sample areal fiber fraction is ~36%: a) left boundary fixed, lower left and bottom node fixed and constant force applied from the right hand side to cause a strain of 1%; b) Lower boundary fixed, lower left and bottom node fixed and constant force applied from the top side to cause a strain of 1%

Table 2: Tensile Modulus as predicted by the OOF based FEA study

Sample	Dir-X	Dir-Y	Ratio (x/y)	Sample	Dir-X	Dir-Y	Ratio (x/y)
M11	9.4	13.2	0.7	M21	15.0	16.5	0.9
M12	11.1	33.6	0.3	M22	9.2	11.8	0.8
M13	15.2	13.0	1.2	M23	9.5	8.4	1.1

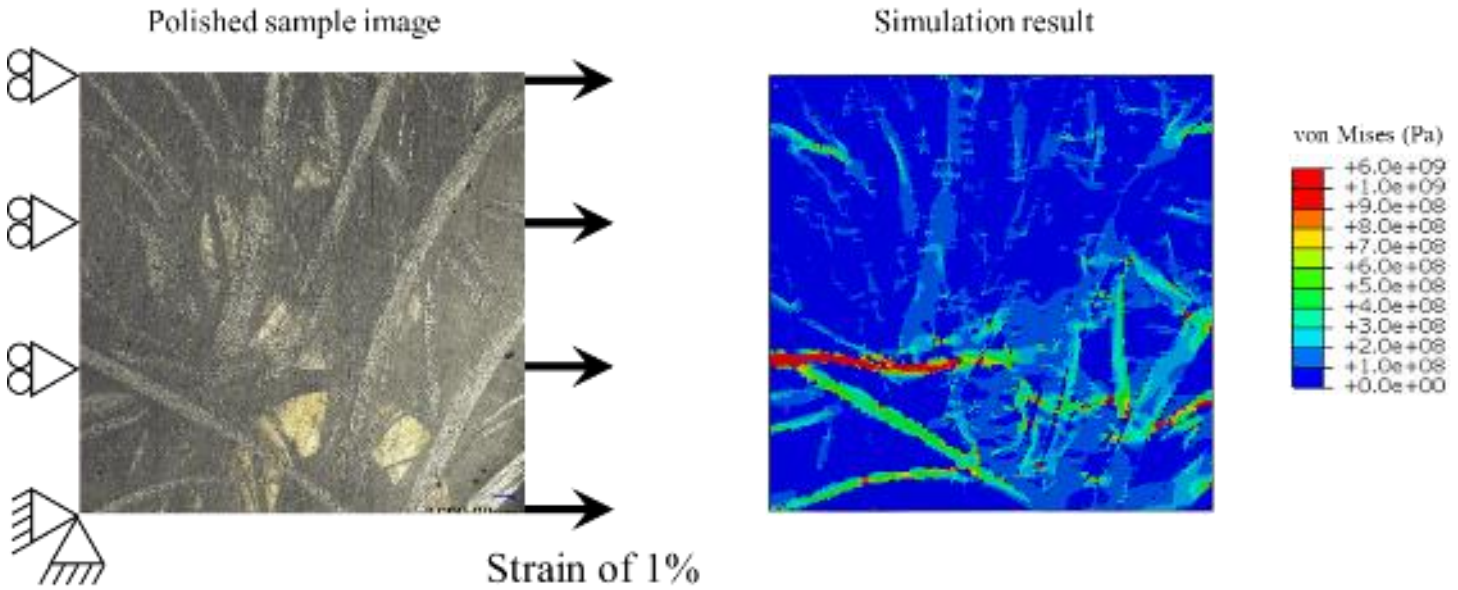

Figure 16: FEA simulation example showing the fibers in the loading direction, bear the load and highlighted in warm colors. while the fibers that are perpendicular to the load direction remain in cold colors as they do not contribute to carrying the load.

Experimental Results

Table 3 summarizes the average tensile properties with respect to the weight fractions for Method 1 and Method 2 plates respectively. 90% of the tensile samples failed in AGM (angled, gage, middle) mode and 10% in LGM (lateral, gage, middle). Table 4 summarizes normalized average tensile properties for each method in respect to unified weight fraction of 33%. The normalized values were assumed based on a linearized fit of the properties based on neighboring a weight fraction. It must be noted that such fit will not be valid for difference of weight fraction above 5%. The linearized fitting equation is [32]:

Figure 17 compares the average experimental tensile Young's modulus of each plate to the theoretical modulus calculated through the Halpin-Tsai equations with respect to their fiber volume fraction. Since each set contained 3 plates, the average values presented in Figure 17 form a cluster distribution of data points. Analysis of the data cluster distribution present higher control and repeatability of fiber weight content with composites made using Method 2 mats with the 3 plates having 28%, 29% and 30% fiber volume ratios. While the composite made with Method 1 mats had larger fiber weight content distribution at 35%, 39% and 37% for plates M1-P1, M1-P2, and M1-P3 respectively.

Evaluation of the experimental versus theoretical values demonstrated that Method 2 composites were much closer in value at 17% below theoretical with an average experimental modulus of 19 GPa and 29% fiber weight content. Method 1 composites had a 31% difference in experimental value from theoretical value with an

experimental modulus of 21GPa and 37% fiber weight content. Figure 18 highlights the individual samples in a scatter distribution in comparison to the values of the theoretical tensile modulus in respect to the fiber weight content. Composites made with Method 2 mats showed a better fit to the theoretical curve with a standard variation of 10% for tensile modulus and less than 3% for fiber weight content. Indicating good fiber distribution and higher consistency in the composite itself. Composites made with Method 1 mats showed a wide distribution and none of them reached the expected theoretical value, the tensile modulus standard deviation varied from 10% to 35%. The fiber weight content standard variation for samples collected from the same plate was above 10%, a direct result of lack of fiber distribution within the mats.

Figure 19 represents the tensile strength comparison between theoretical and experimental values for the plates of both sets. Method 1, plates standard deviation of 21, 31and 36 MPa valued at 20%, 24.2% and 24% respectively.

Method 2, plates showed narrower standard deviation at 15, 17 and 19 MPa valued at 10%,14% and 9.8%. The cluster of the average tensile strength from samples of Method 1 showed a wider spread due to variability in weight content, and an average difference of 46% from theoretical value. The average cluster for Method 2 was closer to the theoretical value with only 28% difference. Such differences can be contributed to voids in the samples as seen in Table 4, the microstructure dependency plays an important role toward the deviation from theory that assumes perfect isotropic material.

Figure 20 focuses on the individual samples in a cluster distribution in comparison to the values of the theoretical tensile strength in respect to the fiber weight

content. There was no fit between the samples and the theoretical tensile strength curve. Still, samples produced through Method 2 mats demonstrated a narrower standard deviation that did not surpass 10%, while the standard deviation for samples produced through Method 1 mats overpassed 20% in value. These results were in accordance with the findings of the tensile modulus for individual samples collected from plates produced using mats from both methods.

Figure 21 shows the normalized tensile values in respect to a unified fiber weight fraction of 33% as presented in Table 4. This bar graph clarifies the improved performance of Method 2 over Method 1 by 16% in Young's modulus value and 52% in ultimate tensile strength. Optimal fiber distribution in Method 2 resulted in closing the gap with the theoretical values as well, with 10% improvement toward theoretical Young's Modulus based on Halpin-Tsai prediction, and 26% improvement in tensile strength based on the Hahn's approach

Figure 22 explores the fracture surface of the tensile samples through SEM imaging. It is clear from Figure 22 (a) that there is significant fiber grouping due to lack of proper dispersion in Method 1. On the other hand, Figure 22 (c) presents a clean break surface with more fiber distribution due to innovation of fiber dispersion in Method 2. A magnification of 500 X, Figure 22 (b) for Method 1 and Figure 22 (d) for Method 2, demonstrated several fibers at random orientations in both methods but an improved bonding in composites made using mats from Method 2.Table 5 summarizes the average flexural properties, weight fractions, and void content for method 1 and method 2 plates respectively. Table 6 summarizes an average of the plates and their standard deviations.

Table 3: Experimental vs theoretical (Halpin-Tsai) tensile data for individual plates. Where the nomenclature Mi Pj, indicates the Method number through i and the plate number through j

Plate	Wf%	E (GPa)	Stde (Gpa)	E (Halpin-Tsai)	% out of Theoretical	StU (Mpa)	Stde (Mpa)	StU (Hahn)	% out of Theoretical
M1 P1	35	22	2	28	77	128	31	230	56
M1 P2	39	20	3	32	64	106	21	239	44
M1 P3	37	20	7	30	66	149	36	234	64
M2 P1	30	19	3	24	79	168	17	217	77
M2 P2	29	19	3	23	83	141	19	214	66
M2 P3	28	20	2	23	88	152	15	211	72

Table 4: Normalized average tensile values for each method based on unified fiber weight fraction of 33%

Method	Wf% Average	E (GPa)	E (Halpin-Tsai)	% out of Theo	σ (Mpa)	StU (Hahn)	% out of Theo
M1	33	19	27	71	114	225	51
M2	33	22	27	83	173	225	77

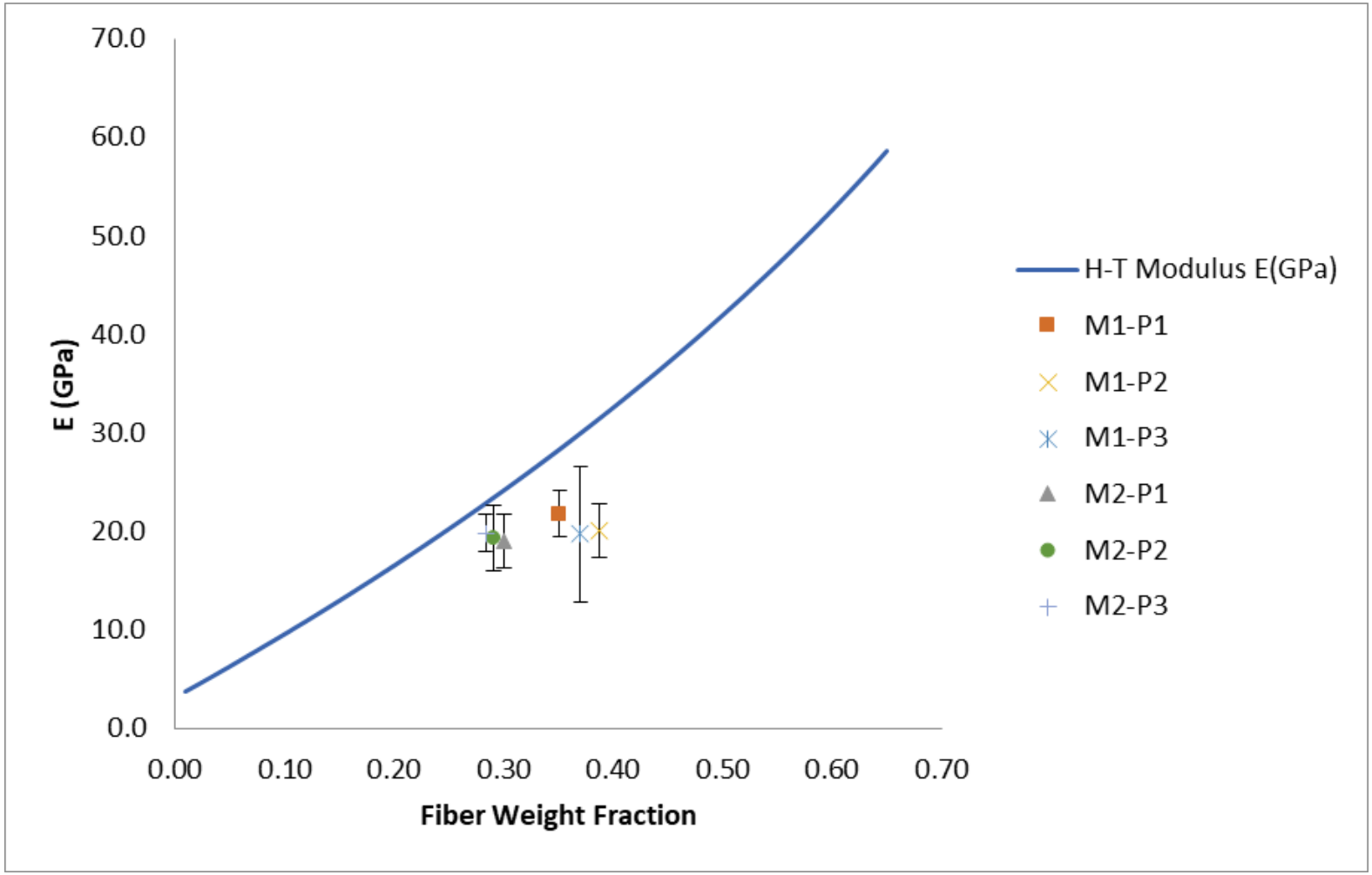

Figure 17: Average tensile modulus versus fiber weight fraction of each plate in both sets of Method 1 and Method 2. The blue line indicates the theoretical value calculated using the Halpin-Tsai equations [28].

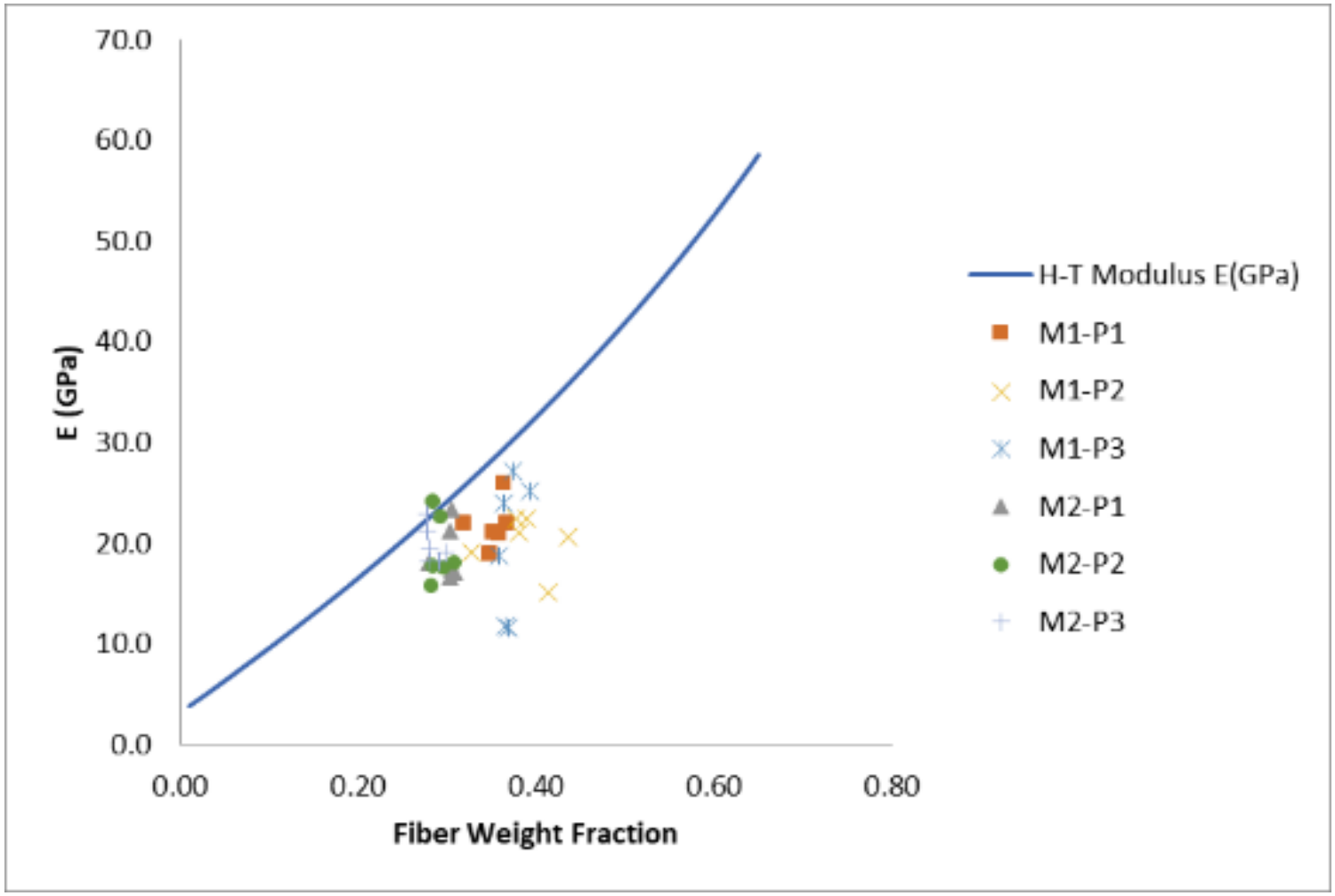

Figure 18: Tensile modulus versus fiber weight fraction of each sample collected from the plates in both sets of Method 1 and Method 2. The blue line indicates the theoretical value calculated using the Halpin-Tsai equations [28].

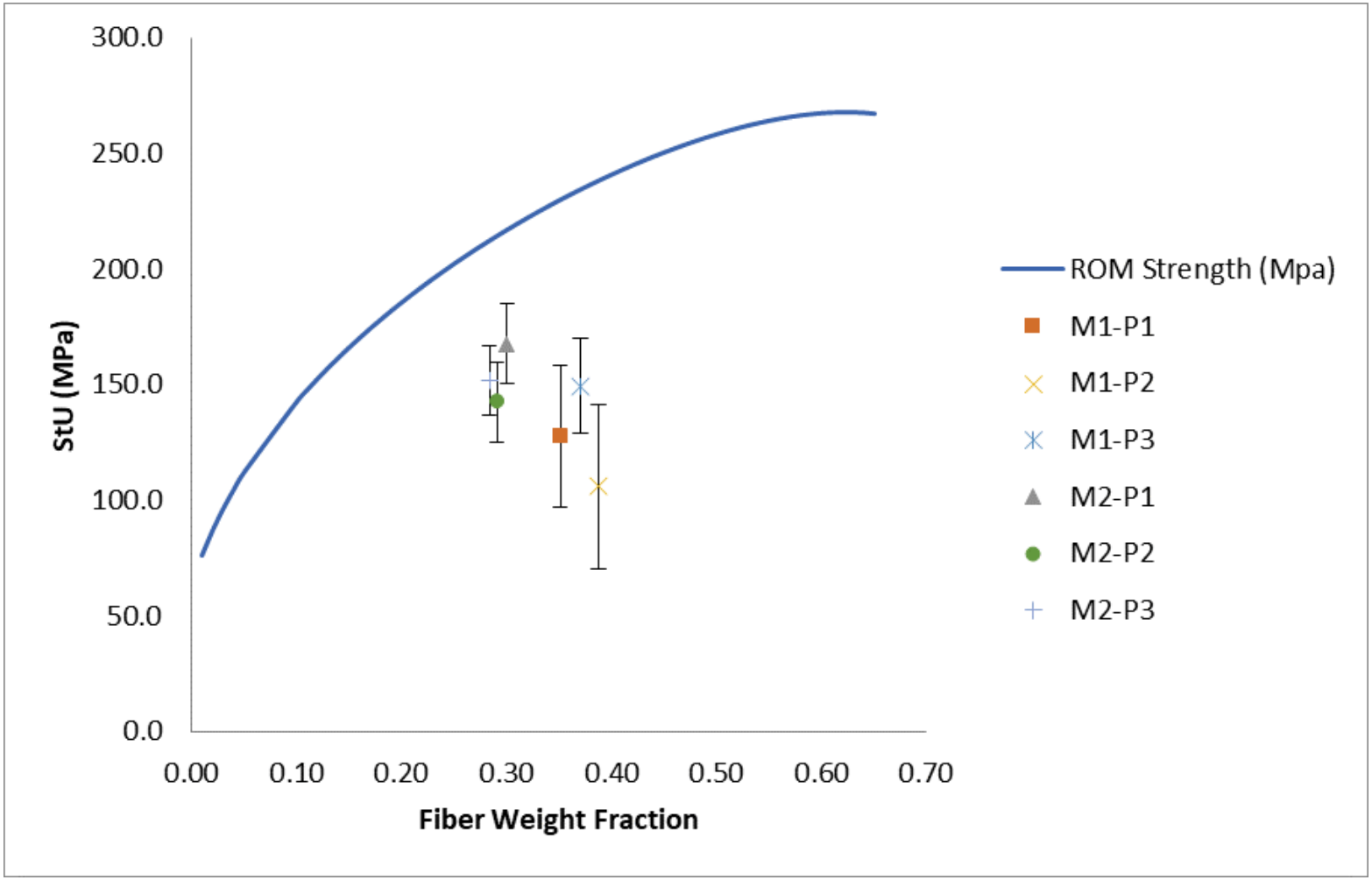

Figure 19: Average tensile strength vs the fiber fraction weight of each of the plates from the sets of each method. The blue curve represents the theoretical value calculated based on the Hahn's equation [31]

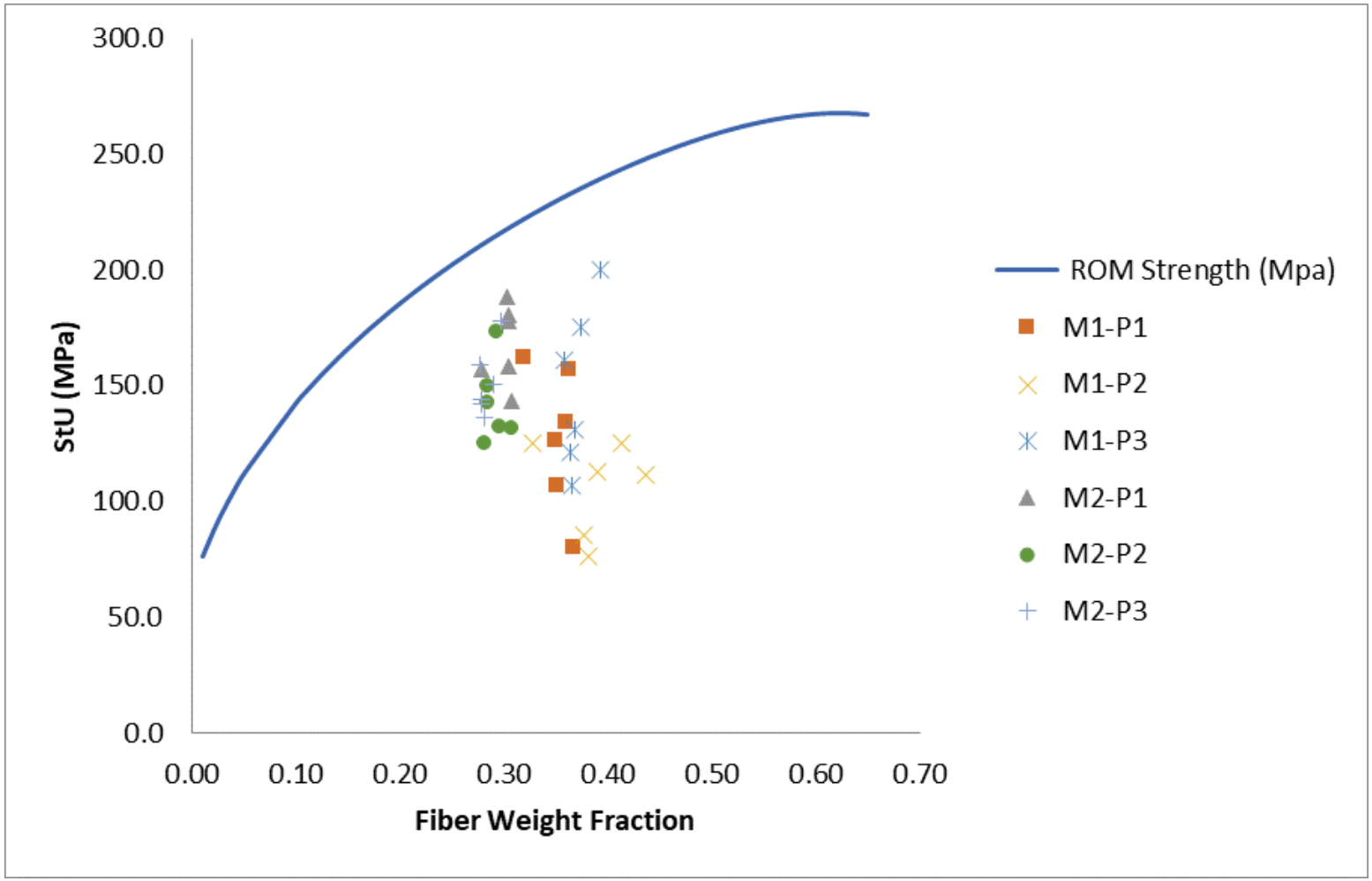

Figure 20: Tensile Strength vs fiber weight fraction of each sample collected from the plates in both sets of Method 1 and Method 2. The blue line indicates the theoretical value calculated using the Hahn's equations [31].

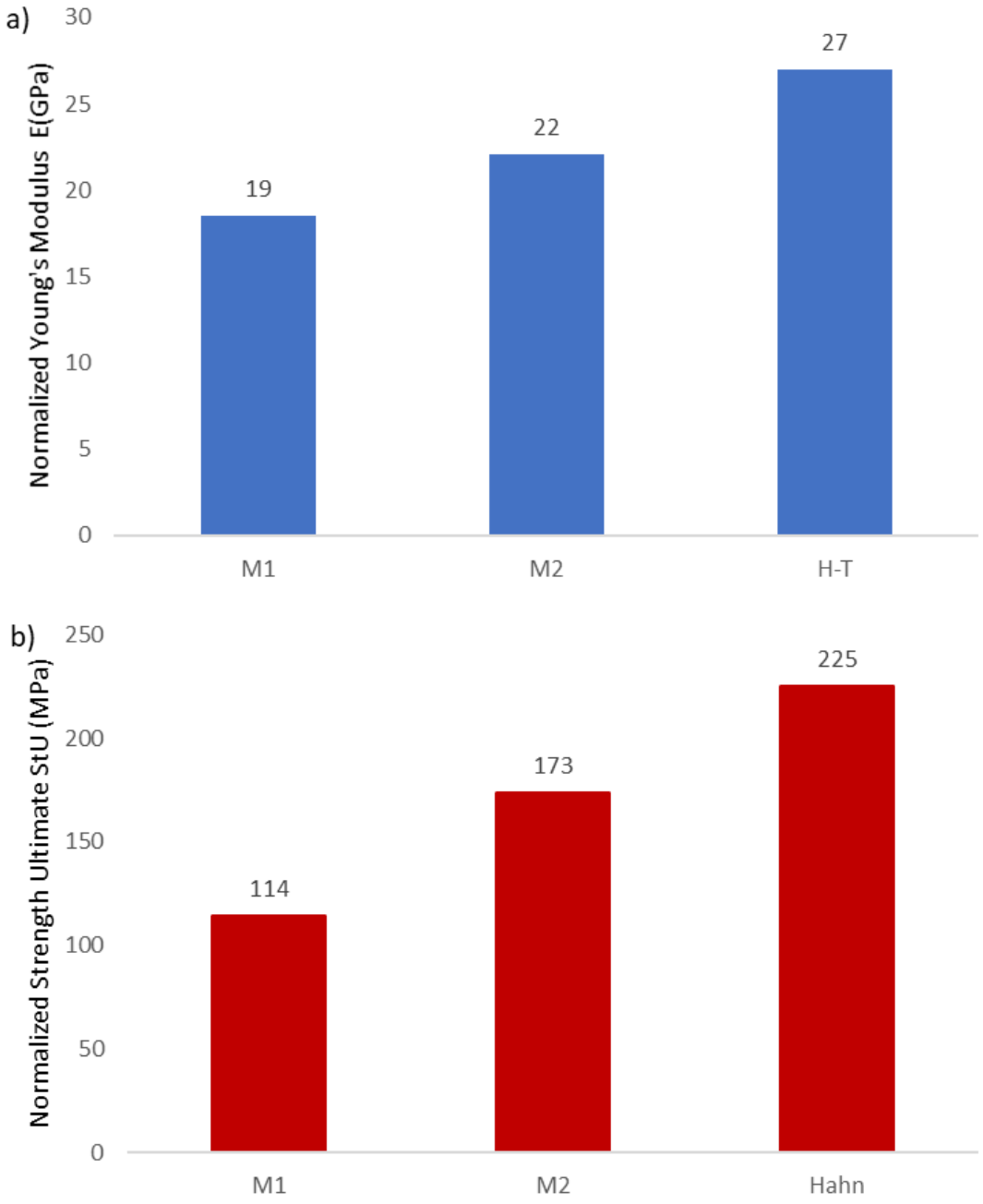

Figure 21: Normalized Tensile properties for each of the method in respect to a unified fiber weight fraction of 33%. Method 2 shows significant improvement in performance over Method 1 both in: a) tensile modulus by 16%, b) tensile strength by 52%

Table 5: Experimental flexural results for the individual plates

Plate	Wf%	Flex Modulus (GPa)	Stde (Gpa)	Stdev (%)	Flex Strength (Mpa)	Stde (Mpa)	Stdev (%)
M1 P1	35	14	6	46	252	85	34
M1 P2	39	13	3	25	242	43	18
M1 P3	37	13	3	22	241	43	18
M2 P1	30	12	1	6	243	23	10
M2 P2	29	12	2	17	239	38	16
M2 P3	28	12	1	11	234	22	10

Table 6: Normalized average flexural values for the plates from each method at a unified fiber weight fraction of 33%

Method	Wf%	Flex Modulus (GPa)	Flex Strength (Mpa)
M1	33	12	219
M2	33	14	270

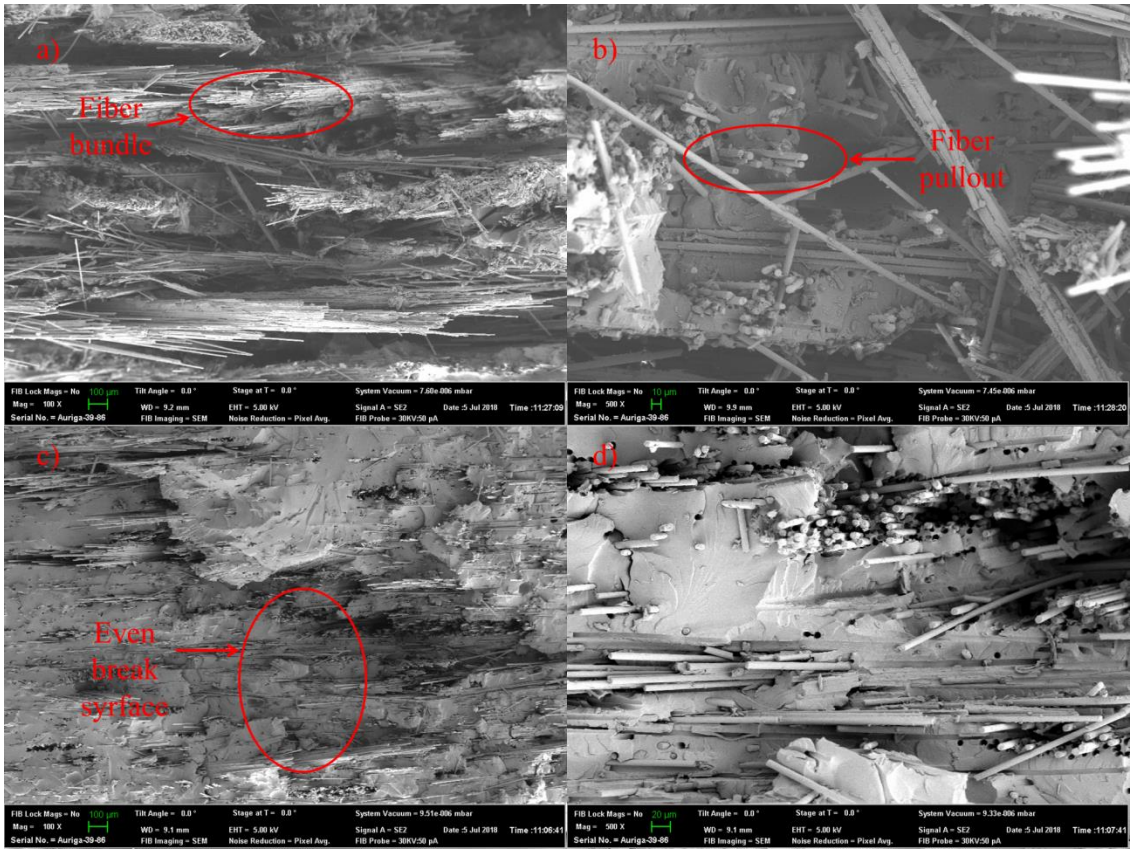

Figure 22: Selected break surface SEM images showing fiber random orientation and dispersion level for: a) Method 1 sample break surface showing high density of bundle fibers, a sign of non-optimal dispersion; b) a zoom in on the break surface of Method 1, showing fibers pointing in multiple directions but with significant fiber pullout, a sign of weak bonding with the matrix; c) Method 2 sample break surface showing a clean area, a sign of optimal fiber dispersion; and d) a zoom in on Method 2 break surface showing no fiber pullout due to resin penetration of fiber dispersion and improved bonding between fiber and matrix.

Figure 23 showed in a bar format the variance of the flexural modulus and strength in each method and a comparison between the normalized results of both methods. The normalized data for a unified fiber weight fraction of 33% shows a significant increase in flexural modulus and strength of 17% and 23% respectively in Method 2 over Method 1. The other significant difference lies in the standard deviation for the individual plates where Method 2 plates have a variance of 6, 17 and 11 % while Method 1 plates have a variance of 46, 25 and 22%.

Table 7 summarizes the average ILSS for each individual plate from both sets. While Table 8 shows the average of each set. Figure 25 highlight the performance in ILSS for both methods with a bar graph showing superiority of Method 2 over Method 1 by 15 MPa. It is hypothesized, that with optimal filament dispersion, increased fiber surface area causes the improvement of the ILSS.

Table 7: Average ILSS of each individual plate from both sets

Plate	Wf %	ILSS (Mpa)	Stdev (Mpa)	Stdev %
M1-P1	35	16.44	5.62	34
M1-P2	39	21.39	3.46	16
M1-P3	37	23.24	5.63	24
M2-P1	30	31.92	2.41	8
M2-P2	29	30.87	2.05	7
M2-P3	28	25.91	1.58	6

Table 8: Normalized average ILSS values of each set for a unified fiber weight fraction of 33%

Plates	Wf%	Normalized ILSS (Mpa)
M1	33	18
M2	33	33

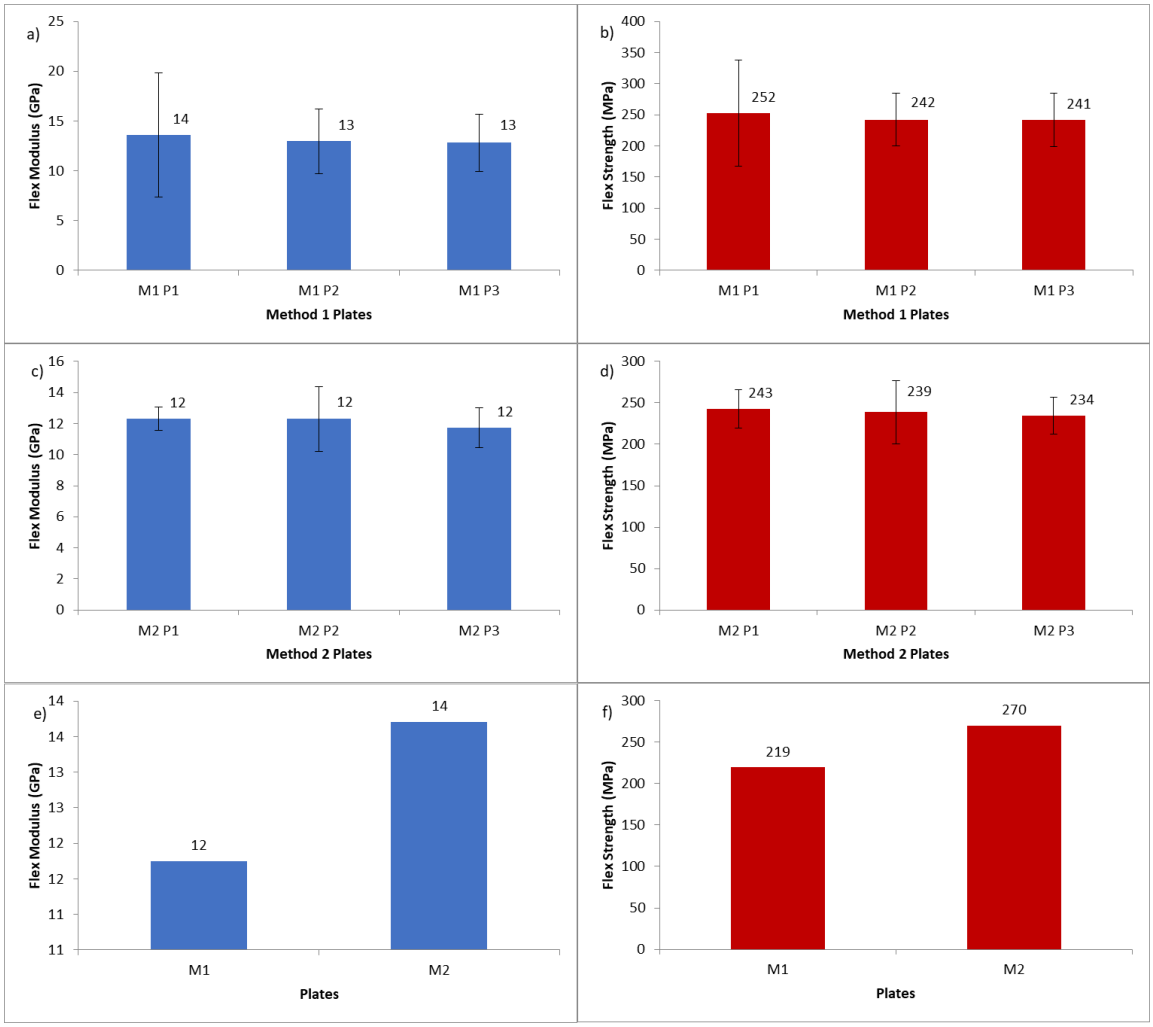

Figure 23: Flexural data for: a) Flex modulus for Method 1 plates, b) Flex strength for Method 1 plates, c) Flex modulus for Method 2 plates, d) Flex strength for Method 2 plates, e) Normalized average flex modulus for Method 1 Set versus Method 2 set for a unified fiber weight fraction of 33%, f) Normalized average flex strength for Method 1 set versus Method 2 set for a unified fiber weight fraction of 33%.

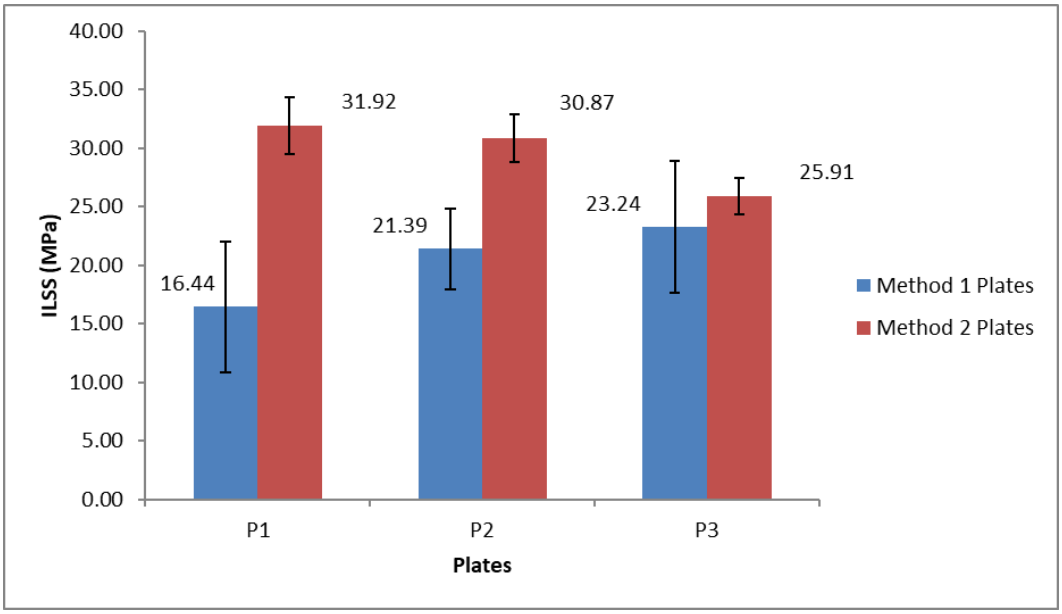

Figure 24: Bar graph representing the average ILSS of each plate from both sets and despite the superiority of fiber weight fraction in Method 1 plates, it is clear that Method 2 plates are outperforming Method 1 plates by values of 10%, to 90% with higher consistency in standard deviation.

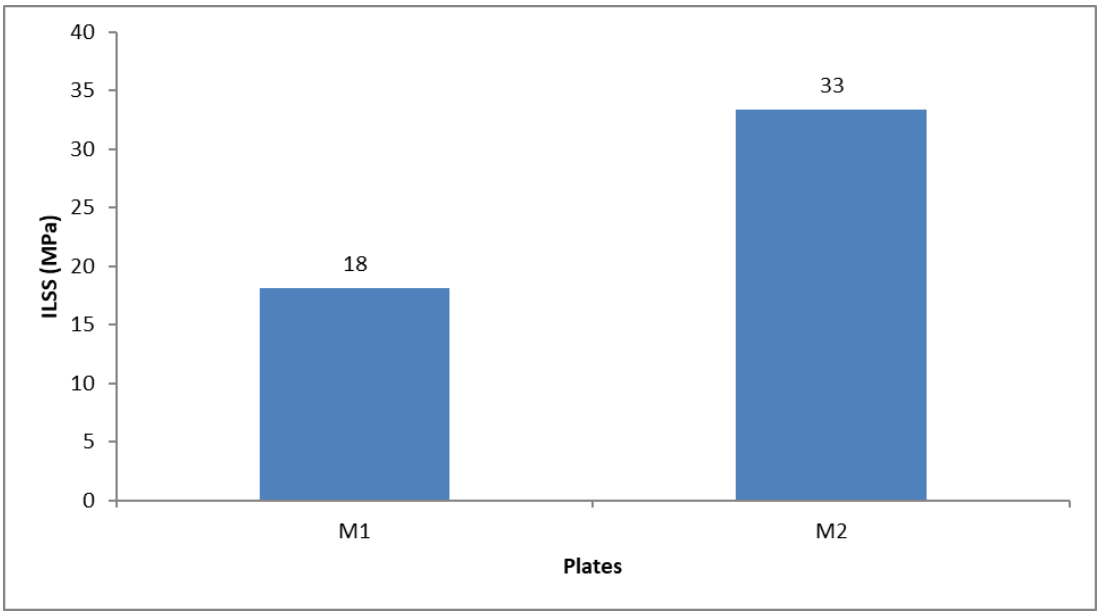

Figure 25: Normalized average ILSS of each set showing the improvement of 83% caused by optimal fiber dispersion in Method 2 when compared to Method 1.

CONCLUSIONS

Two sets of composites were made from WL CF nonwoven mats were consolidated and tested for tensile, flex and ILSS. The mats of each set were prepared through the two mixing regimes, Method 1 and Method 2 presented in Chapter 1. The composites isotropy was validated by computational method through OOF. OOF demonstrated higher isotropy in composites made through Method 2 versus those made through Method 1, thanks to the optimal fiber dispersion achieved in Method 2. The tensile properties were analyzed and compared to Halpin-Tsai prediction for Young's modulus and the Hahn's approach for ultimate tensile strength. The optimal fiber dispersion improved the values of Young's modulus by 16% from Method 1 and got closer to Halpin-Tsai prediction by 10%. The effect of optimal fiber dispersion in Method 2 reflected as well on the flexural properties by an increase of 17% and 23% for modulus and strength respectively. As for the ILSS Method 2 showed a superiority of 83% attributed to the uniform fiber distribution. With these findings it can be concluded that use of WL CF nonwoven mats produced by the innovative Method 2 proposed in Chapter 1 for composites production. These optimized mats helped bridge the gap between theoretical and experimental values, enabling the design and build of complex geometry parts with long discontinuous fibers through low cost manufacturing techniques such as out of autoclave methods and VARTM.

REFERENCES

[1] Pervaiz M, Panthapulakkal S, KC B, Sain M, Tjong J. Emerging Trends in Automotive Lightweighting through Novel Composite Materials. Mater Sci Appl 2016;07:26–38. doi:10.4236/msa.2016.71004.

[2] Akonda MH, Lawrence CA, Weager BM. Recycled carbon fibre-reinforced polypropylene thermoplastic composites. Compos Part A Appl Sci Manuf 2012;43:79–86. doi:10.1016/j.compositesa.2011.09.014.

[3] Chung DDL. Review: Materials for vibration damping. J Mater Sci 2001;36:5733–7. doi:10.1023/A:1012999616049.

[4] Ghossein H, Hassen AA, Paquit V, Love LJ, Vaidya UK. Innovative Method for Enhancing Carbon Fibers Dispersion in Wet-Laid Nonwovens. Mater Today Commun 2018;17:100–8. doi:10.1016/j.mtcomm.2018.08.001.

[5] Yeole P, Ning H, Hassen AA, Vaidya UK. The Effect of Flocculent , Dispersants , and Binder on Wet – laid Process for Recycled Glass Fiber / PA6 Composite 2018;26:259–70.

[6] Lu L, Xing D, Xie Y, Teh KS, Zhang B, Chen S, et al. Electrical conductivity investigation of a nonwoven fabric composed of carbon fibers and polypropylene/polyethylene core/sheath bicomponent fibers. Mater Des 2016;112:383–91. doi:10.1016/j.matdes.2016.09.096.

[7] Deng Q, Li X, Zuo J, Ling A, Logan BE. Power generation using an activated carbon fiber felt cathode in an upflow microbial fuel cell. J Power Sources 2010;195:1130–5. doi:10.1016/j.jpowsour.2009.08.092.

[8] Meng C, Liu C, Fan S. Flexible carbon nanotube/polyaniline paper-like films and their enhanced electrochemical properties. Electrochem Commun 2009;11:186–9. doi:10.1016/j.elecom.2008.11.005.

[9] Shen L, Wang J, Xu G, Li H, Dou H, Zhang X. NiCo2S4nanosheets grown on nitrogen-doped carbon foams as an advanced electrode for supercapacitors. Adv Energy Mater 2015;5:2–8. doi:10.1002/aenm.201400977.

[10] Straumit I, Lomov S V., Wevers M. Quantification of the internal structure and automatic generation of voxel models of textile composites from X-ray computed tomography data. Compos Part A Appl Sci Manuf 2015;69:150–8. doi:10.1016/j.compositesa.2014.11.016.

[11] Wan Y, Takahashi J. Tensile and compressive properties of chopped carbon fiber tapes reinforced thermoplastics with different fiber lengths and molding pressures. Compos Part A Appl Sci Manuf 2016;87:271–81. doi:10.1016/j.compositesa.2016.05.005.

[12] Wan Y, Straumit I, Takahashi J, Lomov S V. Micro-CT analysis of internal geometry of chopped carbon fiber tapes reinforced thermoplastics. Compos Part A Appl Sci Manuf 2016;91:211–21. doi:10.1016/j.compositesa.2016.10.013.

[13] Tseng H, Chang R, Hsu C. Numerical prediction of fi ber orientation and mechanical performance for short / long glass and carbon fi ber-reinforced composites. Compos Sci Technol 2017;144:51–6. doi:10.1016/j.compscitech.2017.02.020.

[14] Feraboli P, Kawakami H, Wade B, Gasco F, DeOto L, Masini A. Recyclability and

reutilization of carbon fiber fabric/epoxy composites. J Compos Mater 2012;46:1459–73. doi:10.1177/0021998311420604.

[15] Caba AC, Loos AC, Batra RC. Fiber-fiber interactions in carbon mat thermoplastics. Compos Part A Appl Sci Manuf 2007;38:469–83. doi:10.1016/j.compositesa.2006.02.024.

[16] Evans AD, Qian CC, Turner TA, Harper L. ., Warrior NA. Flow characteristics of carbon fibre moulding compounds. Compos Part A Appl Sci Manuf 2016;90:1–12. doi:10.1016/j.compositesa.2016.06.020.

[17] Selezneva M, Lessard L. Characterization of mechanical properties of randomly oriented strand thermoplastic composites. J Compos Mater 2016;50:2833–51. doi:10.1177/0021998315613129.

[18] Amaro AM, Reis PNB, Santos JB, Santos MJ, Neto MA. Effect of the electric current on the impact fatigue strength of CFRP composites. Compos Struct 2017;182:191–8. doi:10.1016/j.compstruct.2017.09.032.

[19] Thomason JL. The influence of fibre length and concentration on the properties of glass fibre reinforced polypropylene: 5. Injection moulded long and short fibre PP. Compos Part A Appl Sci Manuf 2002;33:1641–52. doi:10.1016/S1359-835X(02)00179-3.

[20] Langer, S.A. Fuller, E.R. and Carter WC. OOF: an image-based finite-element analysis of material microstructures. Comput Sci Eng 2001;3:15–23. doi:10.1109/5992.919261.

[21] Reid ACE, Lua RC, Garcia RE, Coffman VR, Langer SA. Modelling

Microstructures with OOF2. Int J Mater Prod Technol 2009;35:361. doi:10.1504/IJMPT.2009.025687.

[22] Dong Y, Bhattacharyya D. Morphological-image analysis based numerical modelling of organoclay filled nanocomposites. Mech Adv Mater Struct 2010;17:534–41. doi:10.1080/15376490903399746.

[23] Dong Y, Bhattacharyya D, Hunter PJ. Characterisation and Object-Oriented Finite Element Modelling of Polypropylene/ Organoclay Nanocomposites. Key Eng Mater 2007;334–335:841–4. doi:10.4028/www.scientific.net/KEM.334-335.841.

[24] Cannillo V, Esposito L, Pellicelli G, Sola A, Tucci A. Steel particles-porcelain stoneware composite tiles: An advanced experimental-computational approach. J Eur Ceram Soc 2010;30:1775–83. doi:10.1016/j.jeurceramsoc.2010.01.041.

[25] Bakshi SR, Patel RR, Agarwal A. Thermal conductivity of carbon nanotube reinforced aluminum composites: A multi-scale study using object oriented finite element method. Comput Mater Sci 2010;50:419–28. doi:10.1016/j.commatsci.2010.08.034.

[26] Coffman VR, Reid ACE, Langer SA, Dogan G. OOF3D: An image-based finite element solver for materials science. Math Comput Simul 2012;82:2951–61. doi:10.1016/j.matcom.2012.03.003.

[27] Goel a., Chawla KK, Vaidya UK, Chawla N, Koopman M. Two-dimensional microstructure based modelling of Young's modulus of long fibre thermoplastic composite. Mater Sci Technol 2008;24:864–9. doi:10.1179/174328408X294080.

[28] Affdl JCH, Kardos JL. The Halpin-Tsai equations: A review. Polym Eng Sci

1976;16:344–52. doi:10.1002/pen.760160512.

[29] Shokrieh MM, Moshrefzadeh-Sani H. On the constant parameters of Halpin-Tsai equation. Polym (United Kingdom) 2016;106:14–20. doi:10.1016/j.polymer.2016.10.049.

[30] Mallick PK. Fiber-Reinforced Composites: Materials, Manufacturing, and Design. third edit. Philadelphia: CRC Taylor & Francis Group; 2007.

[31] Hahn HT. On Approximations for Strength of Random Fiber Composites. J Compos Mater 1975;9:316–26. doi:10.1177/002199837500900401.

[32] "Composite Materials Handbook-MIL 17 Volume I: Guidelines for Characterization of Materials 1st edition", Taylor & Francis, 1999

CHAPTER III

EFFECTS OF FIBER LENGTH AND CROWDING FACTOR ON WET LAID MATS FORMATION, THEIR IN-PLANE PERMEABILITY AND LOCAL PERMEABILITY OF COMPLEX SHAPE PARTS

ABSTRACT

Nonwoven textiles are used in automotive and industrial applications due to their low cost and ease of production. Recent advances in Wet Laid (WL) nonwovens produced nonwoven Carbon Fiber (CF) mats with uniform distribution and consistent reproducibility. This study analyzes the permeability of WL nonwoven mats in relation to their gram per square meter (gsm) distribution and fiber length. Nonwoven pores are directly correlated to both these variables as they affect the packing factor and fibers distribution. The mats permeability was measured using the channel flow technique due to least variability in results associated with it. While the permeability constant for mats prepared using 12.7 mm long fibers was higher than the permeability of those prepared with 25.4 mm fibers by 15%, the stacking of three mats together reversed the results with permeability constant for the mats prepared with fibers at 25.4 mm in length higher by 25% than those prepared with 12.7 mm long fibers. Layers stacking play an important role on the apparent effective mean pore diameter. As fibers from consecutive layers, cross path over the pores of previous layers, affecting in its turn the recorded permeability of the material.

INTRODUCTION

Nonwoven textiles are used in automotive and industrial applications due to their low cost and ease of production [1]. It is used in a range of applications including garments, home filters, medical and technical textiles. Lately the focus on nonwoven textiles has expanded in the field of composites [2–6] where they are used as battery

separator, fuel cell membrane, nonstructural parts, and delamination resistors due to random interlocking between layers. The hierarchy and fiber distribution in nonwoven textile is of outmost importance in relation to its performance. Optimal dispersion of fibers is directly related to fiber dimensions and fiber volume fraction [7–9]. Safavi et al. [10] investigated the fiber characteristics effects on fiber dispersion for wet laid (WL) nonwovens, and found that fiber diameter is directly related to dispersion time, thus the importance of fiber diameter and length in dispersing and forming a WL nonwoven. In lab scale WL web formation, fibers are deposited onto a forming surface using a filtration process [11]. Guan et al. [12] and Fathi-Khalfbadam et al. [13] focused on overcoming dispersion challenges of fibers in aqueous system. They emphasized the link between the final quality of the mat to the fiber aspect ratio and volumetric concentration in water. Simmonds et al. [14] presented detailed mathematical work to help design nonwoven fabric with given pore size specifications, using the Bryner model to relate fiber size and fiber volume fraction to average and maximum pore size in a nonwoven sheet. Wölling et al. [15] presented a study that compared processing technologies and the effect of different parameters like fiber source and the gsm of the textile on the final quality of the mats. They reported a challenge with material permeability, highlighting the importance of fiber quality, quantity and length on the final mechanical properties of the composite. Zhu et al. [16] reported that nonwoven fabrics stand out as a unique class of porous media, due to its relatively high volume of air and complex structure due to the random arrangement of fibers; this place importance on accuracy when it comes to permeability study.

Permeability of woven fabric had been studied extensively by researchers [17–20] and study parameters had been stablished for accurate measurements and analysis, but the variability in nonwoven fabric needs further investigations. Sharma et al. [21] revised the accuracy of the methods used in permeability measurements for in-plane isotropic preforms, they found that among various measurement methods described in the literature, it has now been accepted that channel flow technique is better suited with least variability associated with it. Endruweit et al. [22] compared the permeability values of chopped CF preforms through radial and channel flow methods and found that the unidirectional injection experiments, known as the channel flow technique, are more suitable to obtain reliable permeability values for this type of preform.

Ghossein et al. [23] introduced an innovative technique to produce WL CF nonwoven mats with high consistency and close accuracy to the theoretical calculations for pores coverage area. This study expands the work to investigate the effects of fiber length and gsm of the mats on the resin permeability. The local permeability is also studied through a complex geometry mold by using three layers of WL CF nonwoven mats at 200 gsm and 25.4 mm fiber length. The local permeability analysis improved the understanding of necessary fiber wetting information for better composite design and manufacturing. This study focuses on a complex shape composite using the CF WL mats through the Vacuum Assisted Resin Transfer Molding (VARTM). The study deals with fiber wet out and the resulting mechanical performance of complex geometries.

THEORETICAL BACKGROUND

Nonwovens are porous material in which the permeability is influenced by the pores structure. Pores can be idealized by polygons with sides formed by the free length of fibers between fibers crossings. Simmonds et al. [14] derived an equation to calculate the mean pore diameter ($D_{p,mean}$) in respect to the fiber length and the number of fibers per unit area. Table 9 shows the values of the crowding factor n_f and $D_{p,mean}$ calculated using equation 1 [13] and equation 2 [14] for the variables of mats gsm and fiber length in this study.

$$n_f = \frac{2}{3} C_v (\frac{l}{d})^2 \quad \text{Eq (1)}$$

$$D_{p,mean} = \frac{2}{n_f l} \quad \text{Eq (2)}$$

where C_v, l, and d, are volume fraction (ratio of the volume occupied by fibers to the volume of water), fiber length and fiber diameter in (mm), respectively.

Permeability (K) is a measure of the ability of a porous material to transmit fluid. It can be measured using Darcy's Law with the common unit used (cm^2). This method gives one-dimensional measure of fiber permeability. The WL CF nonwoven are thin with thickness bellow 1 mm, thus the through thickness permeability can be ignored. The in plane permeability noted as K_1 and K_2 are the same for isotropic material such as the WL CF nonwoven used in this study. The permeability constant is calculated using empirically derived formula from Darcy's Law which is given in equation 3 [24]:

$$k = \frac{L^2 \, \Phi \, \mu}{2 \, t \, \Delta P} \quad \text{Eq (3)}$$

where L is the length of flow front in (m), ΔP is the pressure difference in (Pa), t is mold fill time in (sec), Φ is fibers weight percentage, μ is viscosity of test fluid in (Pa.sec) and K is permeability constant in (m^2).

MATERIALS AND METHODS

The carbon fiber used in this study was un-sized chopped Zoltek™ PX35 Type 02 CF with a length of 25.4 mm, average diameter of 7 μm, specific gravity of 1.81 g/cm^3, tensile strength of 4137 MPa, and tensile modulus of 242 GPa. The matrix used was a West system epoxy 105/206 mix with a specific gravity of 1.18 g/cm^3, tensile strength of 50.33 MPa and tensile modulus of 3.17 GPa.

Off the shelf Karo syrup was diluted with distilled water at a ratio of 1 to 2 counts for permeability experimentation giving a density of 1.27 g/ml. The National Institute of Standards and Technology (NIST) database on fabric permeability has used diluted corn syrup as the test fluid to calculate the permeability of fibers [25]. Viscosity of the test fluids was measured before and after each experiment by the ball-drop method using a GV-2300 Gilmont Viscometer at room temperature.

Sample preparations and experimental setup

The innovative WL method presented by the author in previous work [23] was used to prepare the WL CF nonwoven with a combination of two variables. For the first set, the mats areal weight was held constant at 100 gsm and the fiber length was changed from 12.7 mm to 25.4 mm. For the second set, the mats areal weight was raised to 200 gsm with fibers used at the length of 12.7 mm and 25.4 mm respectively. The

permeability test was conducted for each combination using 1 layer of WL CF nonwoven mat and 3 layers of WL CF nonwoven mats to investigate the effect of the mats stacking on the resin flow.

To obtain a unidirectional flow, a rectangular mold with cavity dimensions 216mm by 112mm by 3mm was used. The mold consisted of two reservoirs at both ends to gain constant flow throughout the width of the cavity. Compound pressure measuring devices were installed at the bottom of the reservoirs. A transparent top was used to allow the video to capture the flow. Breather material was placed at the reservoirs to saturate the flow and maintain it at an unobstructed constant rate. Vacuum in the mold was maintained at 29" HG during the experiment. Video camera was used to capture the flow front progress and a DAQ system collected the pressure data from the sensors. Figure 26 shows the permeability. From the video captured a plot of L^2 vs t was constructed and the slope equation 1 was used for permeability calculations.

Local permeability experiment and complex geometry composite infusion

Figure 27 shows a drawing of the three cavities mold used for the testing the dependency of local permeability in relation to change in mold geometry. Figure 28 shows a complex geometry part made using the VARTM technique, the vacuum was held at 29" HG during the experiment. The three shapes are labeled D, B and V throughout the work as indicated in Figure 28. The local permeability experiment followed the same design and procedure as the standard permeability setup with the three cavities mold replacing the flat rectangular mold. Three layers of WL CF nonwoven at 200 gsm and 25.4 mm fiber length were formed one by one on the mold and placed under vacuum for

20 min. In consistency with the in-plane permeability experiment, off the shelf Karo syrup was diluted with distilled water at a ratio of 1 to 2 counts for permeability experimentation giving a density of 1.27 g/ml. A video camera recorded the flow front progress with respect to time.

The complex shape composites followed the same procedure as the local permeability. A West system epoxy 105/206 mix was used for infusion.

Discontinuous fiber element analysis

The complex shape composites, discussed in the previous section, were tested in tensile mode. But since no standard exist for data validation, a comparison to a discontinuous fiber finite element analysis (FEA) was conducted. The FEA serves as theoretical expectation of the behavior and performance of complex shape composites made from the WL CF nonwoven mats.

The chopped fiber reinforced composite properties were predicted using MCQ Chopped software from AlphaStar Corporation. The MCQ chopped software combines nano-micro-macro mechanics with finite element and damage progression to predict chopped composite properties based on reinforced particles and matrix individual properties [26].

The MCQ chopped software uses the well-known Mori-Tanaka analysis approach to evaluate anisotropic composite properties from the mixture of anisotropic fiber and isotropic resin [27,28]. The software uses the materials properties, reinforcement and matrix, to generate an isotropic composite with inclusion of fiber-matrix constituent properties including effect of defects (void distribution, fiber waviness) [29]. In this

simulation the fibers are assumed straight with no waviness, and at consistent length of 25.4 mm as the WL method have no fiber length attrition.

Using the predicted isotropic composite properties produced from MCQ chopped software was imported to HELIUS Composites an Autodesk software that allows simulation and calculation of composite laminates properties. The laminate was simulated with unidirectional layers in the following sequence [0/ 90/ +30/ -30/ +45/ -45/ +60/ -60]s at a thickness of 0.1 mm per layer. In HELIUS Composites a quasi-isotropic laminate is designed to simulate the same behavior as the predicted isotropic composite properties produced from MCQ chopped software. The necessity of this step is driven from the requirements of the FEA simulation of the complex shape geometry. While a FEA study of chopped composites is feasible, it is computationally taxing and requires a full knowledge of fibers distribution and mats morphology. Replacing the chopped composite with a quasi-isotropic laminate will result in similar behavior and ease of computation when conducting the FEA analysis. The designed laminate was imported to Abaqus 2017 for FEA analysis of the complex shape composite achieved through the three cavities tool.

The complex shape composite is considered as 3 separate parts as indicated in Figure 28, shape V, shape B and shape D. Each part was subjected to tensile load with rate of 2 mm/min and a grip pressure of 100 KPa. The FEA model used tetrahedral elements and quadratic interpolation to obtain theoretical tensile performance of the complex shape parts under monotonic tensile stress.

.

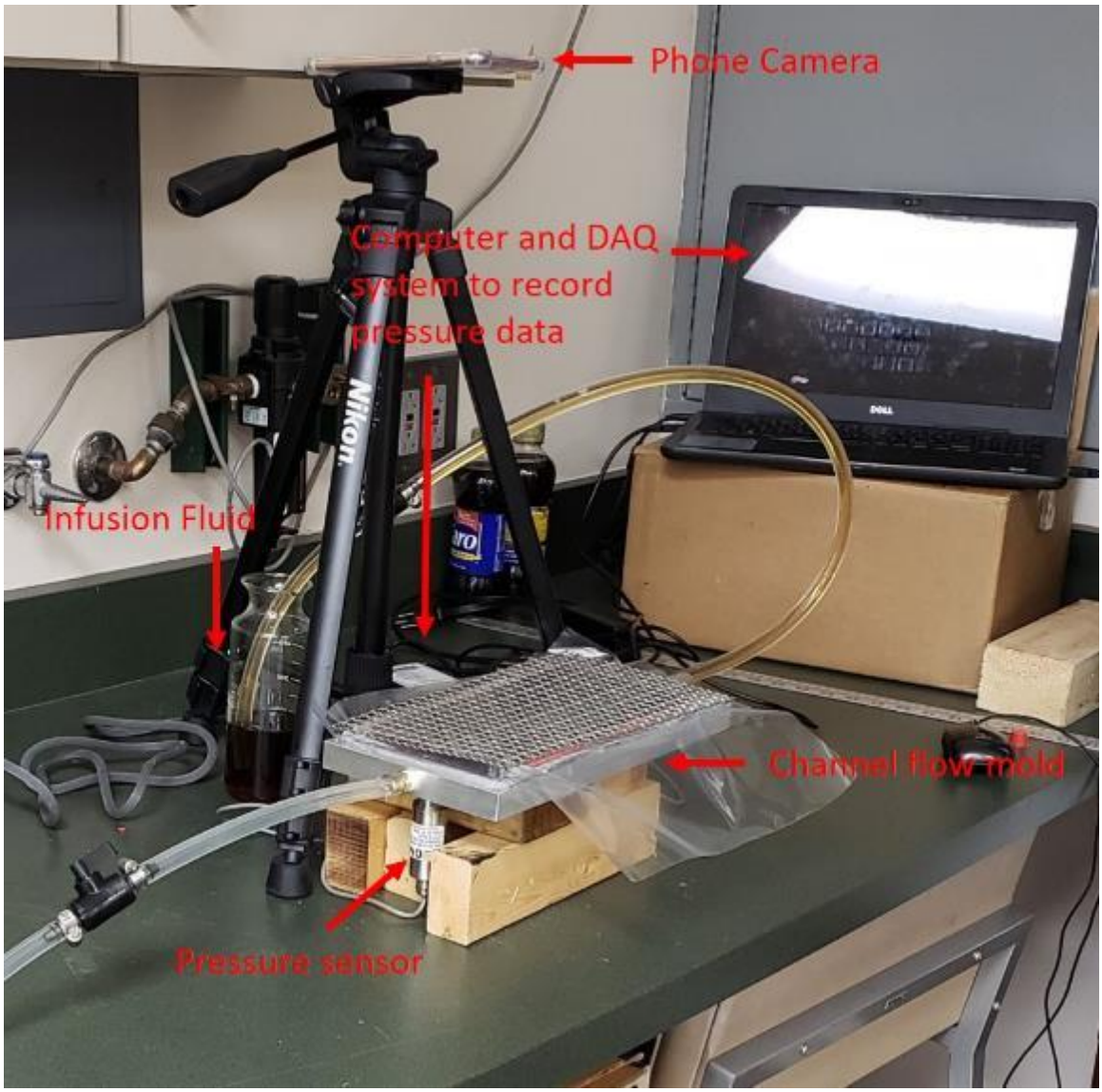

Figure 26: System for measuring in plane permeability of fabric through the channel flow mold technique

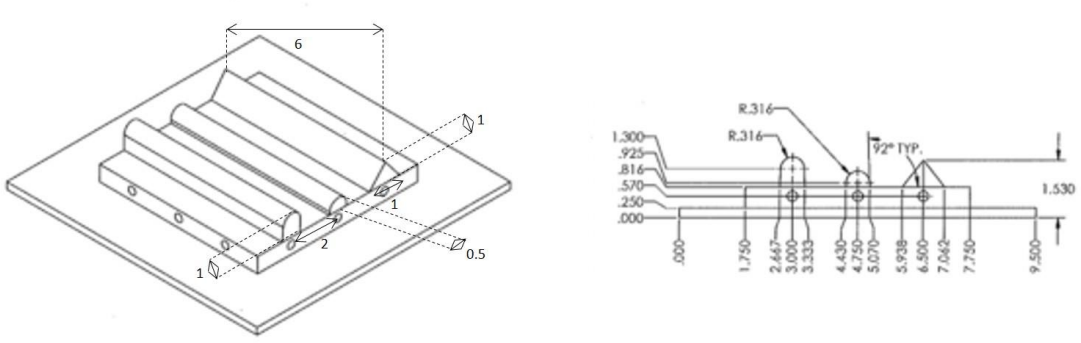

Figure 27: Three cavities mold design, used for analysis of permeability changes with the variance of complex geometry for the WL CF nonwoven preforms

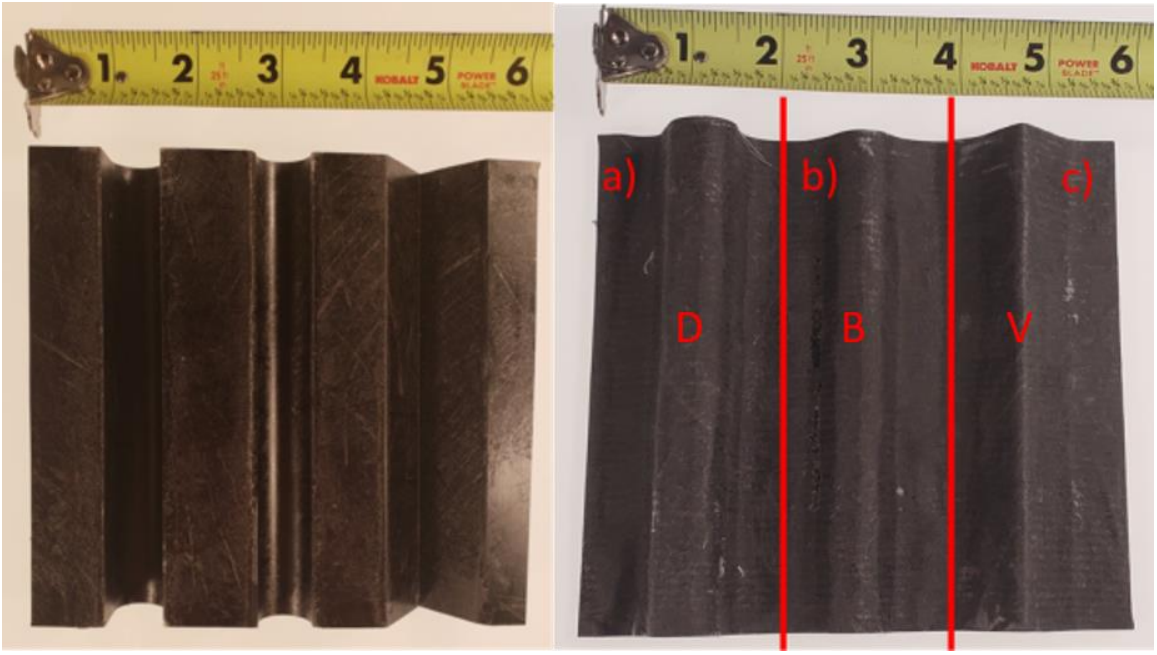

Figure 28: Complex shape composite with 3 cavities made through the VARTM process of three layers of WL CF mats at 200 gsm and using 25.4 mm long CF, the three geometries are as follow: a) Shape A is a semicircle with depth of 25.4 mm, b) Shape B is a semicircle

RESULTS AND DISCUSSION

Permeability results

Table 9 shows the calculated n_f and $D_{p,mean}$ using equation 1 and equation 2. The numbers show an inverse proportionality between n_f and $D_{p,mean}$, this is expected as with the increase in fibers count the fiber crossings increase leading to smaller $D_{p,mean}$. In addition, an increase in fibers count creates higher compaction in the area closing the distance between individual fibers and resulting in smaller$D_{p,mean}$. These numbers allow the prediction of higher permeability for the WL CF nonwoven produced using 12.7 mm fibers over those produced using 25.4 mm. Further, it is hypothesized that increasing the mats gsm should decrease the permeability.

Table 9: n_f and $D_{p,mean}$ calculated in relation to gsm and fiber length

gsm	L_F	C_v	n_f	$D_{p,mean}$
100	25.4	0.03	2.16E+05	3.65E-07
200	25.4	0.05	4.32E+05	1.82E-07
100	12.7	0.03	6.22E+04	2.53E-06
200	12.7	0.05	1.04E+05	1.52E-06

Figure 31 shows an example of the linearity of the flow front during the permeability experiment. This linearity validates the results obtained and calculated from the experiment as it is a result of a consistent and regulated flow of the test fluid throughout the medium.

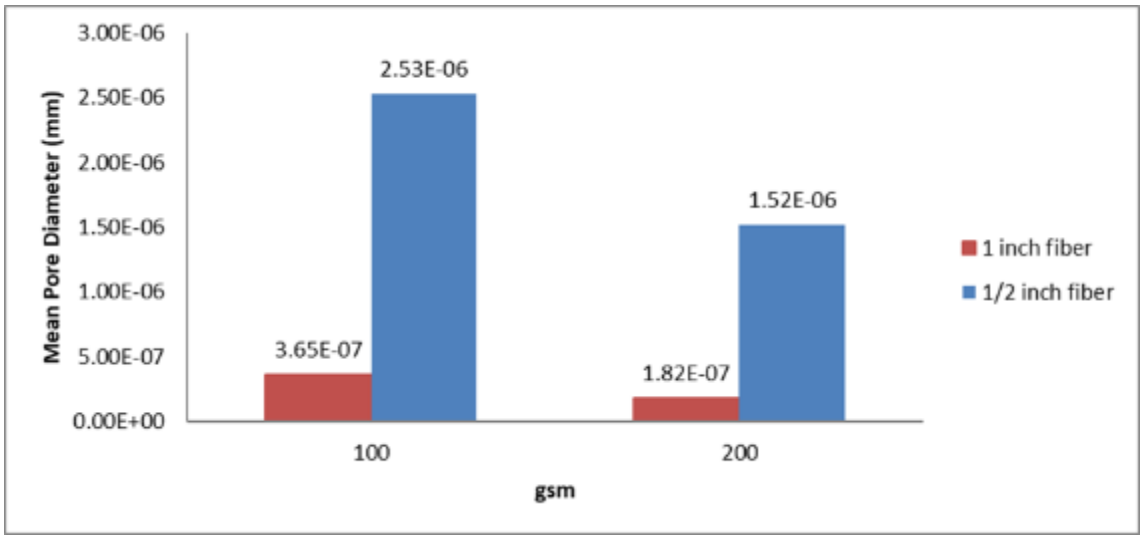

Figure 29: Effect of mats gsm and fiber length on the crowding factor

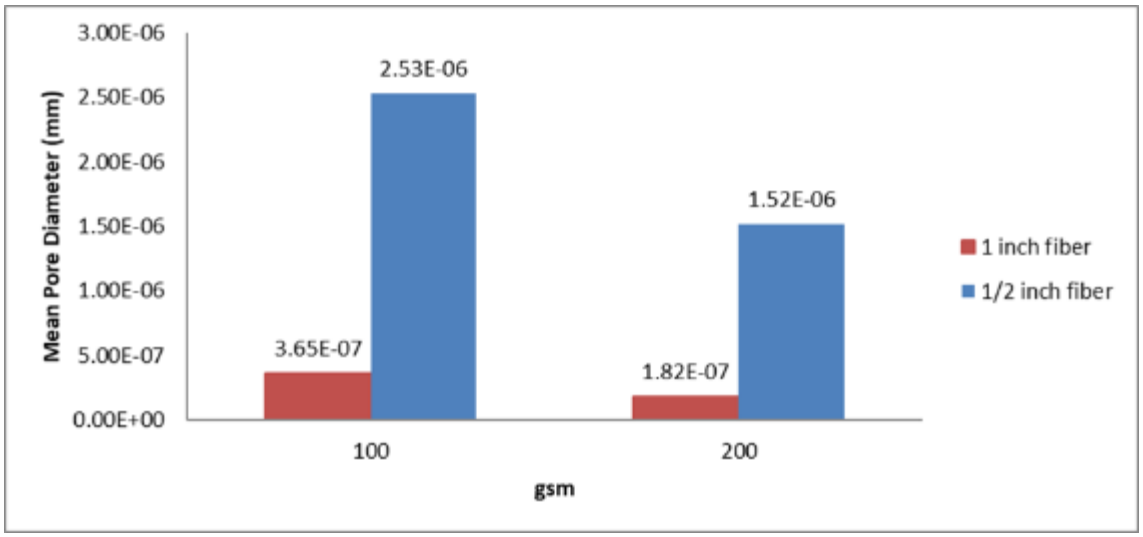

Figure 30: Effect of mats gsm and fiber length on the mean pore diameter

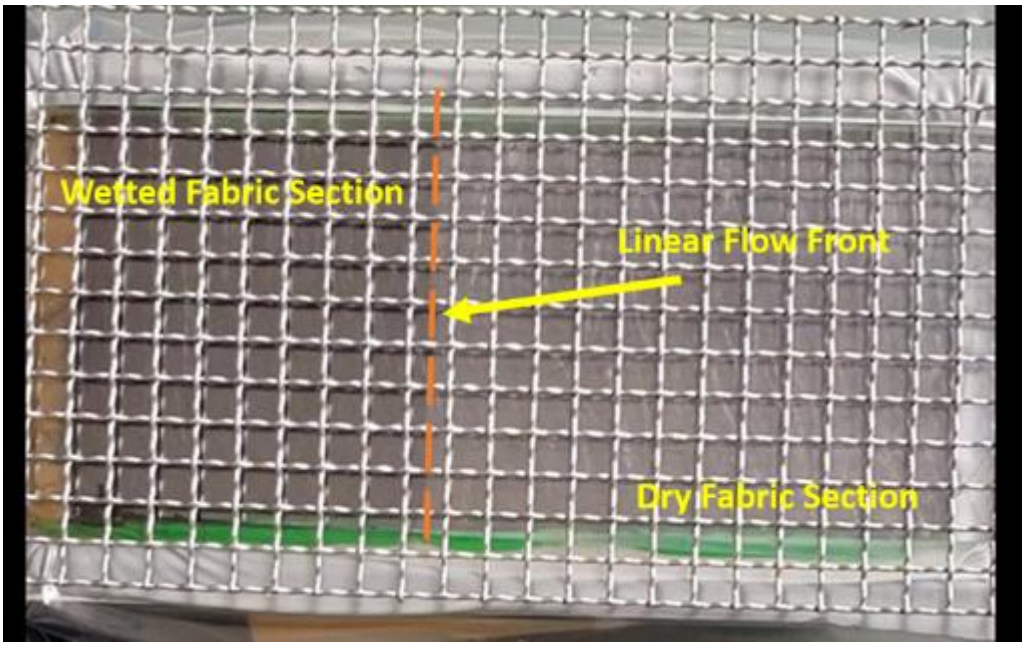

Figure 31: Example of the flow front highlighted by the orange dashed line showing linearity and consistency in shape.

Table 10 shows the values obtained from the permeability test for the various variable combinations selected for this study. Figure 32 displays the trend of change in permeability constant K that falls in accordance with the calculated expectations of $D_{p,mean}$. K shows direct proportionality to $D_{p,mean}$. While the 12.7 mm fiber length mats showed 16 % higher permeability than the 25.4 mm fiber length mats for 100 gsm and 200 gsm, the mats stacking played an important role in permeability reduction. It is to notice that stacking the mats in three layers, those made with 25.4 mm fibers resulted with permeability higher by 10% to 20% than those made with 12.7 mm did. This improved permeability led to the choice of the 24.5 mm fiber length mats when selecting material for the local permeability in dependence on geometrical shape analysis.

Table 10: Permeability experiment results

Mats	(L^2)/t	Viscosity μ (Pa.sec)	Porosity (φ)	ΔP (Pa)	Permeability (K) (m^2)	Stdev (m^2)
100gsm-12.7-1L	10390.0	0.07	0.3	69761.1	1.66E-03	3.33E-05
100gsm-12.7-3L	3629.3	0.07	0.3	70224.2	5.77E-04	1.73E-05
200gsm-12.7-1L	7064.3	0.04	0.3	70152.3	6.26E-04	3.76E-05
200gsm-12.7-3L	2791.9	0.05	0.3	69829.8	2.95E-04	8.86E-06
100gsm-25.4-1L	9095.4	0.07	0.3	68675.9	1.39E-03	5.54E-05
100gsm-25.4-3L	4667.8	0.07	0.3	70423.0	6.93E-04	1.39E-05
200gsm-25.4-1L	3938.2	0.06	0.3	70862.4	5.28E-04	1.32E-05
200gsm-25.4-3L	2791.9	0.06	0.3	68107.1	3.90E-04	3.90E-06

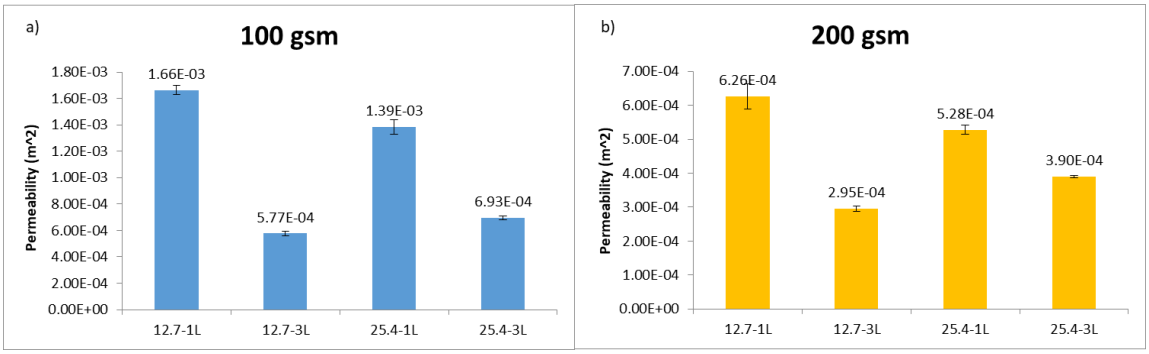

Figure 32: Variance in mats permeability with fiber length while holding areal weight constant for 1 layer and 3 layers thick: a) 100 gsm, b) 200gsm. The x-axis label is as follow: fiber length-count of layers tested, thus 12.7-1L means that the fiber length was 12.7 mm and 1 layer was tested.

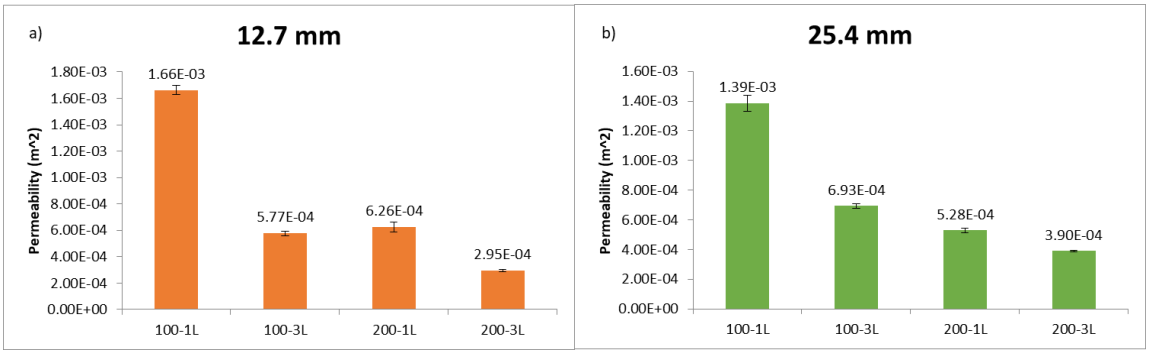

Figure 33: Variance in mats permeability with areal weight while holding fiber length constant for 1 layer and 3 layers thick: a) 12.7 mm, b) 25.4 mm. The x-axis label goes as follow: fiber length-count of layers tested, thus 12.7-1L means that the fiber length was 12.7 mm and 1 layer was tested.

Figure 33 highlights the trend of permeability reduction with the increase in crowding factors even at consistent fiber length. From Figure 33 b), the three layers at 100 gsm had higher permeability than the one layer of 200gsm with fiber length at 25.4 mm. This is due to fiber crossing affecting the distribution of $D_{p,mean}$. Theoretically the value of $D_{p,mean}$ is to be divided by number of layers bringing it to a close value of that calculated for the 200 gsm layer.

Local permeability results

Table 11 shows the results for the local permeability over the three complex geometry barriers presented by the three cavities tool. Figure 27 and Figure 28 show the tool used and a resulting part with code names for each complex geometry respectively. The V shape presented the least resistance for the resin flow, the 60° ramp presented less of an obstacle for the flow front when compared to the 90° climb from the other shapes. Shapes B and D presented higher resistance for resin flow along the vertical wall. Shape D resulted in a decrease of 54% in permeability value in comparison to shape B. The increase in height of shape D played a significant role in reducing the fluid flow.

Table 11: Local permeability results

Shapes	(L^2)/ t	Viscosity μ (Pa.sec)	Porosity (φ)	ΔP (Pa)	Permeability (K) (m^2)	Stdev (m^2)
V	794.3	0.06	0.3	70642.8	1.03E-04	4.12E-06
B	459.6	0.06	0.3	70429.1	5.97E-05	3.34E-06
D	215.6	0.06	0.3	70558.3	2.80E-05	2.24E-06

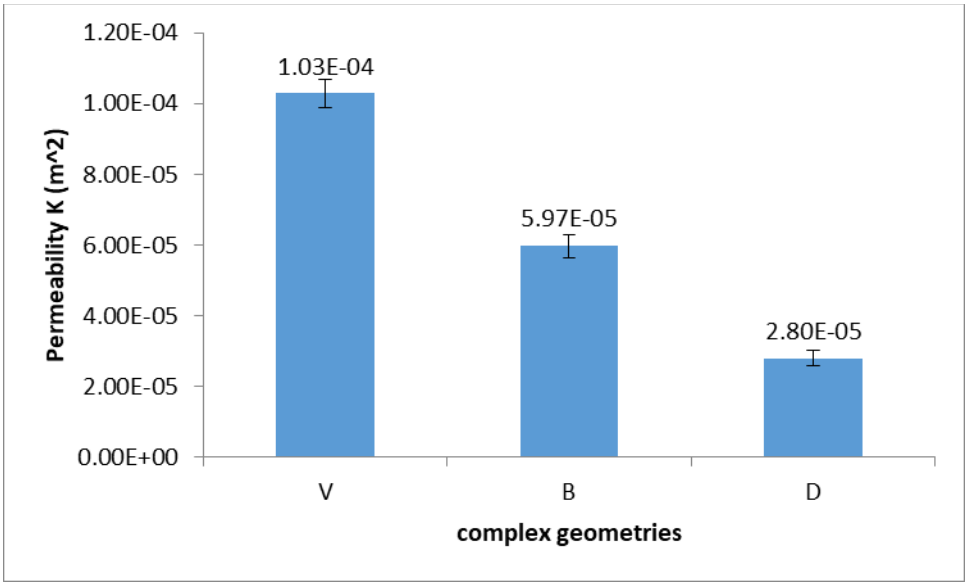

Figure 34: Local permeability changes in respect to complex shape in the mold. The complex geometry is shown in Figure 28 with explanation of the complex shapes labeling.

The permeability values of the complex shapes show a significant decrease of 75% for shape V, 85% for shape B and 93% for shape D in comparison to the in-plane permeability for three layers of WL CF nonwoven mats at 200gsm with fiber length of 25.4 mm.

In-plane permeability is a strong function of both fiber orientation and distribution. The complex shape geometry had a quantifiable change in the local permeability values. Shape V is an isosceles triangle leading to least deformation of fiber microstructure but creating a significant stress point at the peak. Shape D has a steep draw causing the most deformation of fiber alignment in addition to 25,4 mm vertical climb for the resin to overcome. Shape B has a gradual draw leading to low stress concentration and low fiber deformation.

This predicted change in fiber microstructure, and their layout in respect to the direction of applied force should reflect on the mechanical performance of the shapes.

The mechanical response is shown and discussed in the following section. The results shown in Figure 34 were in accordance to the theorized effect of the complex geometries with respect to fibers alignment.

Local permeability information, were taken into consideration during the manufacturing of the complex geometry composite in order to maintain a consistent fiber weight fraction of 30% for all three shapes.

Complex geometry testing

As discussed in the discontinuous fiber finite element analysis section, in order to ease the computational requirement in the FEA analysis, a quasi-isotropic laminate was designed to match the mechanical performance of that of the discontinuous composite. Figure 35 displays the results of the isotropic laminate obtained through theoretical design in HELIUS composite, it shows matching values with the experimental findings of the discontinuous isotropic composite as calculated through the Halpin-Tsai equation [30]. This allows its use in the FEA analysis. Figure 36 displays the results from the FEA analysis, the stress distribution throughout the cavities shows higher concentration at the deepest point, with the small semi-circle cavity holding the highest principal stress followed by the V shape cavity and the lowest stress concentration was found in the deep draw semi-circle. Figure 37 presents the stress vs strain curves, for the three cavities, obtained from FEA model and the load vs displacement obtained from the experimental tensile test. Both results show identical trends that correlate to the stress concentration noted in the FEA model and the theoretical prediction of fiber rearrangement that was discussed in the previous section when looking at local permeability. With more depth in

the cavity the angle between the plane containing the fiber and that of the applied stress becomes greater, this leads to lower loads per displacement as seen in the graphs.

CONCLUSIONS

Permeability constant for WL CF nonwoven have been measured using the channel flow technique and adopting Darcy's law for the calculation. It was found that mats stacking provided a higher permeability constant when using longer fibers as shown in this experiment when comparing 25.4 mm fiber length to 12.7 mm. Both fiber lengths used are above critical aspect ratio for CF, but the higher permeability will ease composite design and guarantee wettability of the part during production. The number of layers stacked has an inversely proportional relation with the in-plane permeability, while this relation is not directly linear, the assumption still holds as the experimental numbers obtained were within 5% margin from each other's as seen in Figure 31. Further investigation, on the relationship of mats stacking and permeability will be conducted to enhance mathematical prediction on the relation between fiber crossings and average pore diameter $D_{p,mean}$. Local permeability variance in relation to complex geometry of a composite was analyzed and showed that the WL CF nonwoven follow the same prediction as unidirectional fibers when it comes to geometry permeability prediction. This conclusion was reflected by the tensile modulus measurements of three different composite with complex geometries.

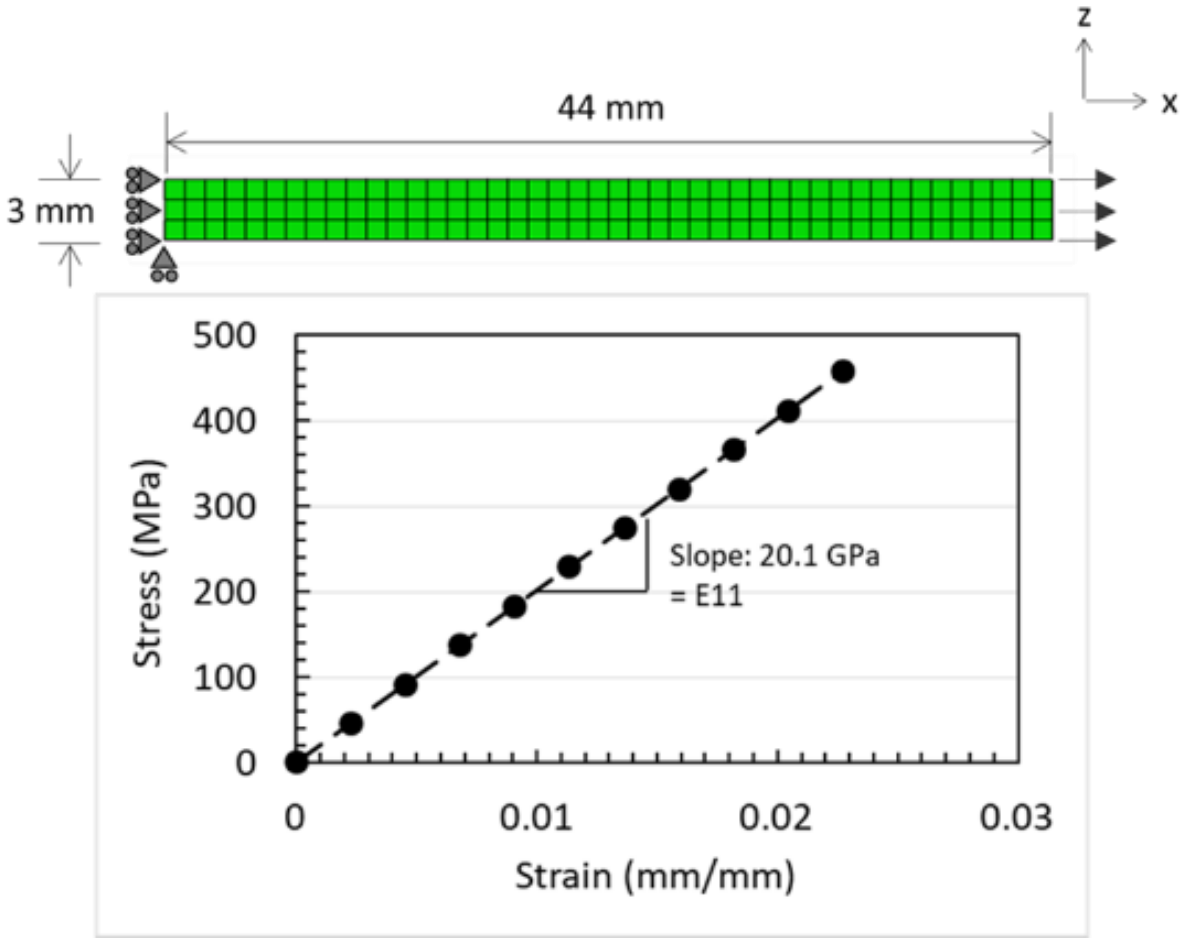

Figure 35: Representation of the quasi isotropic laminate designed in HELIUS composites and its tensile properties. The tensile modulus came in accordance to the calculated tensile modulus of a discontinuous reinforced composite made with the same material based on the Halpin-Tsai equations [30]

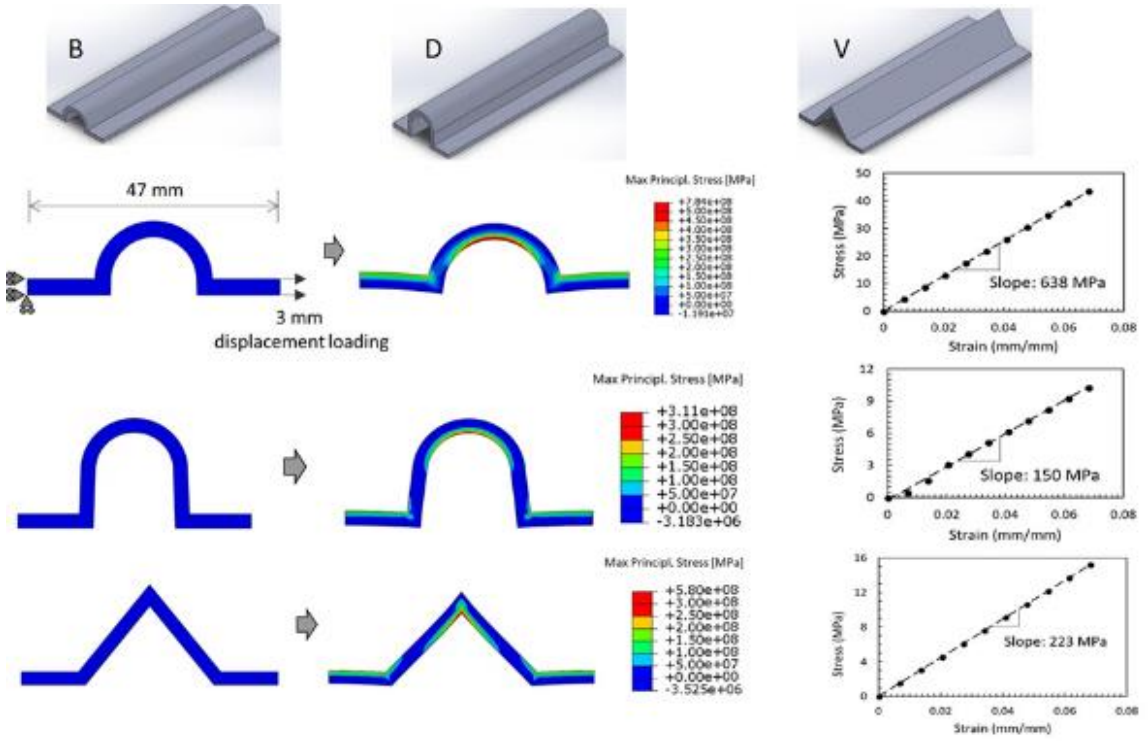

Figure 36: FEA results showing the Max Principal Stress distribution for each of the complex geometry shapes under tensile loading. Theoretical tensile Young's modulus calculations are presented to the right-hand side of each shape respectively.

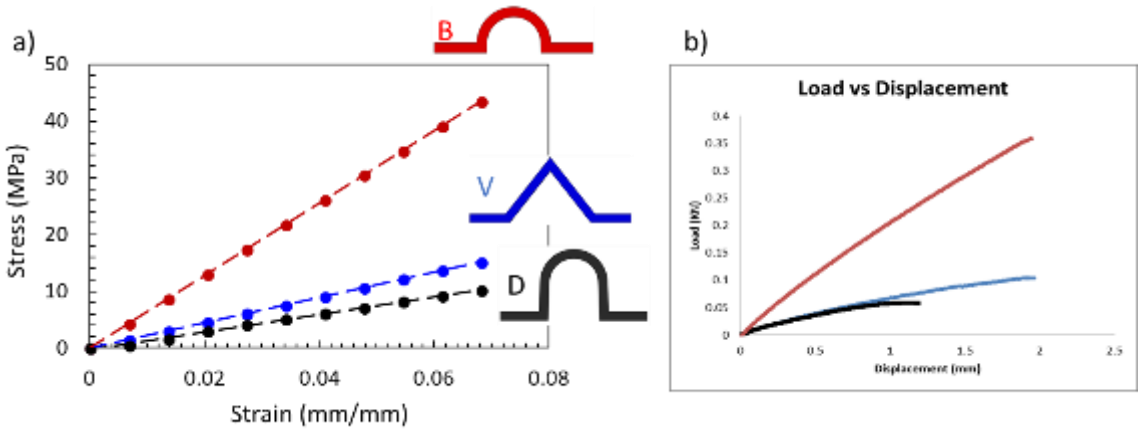

Figure 37: a) Theoretical Stress vs Strain for the three cavities shapes obtained from Abaqus and b) load vs displacement curves obtained through experimental testing.

REFERENCES

[1] Senthil K, Punitha V. An Overview of Nonwoven Product Development and Modelling of Their Properties. J Text Sci Eng 2017;07. doi:10.4172/2165-8064.1000310.

[2] Cai H, Tong X, Chen K, Shen Y, Wu J, Xiang Y. Electrospun Polyethylene Terephthalate Nonwoven Reinforced Polypropylene Separator : Scalable Synthesis and Its Lithium Ion Battery Performance n.d. doi:10.3390/polym10060574.

[3] Megahed AA, Agwa MA, Megahed M. Improvement of Hardness and Wear Resistance of Glass Fiber-Reinforced Epoxy Composites by the Incorporation of Silica/Carbon Hybrid Nanofillers. Polym - Plast Technol Eng 2018;57:251–9. doi:10.1080/03602559.2017.1320724.

[4] Kumar Patnaik T, Nayak SS. Investigation of physico-mechanical and thermo-mechanical analysis of alumina filled needle-punch nonwoven jute epoxy composites. Polym Compos 2018;39:1553–61. doi:10.1002/pc.24099.

[5] Shahzad A, Nasir SU. Validation of fatigue damage model for composites made of various fiber types and configurations. J Compos Mater 2018;52:1183–91. doi:10.1177/0021998317722402.

[6] Lin M-C, Lou C-W, Lin J-Y, Lin TA, Lin J-H. Tensile strength, peel load, and static puncture resistance of laminated composites reinforced with nonwoven fabric. J Mater Sci 2018;53:12145–56. doi:10.1007/s10853-018-2481-3.

[7] Thomason JL. The influence of fibre length and concentration on the properties of glass fibre reinforced polypropylene: 5. Injection moulded long and short fibre PP.

Compos Part A Appl Sci Manuf 2002;33:1641–52. doi:10.1016/S1359-835X(02)00179-3.

[8] Andrić JS, Lindstrom SB, Sasic SM, Nilsson H. Particle-level simulations of flocculation in a fiber suspension flowing through a diffuser. Therm Sci 2017;21:S573–83. doi:10.2298/TSCI160510185A.

[9] Yeole P, Ning H, Hassen AA, Vaidya UK. The Effect of Flocculent , Dispersants , and Binder on Wet – laid Process for Recycled Glass Fiber / PA6 Composite 2018;26:259–70.

[10] Safavi A, Fathi S, Babaei MR, Mansoori Z, Latifi M. Experimental and numerical analysis of fiber characteristics effects on fiber dispersion for wet-laid nonwoven. Fibers Polym 2009;10:231–6. doi:10.1007/s12221-009-0231-5.

[11] Yousfani SHS, Gong RH, Porat I. Manufacturing of fibreglass nonwoven webs using a paper making method and study of fibre orientation in these webs. Fibres Text East Eur 2012;91:61–7.

[12] Guan X, Qian X, Yang Z. Comparison of several image analysis methods for fiber dispersion uniformity in water. J Dispers Sci Technol 2017;38. doi:10.1080/01932691.2015.1088455.

[13] Fathi-Khalfbadam S, Latifi M, Sheikhzadeh-Najar S, Towhidkhah F. Analysis and simulation of fiber dispersion in water using a theoretical analogous model. J Dispers Sci Technol 2011;32:352–8. doi:10.1080/01932691003659833.

[14] Simmonds GE, Bomberger JD, Bryner MA. Designing Nonwovens to Meet Pore Size Specifications. J Eng Fiber Fabr 2007;2:1–15.

[15] Wölling J, Schmieg M, Manis F, Drechsler K. Nonwovens from Recycled Carbon Fibres - Comparison of Processing Technologies. Procedia CIRP 2017;66:271–6. doi:10.1016/j.procir.2017.03.281.

[16] Zhu G, Kremenakova D, Wang Y, Militky J. Air permeability of polyester nonwoven fabrics. Autex Res J 2015;15:8–12. doi:10.2478/aut-2014-0019.

[17] Pierce RS, Falzon BG, Thompson MC. Permeability characterization of sheared carbon fiber textile preform. Polym Compos 2018;39:2287–98. doi:10.1002/pc.24206.

[18] Alhussein H, Umer R, Rao S, Swery E, Bickerton S, Cantwell WJ. Characterization of 3D woven reinforcements for liquid composite molding processes. J Mater Sci 2016;51:3277–88. doi:10.1007/s10853-015-9640-6.

[19] Stig F, Tahir MW, Åkermo M, Hallström S. An experimental study of the influence from fibre architecture on the permeability of 3D-woven textiles. J Reinf Plast Compos 2015;34:1444–53. doi:10.1177/0731684415593351.

[20] Antonucci V, Esposito M, Ricciardi MR, Raffone M, Zarrelli M, Giordano M. Permeability characterization of stitched carbon fiber preforms by fiber optic sensors. Express Polym Lett 2011;5:1075–84. doi:10.3144/expresspolymlett.2011.105.

[21] Sharma S, Siginer DA. Permeability Measurement Methods in Porous Media of Fiber Reinforced Composites. Appl Mech Rev 2010;63:020802. doi:10.1115/1.4001047.

[22] Endruweit A, Harper LT, Turner TA, Warrior NA, Long AC. the Permeability of

Random Discontinuous Carbon Fibre Preforms n.d.:2–3.

[23] Ghossein H, Hassen AA, Paquit V, Love LJ, Vaidya UK. Innovative Method for Enhancing Carbon Fibers Dispersion in Wet-Laid Nonwovens. Mater Today Commun 2018;17:100–8. doi:10.1016/j.mtcomm.2018.08.001.

[24] Ferland P, Guittard D, Trochu F. Concurrent Methods for Permeability Measurment in Resin Transfer Molding. Polym Compos 1996;17:149–58. doi:10.3139/9781569906200.016.

[25] National Institute of Standard and Technology data base on selection of test fluids for permeability measurments. n.d.

[26] Dormohammadi S, Repupilli M, Abdi F, Wan Y, Takahashi J, Huang H. Multi-Scale Computational Modeling of Short Fiber Reinforced Thermoplastics. Am Soc Compos Thirty-First Tech Conf 2016:1–8. doi:10.1111/j.1532-5415.1991.tb04043.x.

[27] Baid HK, Abdi F, Lee MC, Vaidya U. Chopped Fiber Composite Progressive Failure Model under Service Loading, Baltimore MD: SAMPE 2015; 2015, p. 1–17.

[28] Kim JH, Garg M, Kim JH. Research of carbon composite material for nonlinear finite element method 2012:84092T. doi:10.1117/12.923276.

[29] Dormohammadi S, Huang D, Repupilli M, Abdi F, Song Y, Gandhi U. Crush Analysis of Compression Modeled Chopped Fiber Tubes. Proc Am Soc Compos Tech Conf 2016.

[30] Affdl JCH, Kardos JL. The Halpin-Tsai equations: A review. Polym Eng Sci 1976;16:344–52. doi:10.1002/pen.760160512.

OVERALL CONCLUSIONS

The main goal of this dissertation was to introduce an innovative method for CF dispersion that can optimize WL CF nonwoven mats production and to validate their use in composites production. The pre-existing methods of dispersion, called Method 1, were unable to reach optimization of CF dispersion in water due to fiber adaptation to the fluid velocity when rigid body motion is reached during the mixing process.

Proposed innovative mixer

To achieve optimal CF dispersion, the innovated technique of mixing called Method 2, followed the chaotic mixing regime in order to achieve optimal dispersion of CF. Method 2, not only achieved optimal dispersion, but with the help of a systematical numerical analysis its was proven to be a reproducible method with high accuracy.

Validation of mats isotropic nature

The resulting mats, when made into composites were proven isotropic in nature through a numerical computer-simulation analysis using OOF. The simulation explored the tensile behavior of the composites microstructure in two principal directions and made comparison. The optimal dispersion of fibers through Method 2 proved to achieve full isotropy in the composites made with the optimally dispersed mats.

Mechanical performance evaluation of WL CF nonwoven composites

A comparison of the experimentally tested Young's modulus, of the two sets of composites made from each method, showed an improvement of 16% for Method 2 over

Method 1 and 10% improvement toward the fit with the expected calculated values from the well accepted Halpin- Tsai laminated theory. This trend in improvement was reflected on other mechanical properties like flexural strength and ILSS by 23% and 83% respectively.

In-plane permeability and local permeability evaluations

The study explored the in-plane permeability of the nonwoven mats in order to establish an understanding of their behavior when infused with resin.

The optimized dispersion of Method 2 allowed for a better fit with theoretical expectation when calculating the average mean pore in the mats. It was found as well that when stacking several mats together, mats made with fibers at 25.4 mm, had higher permeability than those made with fibers at 12.7 mm. Such information can be critical for design of infusion and manufacturing of composites.

The innovated method of mixing will be adopted for future preparation of WL CF nonwoven. Future work can explore formation of nonwoven composites using various grades of CF, like recycled fibers and mixtures of CF with other synthetic fibers.

VITA

Hicham Kheir Ghossein was born October 18, 1986. He grew up in Zahle, Lebanon until the age of 18. For his undergraduate degree, Hicham attended the Lebanese University in Fanar, Lebanon where he majored in physics. After graduation Hicham moved to the United States, to join his parents in Birmingham Alabama. There Hicham started his graduate school career by obtaining a Master degree in Science from the University of Alabama at Birmingham while majoring in applied physics in 2010. In 2013 Hicham started his PhD work under the guidance of Dr. Uday Vaidya. The two of them moved to the University of Tennessee, Knoxville in 2015. There Hicham finalized his PhD work that is presented in this dissertation. During his tenure in graduate school, Hicham has served on the board of directors for the composite division of the Society of Plastic Engineers, and he was member of the steering committee of the Composite Coalition of East Tennessee. Hicham was awarded the Graduate Automotive Technology Education Fellowship from the Department of Energy and Supported by the Institute of Advanced Composite Manufacturing Innovation.